

THE SEARCH FOR OPTIMAL PULSE CHARGING PARAMETERS AND THE IMPACT OF
THESE PARAMETERS ON LITHIUM ION BATTERIES

A Dissertation

by

JUDY MARIAN AMANOR-BOADU

Submitted to the Office of Graduate and Professional Studies of
Texas A&M University
in partial fulfillment of the requirements for the degree of

DOCTOR OF PHILOSOPHY

Chair of Committee,	Edgar Sánchez-Sinencio
Committee Members,	Anthony Guiseppi-Elie
	Jun Zou
	Kamran Entesari
Head of Department,	Miroslav Begovic

August 2018

Major Subject: Electrical Engineering

Copyright 2018 Judy Marian Amanor-Boadu

ABSTRACT

In this day and age, consumers of electronic devices seek faster battery charging and longer battery runtime. Different methods have been proposed to reduce battery charge time and also increase the battery charge and energy efficiencies, which will in turn improve battery runtime. Of these methods, pulse charging is the most promising and less complex. However, the pulse charge currents used in pulse charging have different factors and factor levels. The different combination of these factors and their levels can result in either poor battery charge and energy efficiencies or longer charge times. These factors also impact the life cycle and impedance characteristics of the battery. Many researchers have investigated the impact of pulse charging on lithium-ion batteries. However, the combined impact of duty cycle and frequency of the pulse charge current on lithium-ion polymer batteries is seldom investigated. This work presents a pulse charger design based on battery polarization characteristics for the Internet-of-Things (IoT) applications. It further proposes an optimization approach, the Taguchi orthogonal arrays (OA), to search for optimal pulse charging parameters that will maximize battery charge and energy efficiencies while decreasing charge time. The same approach is used to determine the impact of the pulse charge current factors on the life cycle of lithium-ion polymer batteries and their impedance parameters.

Experimental results verify that the proposed pulse charger designed for IoT applications reduces the charging time of 100 mAh and 45 mAh li-ion batteries respectively by 37.35% and 15.56% and improves the charge efficiency by 3.15% and 3.27% when compared to the benchmark constant current-constant voltage (CC-CV) charging technique. The pulse charger using optimal parameters obtained from the Taguchi OA approach was compared with the benchmark CC-CV

charging technique. This resulted in a charge time reduction of 47.6% and battery charge and energy efficiencies improvement of 1.5% and 11.3% respectively, at a charge rate of 0.5C. Life cycle also increased by more than 100 cycles.

DEDICATION

Anuonyam nka Onyankopon

ACKNOWLEDGEMENTS

I would like to thank my committee chair and advisor, Dr. Sánchez-Sinencio for his support, advice, mentorship, and guidance throughout my entire research study. I like to acknowledge my committee members, Dr. Guiseppi-Elie for his advice, continuous feedback, and never-ending support, Dr. Zou for his feedback, and Dr. Entesari for his support. I would also like to thank all my committee members for taking time to serve on my committee.

I would also like to express appreciation to my mentors, Dr. Karen Butler-Purry and Shawna Fletcher, for their continual support, encouragement, and advice. I also would like to acknowledge my research colleagues, namely Fernando Lavalle Aviles, Joseph Riad, Kyoo Hyun Noh, Mohamed Abouzied, Sergio Soto Aguilar, and Johan Jair Estrada Lopez, and the ECE department faculty and staff for making my time at Texas A&M University a great experience.

My appreciation also goes to John Aggas and Ankita Bhat of the Center for Bioelectronics, Biosensors, and Biochips (C3B®) in the Department of Biomedical Engineering and Souvik De in the department of Chemical Engineering for their help in performing electrochemical impedance spectroscopy.

I also extend my gratitude to MOSIS (Metal Oxide Semiconductor Implementation Service) who provided a means to fabricate my design through their educational program.

Finally, my gratitude goes to my family for their love and support. A special thanks to my mother for her continual prayers and encouragement.

CONTRIBUTORS AND FUNDING SOURCES

This work was supported by a dissertation committee consisting of Professor Sánchez-Sinencio, research advisor, and Professors Zou and Entesari of the Department of Electrical and Computer Engineering, and Professor Guiseppi-Elie of the Department of Biomedical Engineering.

Access to the equipment used to perform electrochemical impedance spectroscopy was provided by Professor Guiseppi-Elie, who also provided research direction in investigating the use of Design of Experiments approaches to determine optimal parameters for charging. Professor Lutkenhaus in the Department of Chemical Engineering also provided access to one of the labs in order to perform battery impedance measurements. All other work conducted for the dissertation was completed by the student independently.

The first year of graduate study was supported by a fellowship from Texas Instruments Inc. Funding for all other years has been provided through assistantships from the College of Engineering. Fees, testing materials, and other minor expenses were also covered by support from Texas Instruments Inc.

NOMENCLATURE

ac	alternating current
dc	direct current
PMOS	p-type metal-oxide-semiconductor
NMOS	n-type metal-oxide-semiconductor
IC	integrated circuit
CAD	computer-aided design
PCB	printed circuit board
RF	radio frequency

TABLE OF CONTENTS

	Page
ABSTRACT.....	ii
DEDICATION.....	iv
ACKNOWLEDGEMENTS.....	v
CONTRIBUTORS AND FUNDING SOURCES	vii
NOMENCLATURE	viii
TABLE OF CONTENTS.....	ix
LIST OF FIGURES	xii
LIST OF TABLES.....	xvi
1. INTRODUCTION	1
1.1 Organization of dissertation.....	4
2. ENERGY STORAGE DEVICES.....	7
2.1 Electrical energy storage devices: Supercapacitors	7
2.2 Electrochemical energy storage devices: Secondary batteries	9
2.2.1 Secondary batteries market.....	11
2.2.2 Recent development in secondary batteries	13
2.2.3 Battery terms definition	15
2.3 Lithium-ion chemistry based batteries.....	17
2.3.1. Types of positive electrodes for li-ion chemistry based batteries.....	18
2.3.2. Li-ion battery formats	19
2.3.3. Li-ion polymer (LiPo) battery.....	20
2.4 Mechanism of LiPo battery operation during the charge and discharge processes	20
2.5 Li-ion battery models.....	22
2.6 Electrochemical impedance spectroscopy (EIS).....	26
3. BATTERY CHARGERS.....	31
3.1 Battery charging algorithms.....	31
3.2 Li-ion battery charging algorithms	32
3.2.1 Constant current - constant voltage charging algorithm.....	33

3.2.2	CC-CV based li-ion battery chargers	35
3.2.2.1	Linear chargers	35
3.2.2.2	Switch-mode chargers	36
4.	PULSE CHARGING	39
4.1	Basics and benefits of pulse charging.....	39
4.2	Previous works on li-ion pulse charging.....	44
4.3	Design of a pulse-based charger for IoT applications	46
4.3.1	Proposed pulse charger system level overview.....	47
4.3.2	Implementation of proposed pulse charger for IoT applications	52
4.3.3	Testing setup and experimental results	57
4.3.3.1	Summary of experimental results	67
4.4	The need for searching for optimal pulse charging parameters.....	68
5.	TAGUCHI ORTHOGONAL ARRAYS.....	70
5.1	Overview of Taguchi orthogonal arrays	73
5.2	Design and analysis of Taguchi OA	74
5.3	Design example using Taguchi OA	78
6.	THE SEARCH FOR OPTIMAL PULSE CHARGING PARAMETERS.....	82
6.1	Previous li-ion battery charging works using Taguchi OA	82
6.2	Search for optimal pulse charging parameters.....	83
6.2.1	Characterization of li-ion polymer batteries	84
6.2.2	Taguchi OA model design	87
6.2.2.1	Control factors identification and level determination	87
6.2.2.2	Tolerance design.....	88
6.2.2.3	OA size selection	89
6.2.2.4	Conduction of experiments.....	91
6.2.2.5	Data analysis.....	91
6.2.2.6	Optimal parameters evaluation.....	92
6.2.3	Pulse charger design	92
6.3	Experimental results	94
6.4	Summary.....	105
7.	THE IMPACT OF PULSE CHARGING PARAMETERS ON LI-ION POLYMER BATTERY LIFE CYCLE.....	107
7.1	Techniques for determining the impact of charging parameters on batteries.....	107
7.2	Overall experimental test configuration	108
7.3	Experimental results and observations	110
7.3.1	The impact of charging characteristics on battery impedance parameters	110
7.3.2	The impact of charging characteristics on battery life cycle	117
7.3.3	Impact of pulse charge current factors and factor levels on battery characteristics	120

7.3.4 Summary of experimental results	124
8. CONCLUSION.....	126
8.1 Contributions	128
8.2 Future research direction	128
REFERENCES	130
APPENDIX.....	164

LIST OF FIGURES

	Page
Figure 1 A typical charging system	2
Figure 2 Conventional capacitor vs supercapacitor	8
Figure 3 Ragone plot.....	9
Figure 4 Energy density comparison of different batteries.....	11
Figure 5 Different battery formats	18
Figure 6 Charge and discharge processes in a battery	21
Figure 7 Different li-ion battery models	24
Figure 8 Li-ion battery model incorporating inductance	24
Figure 9 Li-ion battery model with constant phase element.....	25
Figure 10 Typical Nyquist plot of a li-ion battery	27
Figure 11 Typical Bode magnitude and phase plot of li-ion battery	27
Figure 12 Nyquist plots of discussed li-ion battery models.....	28
Figure 13 Fitting of different li-ion battery models to measured EIS data using Nyquist.....	29
Figure 14 Fitting a modified Randles equivalent circuit to measured li-ion battery data.....	30
Figure 15 Macro model representation of different charging algorithms.....	33
Figure 16 CC-CV charging algorithm	34
Figure 17 Linear and switch mode CC-CV li-ion battery charger.....	37
Figure 18 Pulse charge current characteristics.....	41
Figure 19 Bode impedance magnitude plot showing minimum impedance occurrence	42
Figure 20 Flow chart of proposed pulse charger for IoT applications.....	48
Figure 21 Changes in battery polarization with respect to SoC.....	49
Figure 22 Block level diagram of proposed pulse charger for IoT applications	51

Figure 23	Simulation results showing variation of power consumption and charge time versus fast charge phase duty cycle of proposed pulse charger	51
Figure 24	Implementation of proposed pulse charger	52
Figure 25	(a) Micrograph of designed pulse charger (<i>Left</i>) (b) Packaged IC (<i>Right</i>).....	57
Figure 26	Bode impedance magnitude plot for different li-ion batteries under test.....	58
Figure 27	Measured minimum impedance vs the frequency at which it occurs for different battery capacities.....	59
Figure 28	Nyquist plots for different li-ion batteries in coin format under test.....	60
Figure 29	Experimental setup for testing designed pulse charger	61
Figure 30	Proposed pulse charging algorithm vs CC-CV for a 100 mAh li-ion battery	63
Figure 31	Proposed pulse charging algorithm vs CC-CV for a 45 mAh li-ion battery	63
Figure 32	100 mAh battery surface temperature for both pulse charging at f_{Zmin} vs CC-CV ...	66
Figure 33	45 mAh battery surface temperature for both pulse charging at f_{Zmin} vs CC-CV	66
Figure 34	A typical system undergoing an experiment	70
Figure 35	Pictorial representation of an experimental system with three input factors.....	71
Figure 36	General procedure for a DoE flow chart	73
Figure 37	Pictorial representation of a Taguchi OA with 3 factor inner array and 2 factor outer array	75
Figure 38	Main effects plot for yield	80
Figure 39	S/N (larger-the-better) for factor levels	80
Figure 40	Proposed method for search of pulse charging optimal parameters.....	84
Figure 41	Bode and Nyquist impedance plot of LiPo batteries under test	85
Figure 42	PDFs for extracted LiPo batteries under test impedance parameters	86
Figure 43	Taguchi OA model design procedure.....	87
Figure 44	PDF for Z_{intmin} and f_{Zmin} of batteries under test	89
Figure 45	Pulse charger schematic	93

Figure 46	Designed pulse charger waveforms.....	94
Figure 47	Experimental test setup for searching for optimal pulse charger parameters for LiPo batteries	95
Figure 48	Main factor effects for output response using ANOM.....	97
Figure 49	Main factor effects for output response using S/N	98
Figure 50	η_{BC} , η_{BE} , t_c vs D	100
Figure 51	CC-CV charge method vs Pulse charge method (50% duty cycle, f_{Zmin}).....	100
Figure 52	CC-CV vs Pulse at room temperature (23°C) at 0.5C charge rate	102
Figure 53	Battery charge curves at different charge rates	103
Figure 54	Battery surface temperature during charging at different charge rates	103
Figure 55	JEITA guidelines for li-ion battery charging.....	105
Figure 56	Experimental setup for determining impact of pulse charging parameters on LiPo batteries.....	109
Figure 57	Pulse charger design for conducting experiments.....	109
Figure 58	$R_s + R_{ct}$ vs number of charge and discharge cycles at 100% DoD	111
Figure 59	Q_{dl} vs number of charge and discharge cycles at 100% DoD.....	111
Figure 60	$R_s + R_{ct}$ vs number of charge and discharge cycles at 100% DoD separated at different temperatures	113
Figure 61	Q_{dl} vs number of charge and discharge cycles at 100% DoD separated at different temperatures.....	114
Figure 62	Z_{min} vs number of charge and discharge cycles at 100% DoD	115
Figure 63	Z_{min} vs number of charge and discharge cycles at 100% DoD separated by temperature	116
Figure 64	Accelerated aging of LiPo batteries subjected to pulsing at optimal parameters and conventional CC-CV algorithm	118
Figure 65	Life cycle of batteries subjected to CC-CV charging algorithm	118
Figure 66	Pulse charging factors and factor level impact on battery life cycle.....	120

Figure 67 Pulse charge current factor effects on battery impedance parameters 121

LIST OF TABLES

	Page
Table 1 Advantages and disadvantages of different secondary batteries	12
Table 2 Comparison of different positive electrodes used in li-ion batteries	19
Table 3 Extracted battery parameter values from fitted curve using Levenberg-Marquardt.....	30
Table 4 Advantages and disadvantages of switch mode and linear chargers	38
Table 5 Impedance parameters of characterized li-ion batteries	60
Table 6 Summary of experimental results for 100 mAh li-ion battery	64
Table 7 Summary of experimental results for 45 mAh li-ion battery	65
Table 8 Typical orthogonal array.....	76
Table 9 Standard Taguchi orthogonal arrays [204]	77
Table 10 Design scenario example factors and factor levels.....	78
Table 11 L_4 OA showing experimental runs	79
Table 12 Extracted mean values of the impedance parameters of the batteries under test.....	86
Table 13 Factors levels under test.....	89
Table 14 $L_{36}(3^2 \times 6^1)$ Orthogonal array.....	90
Table 15 Output responses of Taguchi OA experiment.....	96
Table 16 Charge improvement - Pulse charge vs CC-CV at 0.5C charge rate.....	101
Table 17 Output responses at the different charge rates	102
Table 18 Output evaluated responses	119
Table 19 ANOVA table for battery life cycle.....	122
Table 20 ANOVA table for battery impedance parameters.....	123

1. INTRODUCTION

Processing power for different portable electronic devices has been increasing over the past few years. This is primarily driven by the need for devices to perform more functions and these devices should perform these functions in a short amount of time. Most of these devices are powered by secondary energy storage devices such as batteries and supercapacitors. These energy storage devices can have their energy replenished once it has been depleted. They provide consumers with the convenience of not always needing to connect their devices to an external power source via wires. Driven by their ubiquitous use in many applications, secondary energy storage devices continue to increase their market share in the battery market. The rechargeable battery market size, for example, is increasing every year and it is projected to exceed \$111 billion by 2019 [1]. This estimated growth is primarily driven by the automotive, consumer electronics, and grid energy storage industries [2], [3]. The supercapacitor market is also projected to exceed \$2.18 billion by 2022 [4] driven by the memory, aviation, solid state drives, automotive, and energy harvesting markets.

These energy storage devices need to have their energy replenished once it has been depleted, and this replenishment can be achieved by using a system known as a charger. A typical charging system is shown in Fig. 1. A charging system is composed of special circuits that ensure that the energy delivered to the energy storage devices is conditioned properly. It will typically take its inputs from a universal serial bus (USB), an ac adapter, energy harvesting sources or a combination of these inputs. Most of today's portable electronic devices have embedded USB ports and offer the convenience of easily charging whatever energy storage device is present. USBs are now able

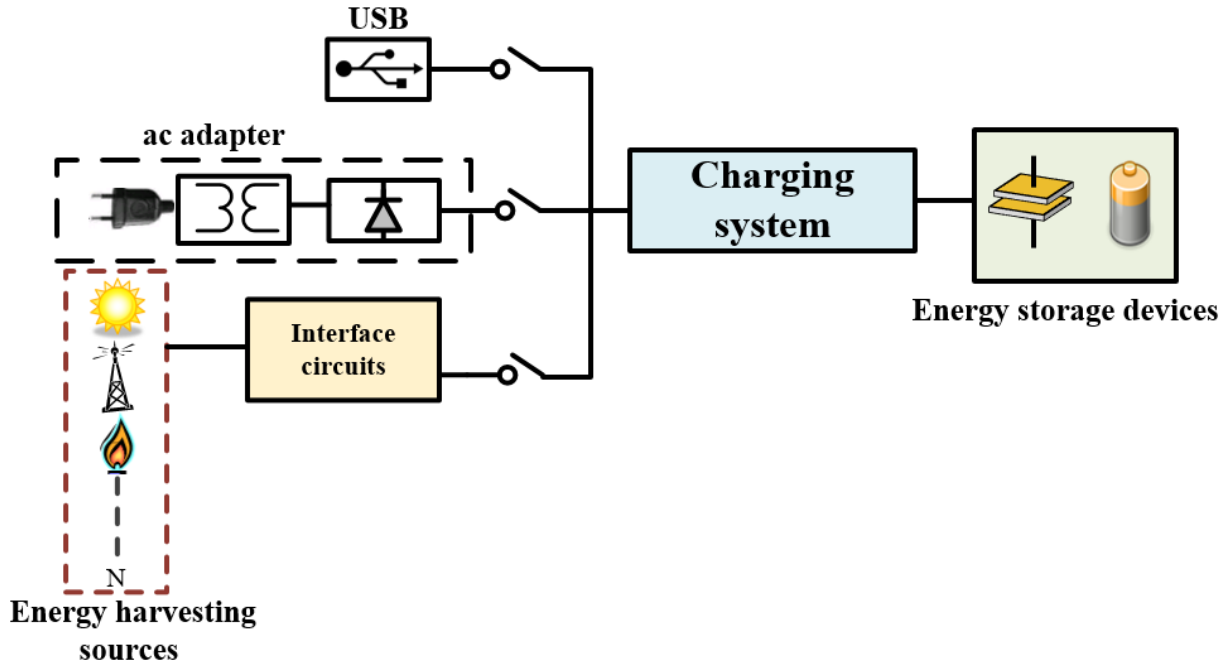


Figure 1: A typical charging system

to supply up to a 100W of power [5], thereby offering more flexible power delivery to many devices. The use of power adapters, also known as ac adapters, is one of the most popular input power sources from which energy storage devices in portable electronics are recharged. These adapters consist of a step-down transformer to reduce the mains voltage to a suitable voltage that can be rectified and conditioned for use with the charging system. They are connected to the mains or wall outlet via a plug. Within the past few decades, the use of environmental energy as power sources have been established. Potential energy that can be harvested from the environment for use with charging systems include solar, thermal, RF, and vibrations. Special transducers, such as photovoltaic cells for solar energy, thermoelectric generators for thermal, antennas for RF, and piezoelectric generators for vibrations are needed in order to harvest environmental energy and convert it to electrical energy. The harvested power is then conditioned for use with the charging

system by using interface circuits that might include maximum power point tracking (MPPT) circuits, charge pumps, or switching dc-dc converters. These charging systems play a very important role in many applications as they are needed to ensure that energy storage devices are replenished in a timely and efficient manner.

Consumers expect their portable electronic devices to be quickly charged when connected to various inputs power sources. They also expect longer runtimes when their devices are not connected to input power sources. Unfortunately, energy storage devices used in many electronic applications have not been able to keep up with the power requirements needed by their hosts [6]. To keep consumers satisfied and also to solve the problem of the slow advancement of increased energy storage capacities and energy densities that are safe for consumer use, original equipment manufacturers (OEMs) have implemented several techniques to lower power consumption in order to improve battery runtime. These techniques include power management circuits with ultra-low power consumption, such as state of the art switching regulators [7], power control techniques using software approaches [8]-[11], and relying on environmental energy, such as solar [12]-[15], thermal [16]-[20], and radio frequency (RF) [21]-[27] to increase battery runtime. Another technique that can extend runtime is the use of larger capacity energy storage devices which results in increased cost and form factors. For example, when comparing a 0.7 F supercapacitor to 120 F, the physical size increases by a factor of 3 [28], and when comparing a battery with a capacity of 85 mAh to a 500 mAh battery of the same chemistry, the physical size increases by a factor of 1.5 [29].

To satisfy the consumer need for reduced charge time, companies, such as Qualcomm Inc., have implemented a fast charging technology called Quick Charge [30]. This technology increases the charge rate in the beginning stages of charging by using a higher voltage, resulting in an increased power transfer rate. Qnovo has also created a technology that uses software techniques to achieve adaptive fast charging [31]. Companies, such as Apple, Samsung, Motorola, and Huawei, have different implementations for achieving fast charging based on either an increased charge voltage or current. However, safety mechanisms must be incorporated in these technologies to prevent overheating and ensure safety for both the consumer and device.

Energy storage devices and their corresponding charging systems are crucial to the operation of many electrical applications. To keep consumers satisfied, there is therefore a need for long runtime, fast charging, and long life cycle energy storage devices. Consequently, this work will review energy storage devices and focus on the implementation of charging systems that concentrate on fast charge time, improved run time, and increased life cycle.

1.1 Organization of dissertation

Charging systems use various charging algorithms and to determine the algorithm that results in reduced charge time, longer runtime, and increased life cycle is very important to ensure consumer safety and satisfaction. The objective of this work is to therefore design a battery charging system based on an efficient charging algorithm to improve safety without compromising fast charging and increased battery life cycle. It also searches for the optimal charging parameters that reduces the charge time and at the same time increases the battery charge and energy efficiencies. This work will also evaluate the impact of the chosen charging algorithm on the life cycle and characteristics of the battery. This document is organized as follows:

Section 2 will review popular secondary energy storage devices, their applications, and definition of some terms used in datasheets. It will focus primarily on lithium-ion batteries, their formats, and equivalent circuit models and discuss why lithium-ion polymer batteries are the chosen energy storage of choice in this work.

Section 3 reviews battery charging methods or techniques, battery chargers, and why battery charging is important. It will also discuss the current benchmark charging technique, the constant current - constant voltage charging algorithm, and its drawback.

Section 4 gives a background on pulse charging and why it is the chosen method of charging in this work. It also discusses why pulse charging improves the battery charge efficiency and reduces charge time. It also analyzes some previous works in literature. A pulse charger, specifically for low power applications, such as the Internet of Things (IoT), is designed, fabricated, and tested. The results are compared with the benchmark constant current - constant voltage charging technique, and conclusions are drawn from this design. This work has been presented in [32].

Section 5 discusses the design of experiments approaches, specifically, Taguchi orthogonal arrays, their design, analysis, and applications. It also discusses why there is a need to incorporate this approach in battery charging.

Section 6 discusses why there is a need to search for optimal charging parameters to reduce charge time and increase battery charge and energy efficiencies. It further describes an optimization procedure, Taguchi orthogonal arrays, to find the pulse charge parameters that have the greatest

impact on output parameters such as charge time and battery charge and energy efficiencies. These optimal parameters are then applied to a designed pulse charger and the experimental results compared with the benchmark constant current - constant voltage charging algorithm. This work has been presented in [33].

Section 7 discusses the impact of pulse charging parameters on battery impedance parameters and life cycle. This section also examines the impact of pulse charging parameters on the LiPo batteries under test and compares it with LiPo batteries subjected to the benchmark constant current - constant voltage charging algorithm.

In section 8, a summary is given, contributions are highlighted, and other potential research areas in the area of battery charging are discussed.

2. ENERGY STORAGE DEVICES

Energy storage devices can be found in many stationary, motive, and portable applications. They provide numerous benefits depending on the application in which they are used. For stationary applications, which include data storage centers, utility grid storage, and energy harvesting, energy storage devices primarily serve as backup power sources. Motive applications include automobiles, marine transport, aviation, and unmanned underwater, aerial, and ground systems. The use of energy storage for portable applications include mobile phones, personal computers, smart watches, cameras, and many other consumer electronic devices. The ubiquitous use of energy storage devices in many of these applications signifies its importance in improving the quality of life of consumers and providing the convenience and security needed. The projected growth for the stationary energy storage, for example, is expected to top \$35 billion by 2030 [34].

Energy storage devices can be categorized as mechanical, chemical, electrochemical, electrical, or thermal [35], [36]. In this work, electrochemical energy storage devices, specifically batteries, and electrical energy storage devices, specifically supercapacitors, will be reviewed as they are the most popular energy storage devices used in stationary, motive, and portable electrical applications.

2.1 Electrical energy storage devices: Supercapacitors

Supercapacitors, also known as ultracapacitors, have relatively higher capacitances and energy densities when compared to conventional capacitors. Conventional capacitors have a dielectric material between two metal plates while supercapacitors have two metal plates, that are coated with an activated carbon-based material, immersed in an electrolyte [37], [38]. The two metal

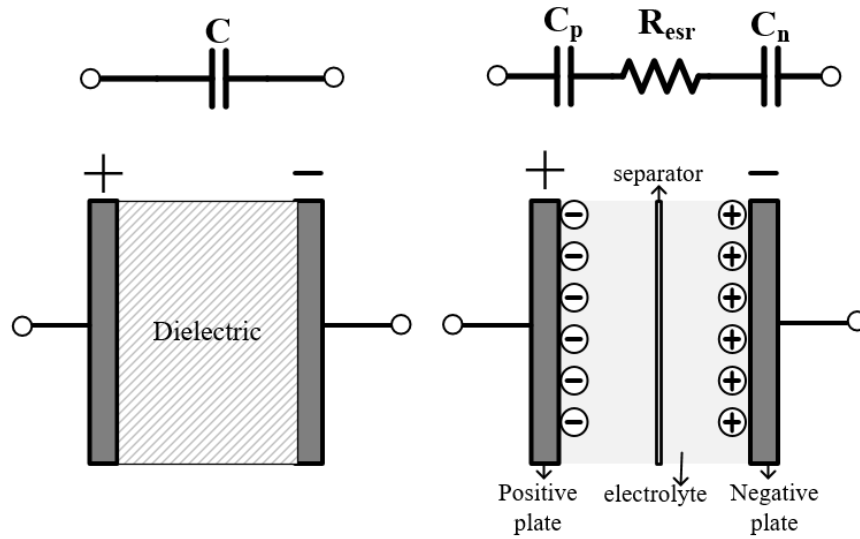


Figure 2: Conventional capacitor vs supercapacitor

plates are separated from each other by a film known as a separator. During charging, the supercapacitor accumulates ions on each metal plate. The ions accumulated on one plate is equal and opposite in polarity to the ions on the other plate, hence an electric field is form between these two plates. Each charged region of the electrode can be represented as a single conventional capacitor as shown in Fig. 2. Therefore, the supercapacitor can be modelled as two capacitors, C_p and C_n , in series with a resistor, R_{esr} , which represents the resistance of the electrolyte, separators, and other contact resistances. Fig. 2 compares the conventional capacitor with the supercapacitor.

Supercapacitors are found in numerous applications including consumer electronics, power tools, back-up energy storage, and hybrid vehicles [39]. They have the advantages of low cost, longer life cycle, faster charging capability, rugged operation, and higher power densities when compared to batteries. A Ragone plot, which is used to compare the performance of various energy storage

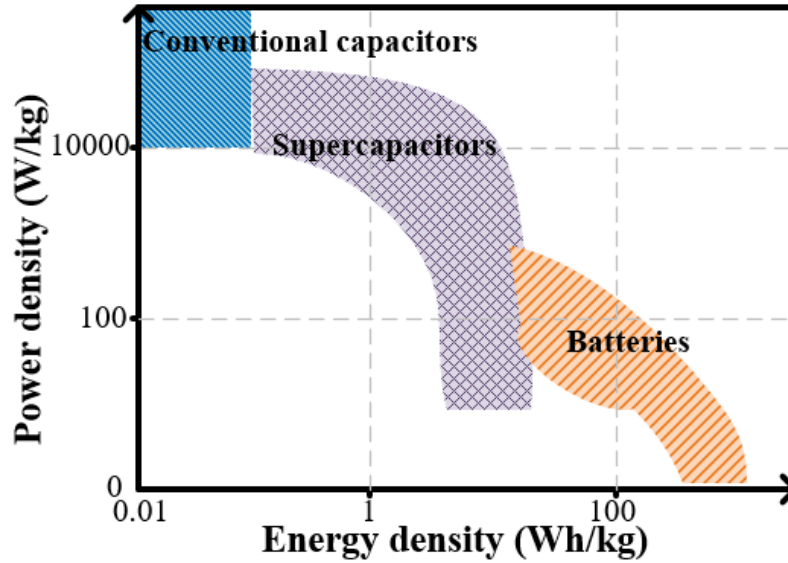


Figure 3: Ragone plot

devices, is shown in Fig. 3. This plot compares conventional capacitors, supercapacitors, and batteries in terms of their energy and power densities [40]-[42].

2.2 Electrochemical energy storage devices: Secondary batteries

Batteries can be categorized as primary or secondary. Primary batteries, such as alkaline and zinc carbon, are non-rechargeable and must be disposed of once their energy is depleted. Secondary batteries, unlike their primary counterparts, are rechargeable and their charge can be replenished once depleted. Therefore, the frequency of replacement is decreased. These types of batteries are needed to provide the flexibility of movement without the impediment and inconvenience of wires. They also serve as backup energy sources in the absence of connection to the electrical grid or insufficient environmental energy. Every secondary battery has a pair of electrodes immersed in an electrolyte. Depending on the construction and chemistry, there are several popular secondary

batteries on the market today: nickel chemistry based batteries, lead acid variations, and lithium-ion chemistry based batteries [43].

- **Nickel chemistry based batteries:** These batteries use nickel oxides for their positive electrodes [43], [44]. Depending on the chemical composition of the negative electrode, different types of nickel chemistry based batteries can be realized, e.g. nickel cadmium (NiCd), nickel metal hydride (NiMH), nickel zinc (NiZn), and nickel iron (NiFe). The use of these batteries is advantageous because of their ability to be deeply discharged without needing special recovery circuits, their simple charging circuits, and their use in rugged environments. However, they have high self-discharge rates, low energy densities, and the tendency to be susceptible to memory effect [44], where the battery loses its full capacity if it is constantly charged below its full capacity. They are usually used in digital cameras and MP3 players [45].
- **Lead acid batteries:** These batteries are found in many of today's automobiles [46] and also serve as storage for standby power applications [47], [48]. They use lead dioxide as the positive electrode and lead as the negative electrode, with sulfuric acid as the electrolyte [43], [46]. Apart from being low cost, lead acid are good for rugged applications and have a low self-discharge rate. However, due to their size and weight, they are limited in many portable applications. Different variations of lead acid, such as valve regulated lead acid and absorbed glass mat, have been developed to account for the potential spillage and electrolyte top off [46], [48], [49].
- **Lithium ion (li-ion) chemistry based batteries:** These batteries have the advantages of very low self-discharge rate, no memory effect, and most importantly, high energy density [43]. These properties make li-ion chemistry based batteries suitable for portable

applications and hence their ubiquitous use in many consumer electronics. Their positive and negative electrodes consist of a lithium-based oxide material and a carbon or graphite material, respectively [50]. Depending on the material used for the positive electrode, the battery capacity, voltage, density, cost, and life cycle will vary.

Fig. 4 shows the energy density comparison of the discussed secondary batteries and Table 1 summarizes the advantages and disadvantages of the various secondary batteries.

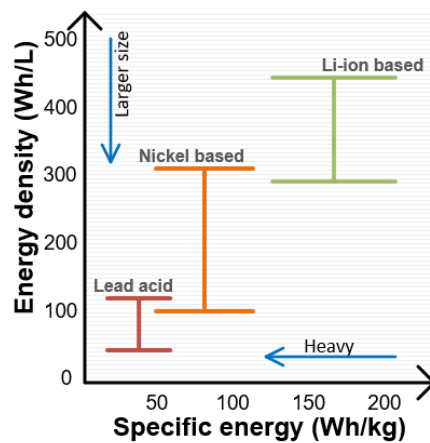


Figure 4: Energy density comparison of different batteries

2.2.1 Secondary batteries market

The secondary battery market is predicted to exceed \$111 billion by 2019 [1]. The consumer electronics market, driven by mobile phone, tablets, digital cameras, and personal computer applications, is expected to exceed \$43.7 billion by 2022 [51] and the transportation sector battery

Table 1: Advantages and disadvantages of different secondary batteries

Battery type	Advantages	Disadvantages
Nickel chemistry based	<ul style="list-style-type: none"> • Can be deeply discharge • Good for rugged applications 	<ul style="list-style-type: none"> • High self-discharge rate • Susceptible to memory effect
Lead acid based	<ul style="list-style-type: none"> • Inexpensive • Robust • Low self-discharge 	<ul style="list-style-type: none"> • Low energy density • Bulky size • Sizeable weight
Lithium-ion chemistry based	<ul style="list-style-type: none"> • High energy density • No memory effects • Low self-discharge rate 	<ul style="list-style-type: none"> • Expensive • Complex charging circuits

market is forecasted to exceed \$17.26 billion by 2021 [52]. When it comes to battery chemistries, lead acid chemistry based and li-ion chemistry batteries have the greatest market shares. The lead acid battery market share is mainly driven by the transportation sector, uninterruptible power supplies, and telecommunications while the li-ion chemistry based batteries are driven by consumer electronics. With the current trend of li-ion chemistry based batteries replacing lead acid batteries in the transportation sector, primarily electric and unmanned vehicles, li-ion chemistry

based batteries are predicted to overtake their lead acid counterparts by 2024 and become the largest of the battery market share [53].

Key industry players include Panasonic Corp, Exide, Johnson Controls, and EnerSys for the manufacturing of lead acid batteries and Panasonic Sanyo, BYD, LG Chem, and Samsung for li-ion chemistry based batteries [54]. As of 2018, Panasonic Sanyo had the largest, about 33%, of the li-ion battery manufactures market share while BYD has 18% [54].

Asia pacific and North America have the largest li-ion battery market share when it comes to regional battery market share [55]. In the Asia pacific region, China, India, and Japan have the greatest market shares, while in North America, United States, Canada, and Mexico have the largest shares.

With li-ion chemistry based batteries being the most popular batteries for portable electronic applications due to their properties of low self-discharge rate, high energy density, no memory effect, and low maintenance [2], [53], this work will focus on designing charging systems for li-ion batteries.

2.2.2 Recent development in secondary batteries

Even though li-ion batteries are a more matured technology and large-scale manufacturing processes have been established, they still have the limitations of safety at higher energy densities and their inability to keep up with demands of current electrical applications. These limitations have pushed researchers to look for alternative battery chemistries that will have much higher energy densities and are much safer.

One of the battery research developments is the use of graphene in batteries. This is seen to be very promising for the rechargeable battery market due to graphene being one of the strongest and thinnest materials [56], [57]. It is primarily used as a hybrid combination with other materials for the battery electrodes, which enables the batteries to be light-weight, have shorter charger times, and higher capacities [58]. Several graphene-based batteries have been reported in literature, including graphene lithium sulphur batteries [59] and graphene metal oxide composite electrodes [60]. Graphene based batteries are still under development and promises to have a much higher potential than li-ion batteries.

Metal-air batteries are another of such potential development. These kinds of batteries use the surrounding air as one of their electrodes [61]. Theoretically, they have much higher energy densities than li-ion batteries but there are serious disadvantages that need to be addressed before they become prevalent on the market. These disadvantages include the tendency of dendrite growth, instability in chemical reactions, and lower life cycle [61]-[63]. Lithium-air [62], [64], [65], zinc-air [64], [66], and aluminum-air [67], [68] are some examples of metal-air batteries. Renata Batteries currently have zinc-air batteries on the market today that are used for hearing aids [69].

Solid-state lithium ion batteries also offer higher energy densities and improved safety than li-ion batteries [70]. They also offer faster charging rates. However, they suffer from limited ionic conduction and are expensive to manufacture [71], [72]. They differ from their li-ion counterparts by using solid electrolytes and electrodes.

Other research developments in the area of rechargeable batteries include foam batteries [73], [74], nanowire batteries [75], [76], and liquid metal batteries [77].

Unfortunately, most of these new battery chemistries are still in their developmental stages and have not yet been widely adopted and till that happens, li-ion batteries will continue to rule the battery market.

2.2.3 Battery terms definition

This section will define some of the common battery terms that will be used in this work.

- **Battery capacity:** This is the electric charge available in the battery that can be transferred to a load at a certain discharge current and time. It is usually expressed as mAh.
- **State of Charge (SoC):** This is the ratio of the current battery capacity to the overall capacity of the battery. SoC is usually expressed as a percentage.
- **Depth of Discharge (DoD):** This is the extent to which a battery can be discharged and it is usually expressed as a percentage.
- **Life cycle:** This is the number of times a battery can be charged and discharged before its original capacity is reduced by 20%.
- **Energy density:** This is the battery energy capability per unit volume expressed as Wh/L.
- **C-rate (C):** This is the rate of charge or discharge of the battery based on the capacity, e.g. if a battery is rated at 100 mAh and discharged at 50 mA constant current, then the discharge rate is 0.5C.
- **Battery energy efficiency (η_{BE}):** This is defined as the ratio of the energy recovered from a battery to the energy needed for its recharge. It is mathematically expressed as

$$\eta_{BE} = \frac{\int_0^{t_d} V_d I_d dt}{\int_0^{t_c} V_c I_c dt} * 100 \quad (1)$$

where t_c and t_d are the charge and discharge times, respectively, I_d and I_c are the discharge and charge currents, respectively, and V_c and V_d are the average battery charge and discharge voltages, respectively.

- **Battery charge efficiency (η_{BC}):** This is defined as the ratio of the charge recovered from a battery under a defined load to the total charge consumed during its charging. η_{BC} is expressed as

$$\eta_{BC} = \frac{\int_0^{t_d} I_d dt}{\int_0^{t_c} I_c dt} * 100 \quad (2)$$

- **Polarization:** This is the effect that causes the battery voltage to deviate from its equilibrium value. It affects the performances of batteries. There are three types of polarization [78].

- *Ohmic polarization:* This represents the resistance of the electrolyte, interconnects, and other contacts of the battery. This is characterized as a current-resistance (IR) drop.
- *Concentration polarization:* This is as a result of the mass transport effects in the battery and it is characterized by the Nernst equation shown in (3) [78].

$$E = E^o - \frac{RT}{nF} \ln Q_c \quad (3)$$

where E is the cell potential in V , E^o is cell potential at standard state conditions in V , R is the ideal gas constant in $J/mol \cdot K$, T is temperature in K , n is number of moles of electrons, F is Faraday constant in C , and Q_c is reaction quotient.

- *Activation polarization*: This effect is due to the charge transfer reactions of the battery and can be characterized by the Tafel equation [79] shown in (4).

$$\eta_{activation} = S \log \frac{i}{i_o} \quad (4)$$

where i is the current density in A/m^2 , i_o is the exchange current density in A/m^2 , and S is the Tafel slope.

- **Overpotential**: This is the voltage drop that occurs in the battery due to polarization effects.
- **State of Health (SoH)**: This is the current state of the battery when compared to its unused or new state. It describes how the battery can perform as it ages.
- **Open circuit voltage (OCV)**: This is the voltage seen at the terminals of the battery under no load conditions.
- **Nominal voltage**: This is the voltage that refers to the midpoint of the charge-discharge cycle and normally quoted on datasheets by battery manufacturers.

2.3 Lithium-ion chemistry based batteries

A li-ion chemistry based battery typically has the negative electrode as carbon or graphite and a lithium based metal oxide as the positive electrode. In some special types of li-ion batteries, the negative electrode can be lithium titanate (Li_4TiO_{12}) [43]. Batteries using Li_4TiO_{12} as the negative electrode have higher power densities and charge rate capabilities and hence it is capable of fast charging with improved safety [80]. However, it suffers from lower cell voltage, limited life cycle, and low ion conductivity [43]. There are very few applications using these types of batteries. This work focuses on li-ion batteries with graphite/carbon based negative electrodes, hence section 2.3.1 describes popular chemistries used for the positive electrode.

2.3.1. Types of positive electrodes for li-ion chemistry based batteries

Depending on the chemistry of the electrode used for the positive electrode, the cell voltage, capacity, life cycle, power density, and safety characteristics of the li-ion battery will vary.

Examples of popular positive electrodes used are

- Lithium cobalt oxide (LiCoO_2)
- Lithium iron phosphate (LiFePO_4)
- Lithium manganese oxide (LiMn_2O_4)
- Lithium nickel manganese cobalt oxide (NMC)
- Lithium nickel cobalt aluminum oxide (NCA).

Table 2 summarizes the characteristics of these positive electrodes [43], [81]-[84]. The chemical structure of the positive electrodes matters because it determines the electrical conductivity and hence, the capacity of the battery.

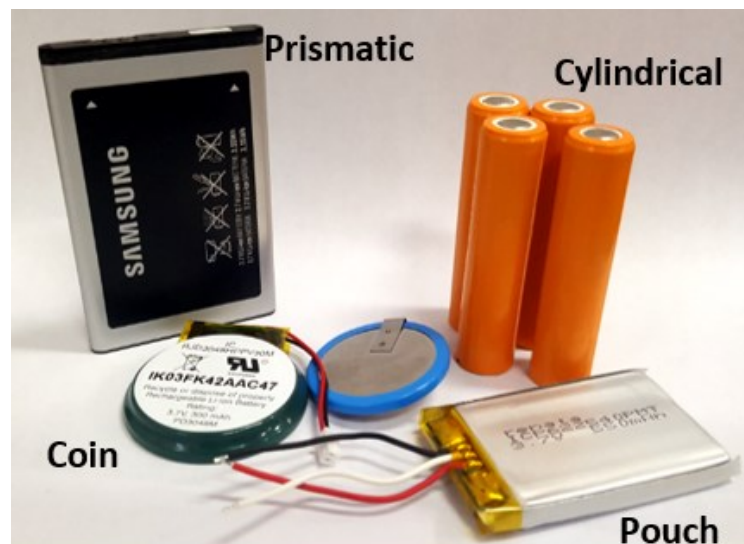


Figure 5: Different battery formats

Table 2: Comparison of different positive electrodes used in li-ion batteries

Battery Parameters	LiCoO₂	LiFePO₄	LiMn₂O₄	NMC	NCA
Life cycle	Fair	Good	Good	Good	Good
Power capability	Good	Good	Best	Good	Best
Battery voltage	4.2V	3.6V	4.2V	4.2V	4.0V
Safety	Fair	Best	Good	Fair	Fair
Cost	x	2x	3x	3x	2x
Energy density	High	Low	Highest	High	High
Chemical structure	Layered	Olivine	Spinel	Layered	Layered

2.3.2. Li-ion battery formats

Li-ion batteries can be characterized by their different formats depending on how they are manufactured [43], [85]. The different formats are

- Cylindrical
- Prismatic
- Coin or button

- Pouch

Fig. 5 shows the different formats of these batteries.

2.3.3. Li-ion polymer (LiPo) battery

These batteries are similar to their li-ion counterparts and use the same electrodes, but the difference lies in the electrolyte. In the regular li-ion batteries, they make use of liquid electrolytes. These electrolytes are based on lithium salt organic solvents, e.g. lithium hexafluorophosphate. Li-ion polymer batteries use a high conductivity polymeric semisolid to support the electrolyte and improve ion movement compared to li-ion batteries which use liquid electrolyte [43], [86]-[89]. There are three types of li-ion polymer batteries, i.e. dry solid state polymer, gel-like polymer, and different polymer composites [90]. The polymeric semisolid allows the battery to be formed in different form factors with the additional advantages of improved safety and good mechanical strength. LiPo batteries are therefore used in many portable electronic devices because of these favorable characteristics and usually packaged in the pouch format.

2.4 Mechanism of LiPo battery operation during the charge and discharge processes

A typical LiPo battery has a lithium metal oxide positive electrode (cathode), graphite negative electrode (anode), and a gel-like polymer electrolyte. Both electrodes are separated from each other by a microporous film. In the gel-like polymer battery, the polymer also acts as a separator [43], [91]. During the first charge cycle, a solid electrolyte interface (SEI) is formed on the surface of the electrode. This permeable membrane passivates the electrode, protecting the electrode from the electrolyte but allowing the ions to pass through it [92].

Fig. 6 shows a typical LiPo battery undergoing the charge and discharge process. During charging, the lithium ions (Li^+) are dislodged from the cathode (chemical oxidation), travel through the

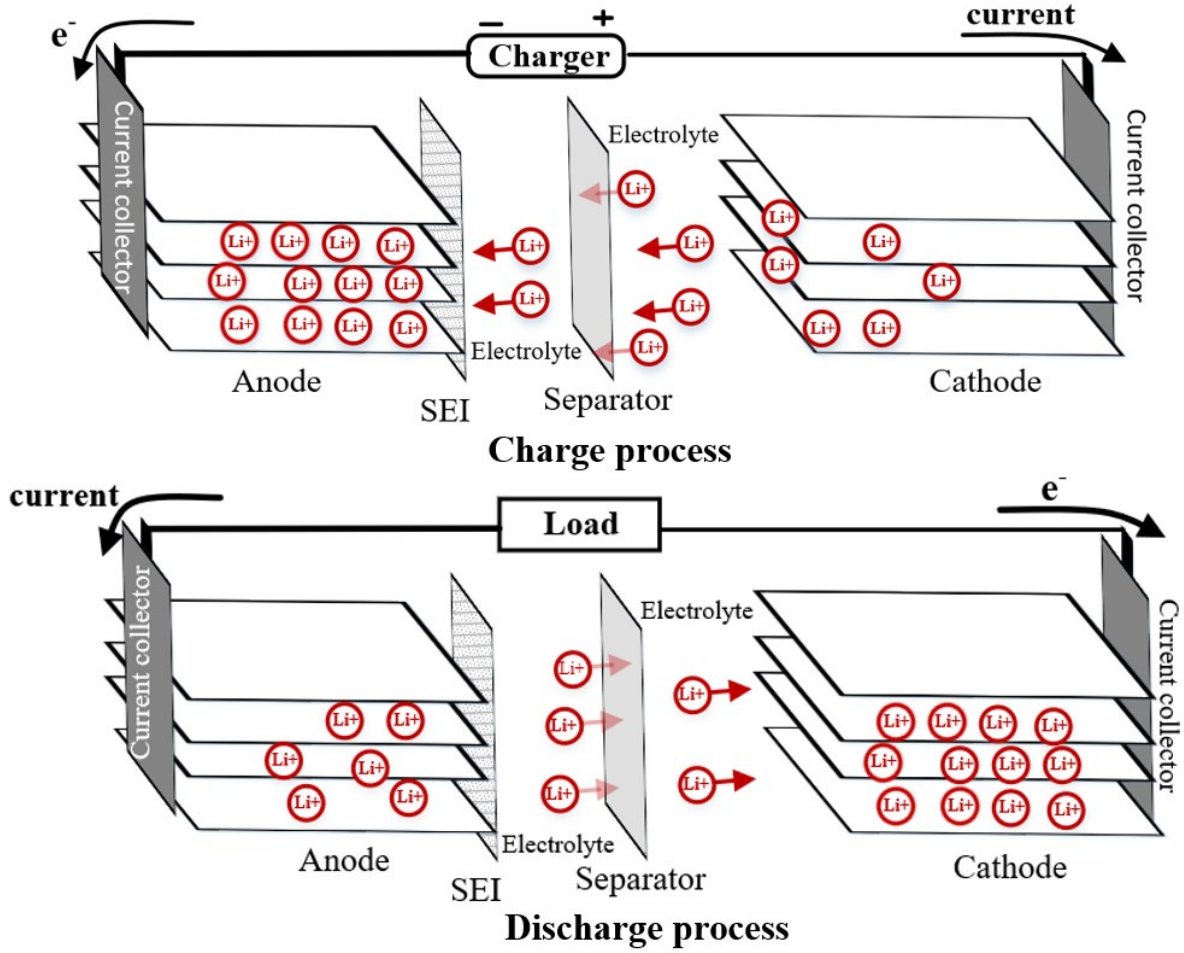
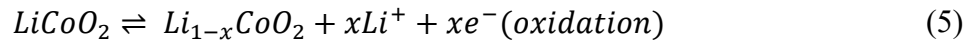


Figure 6: Charge and discharge processes in a battery

electrolyte and insert themselves or intercalate into the negative electrode (chemical reduction) [93]. This process is known as intercalation. The chemical oxidation and reduction (redox) equations [94] for a li-ion battery using a LiCoO_2 are shown below:



2.5 Li-ion battery models

From Fig. 6, the battery can be characterized in many ways due its inherent properties. These can be categorized as kinetic effects, diffusion effects, and double layer effects [78], [93]. Kinetic effects are due to the limitations of the charge transfer reactions in the battery. This is normally characterized as a charge transfer resistance (R_{ct}). Diffusion effects refer to the movement of ions by migration or diffusion. It can result in a concentration gradient or an electric field [93], [95]. This is characterized by an impedance known as the ‘Warburg element’, Z_w [96]. This impedance is expressed as

$$Z_w = \frac{\theta}{\sqrt{\omega}} - j \frac{\theta}{\sqrt{\omega}} \quad (8)$$

where θ is the Warburg coefficient in Ω/\sqrt{s} and ω is the frequency in rad/s . Double layer effects are caused by the charge buildup at the interface between the electrode and the electrolyte. These are characterized by a capacitor, C_{dl} , or a constant phase element, Q_{dl} [97], [98]. Q_{dl} is sometimes used because the charged area does not behave like an ideal capacitor and its impedance can be expressed as

$$Q_{dl} = \frac{1}{C(j\omega)^\alpha} = \frac{1}{C\omega^\alpha} \left(\cos \frac{\alpha\pi}{2} - j \sin \frac{\alpha\pi}{2} \right) \quad (9)$$

where C is capacitance and α is an empirical constant usually less than one [98]. The interconnects, current collectors, contacts, and electrolyte can be represented by a resistance, R_s .

Several models have been proposed for li-ion batteries [99]-[102], some of which are discussed below.

- **I-R model:** This is a very simple model where R_s represents the internal resistance of the battery. The battery terminal voltage, V_{batt} , will be higher during charging and lower

during discharge according to (10). The battery current, I_{batt} , is positive during charge and negative during discharge.

$$V_{batt} = V_{oc} \pm I_{batt} \quad (10)$$

where V_{oc} is the open circuit voltage. V_{oc} is dependent on SoC, SoH, and temperature.

- **1st order RC model:** This model includes the charge transfer resistance and the double layer effects capacitor.
- **Randles equivalent circuit:** This model was proposed by J.E.B. Randles [103] to model the electrodes and electrolyte. It incorporates the ohmic resistance, double layer effects, and the charge transfer resistance.
- **Modified Randles equivalent:** This model incorporates the Warburg impedance element.
- **Two-time constant model:** This model uses two parallel RC circuits to represent the kinetic effects, R_K , and the diffusion effects, R_D .

These models are shown in Fig. 7. An inductance, L , can be added to any of these models to take the geometry and wiring of the battery into account [95]. An example is shown in Fig. 8.

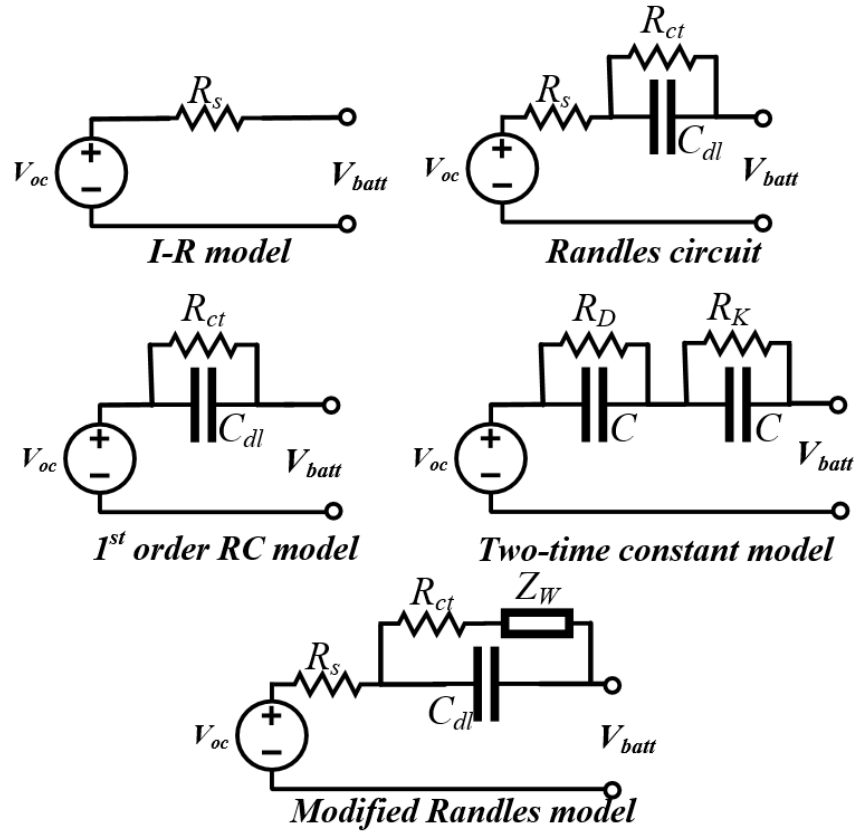


Figure 7: Different li-ion battery models

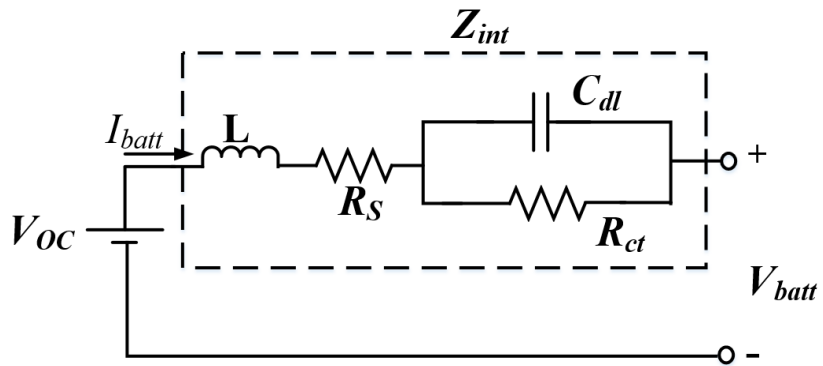


Figure 8: Li-ion battery model incorporating inductance

For the Randles equivalent circuit incorporating the inductance as shown in Fig. 8, the battery impedance, Z_{int} , can be expressed as

$$|Z_{int}(\omega)|^2 = \left(R_s + \frac{R_{ct}}{1 + C_{dl}^2 R_{ct}^2 \omega^2}\right)^2 + \left(\omega L - \frac{C_{dl} R_{ct}^2 \omega}{1 + C_{dl}^2 R_{ct}^2 \omega^2}\right)^2. \quad (11)$$

In the case, where C_{dl} is replaced with Q_{dl} as shown in Fig. 9, the battery impedance can be expressed as

$$Z_{int} = R_s + \frac{R_{ct}(1 + \tau\omega^\alpha X)}{1 + 2\tau\omega^\alpha X + (\tau\omega^\alpha)^2} + j\left(\omega L - \frac{R_{ct}(\tau\omega^\alpha Y)}{1 + 2\tau\omega^\alpha X + (\tau\omega^\alpha)^2}\right) \quad (12)$$

where $\tau = R_{ct}Q_{dl}$, $X = \cos \frac{\alpha\pi}{2}$, and $Y = \sin \frac{\alpha\pi}{2}$.

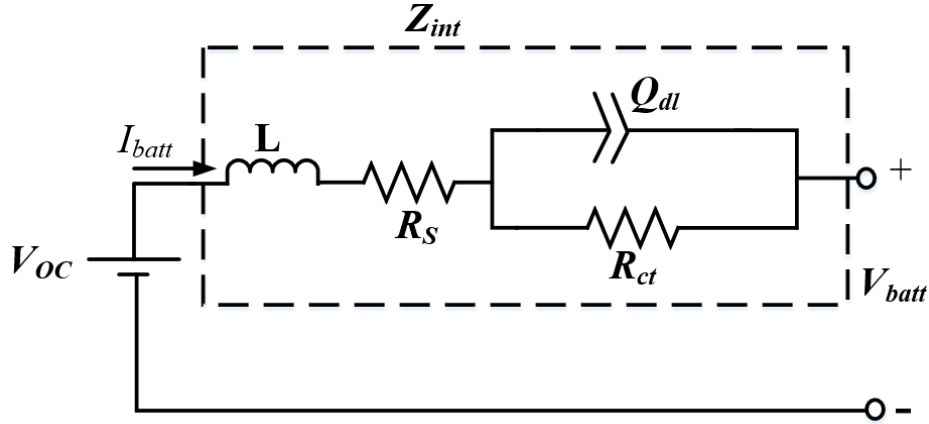


Figure 9: Li-ion battery model with constant phase element

The parameters of these models are dependent on SoC, SoH, and temperature. Their values are obtained by performing an electrochemical impedance spectroscopy (EIS).

2.6 Electrochemical impedance spectroscopy (EIS)

EIS can be used to analyze the characteristics of the battery and obtain the battery impedance parameters [104]. It is performed by perturbing the battery with a small ac signal over a wide range of frequencies. If the ac signal is a voltage, $V(t)$, then the impedance, $Z(t)$, can be found by the expression

$$Z(t) = \frac{V(t)}{I(t)} \quad (13)$$

where $I(t)$ is the measured current. For a perturbation signal, $v(t) = V_o \cos \omega t$, the resulting current will be $i(t) = I_o \cos(\omega t - \varphi)$, and hence $Z(t)$ can be found using (13),

$$Z(t) = \frac{V_o \cos \omega t}{I_o \cos(\omega t - \varphi)} = Z_o (\cos \varphi + j \sin \varphi) \quad (14)$$

where V_o , I_o , and Z_o are the dc values. A Nyquist plot or a Bode plot can be generated from the above analyses. From these plots, the battery parameter values can be obtained by fitting one of the battery models that best represents the measured data. A typical Nyquist plot showing how to obtain the various battery parameters is shown in Fig. 10.

An example of a typical Bode magnitude and phase plot is shown in Fig. 11. Fig. 12 shows the Nyquist plots for the various models discussed in Fig. 7 to Fig. 9.

When the C_{dl} is replaced with Q_{dl} , the Nyquist plot no longer consists of a perfect semi-circle but a depressed semi-circle as shown in Fig. 12.

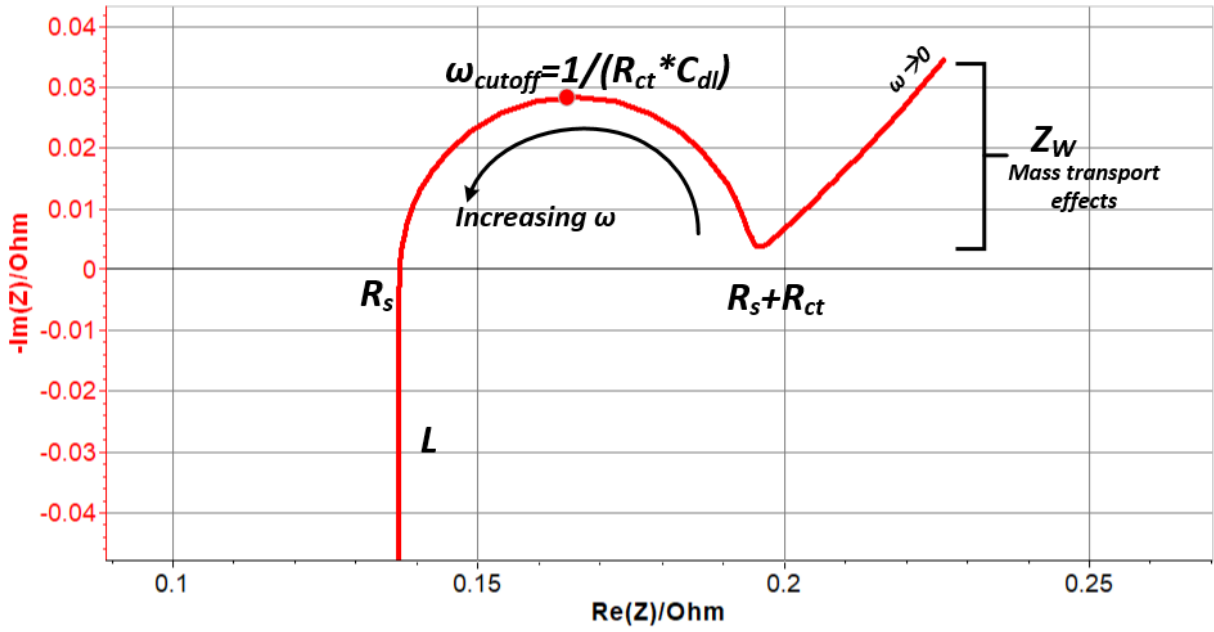


Figure 10: Typical Nyquist plot of a li-ion battery

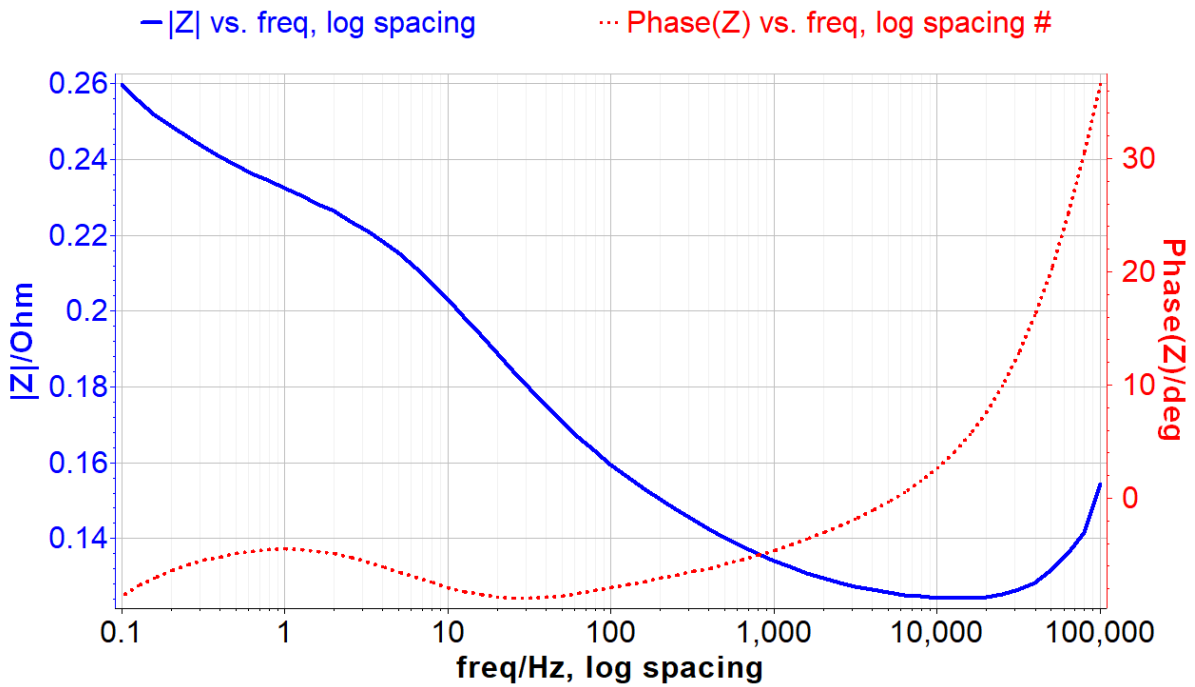


Figure 11: Typical Bode magnitude and phase plot of li-ion battery

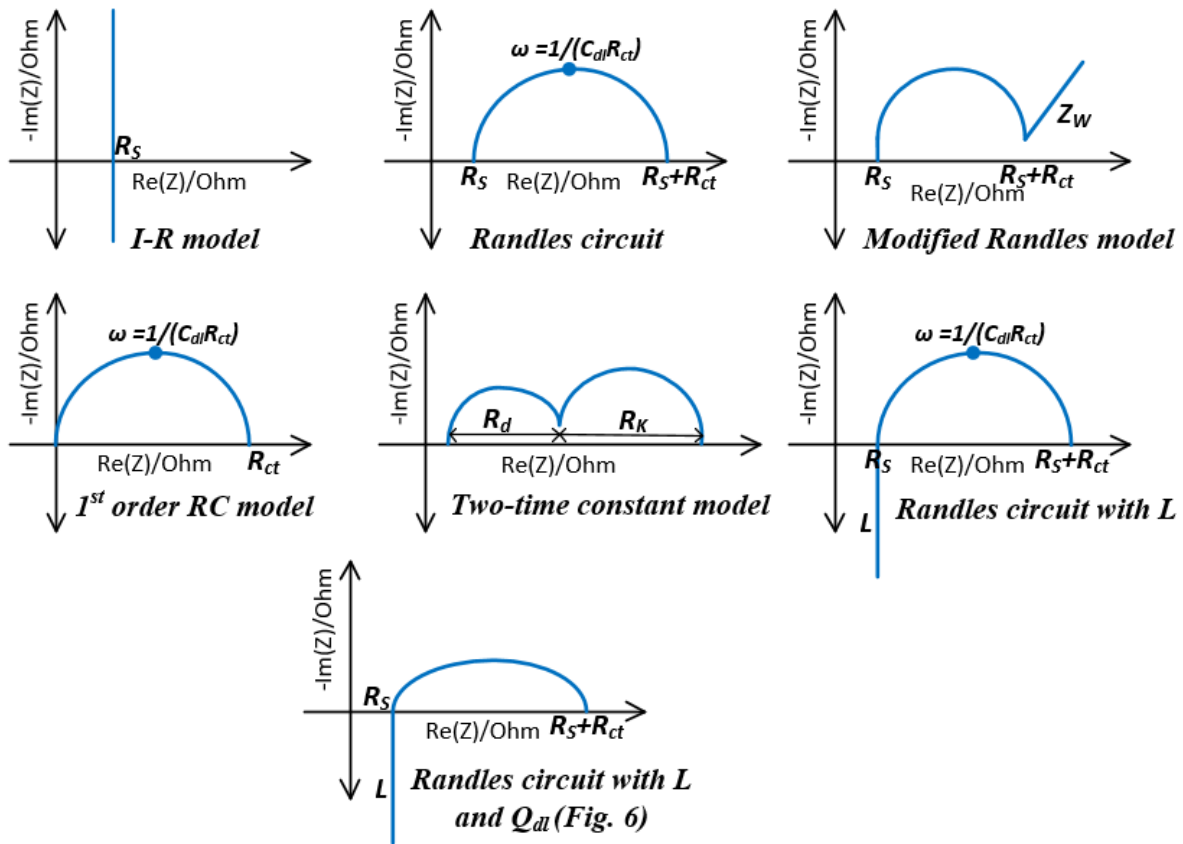


Figure 12: Nyquist plots of discussed li-ion battery models

Fig. 13 shows the fitting of different models to a measured EIS battery impedance data. Depending on the model used, the accuracy of the fitting will differ.

The fitting of different li-ion battery models to a measured EIS data to obtain battery parameter values is achieved by using curve fitting algorithms, such as Levenberg-Marquardt, least squares method, trust region [102], and Simplex algorithms[105]. These algorithms operate using the same basic approach: start with an initial guess and iterate until error is minimized. These algorithms have been embedded in EIS analysis software such as ZView[®] [106] and EC-Lab[®] [107]. Fig. 14

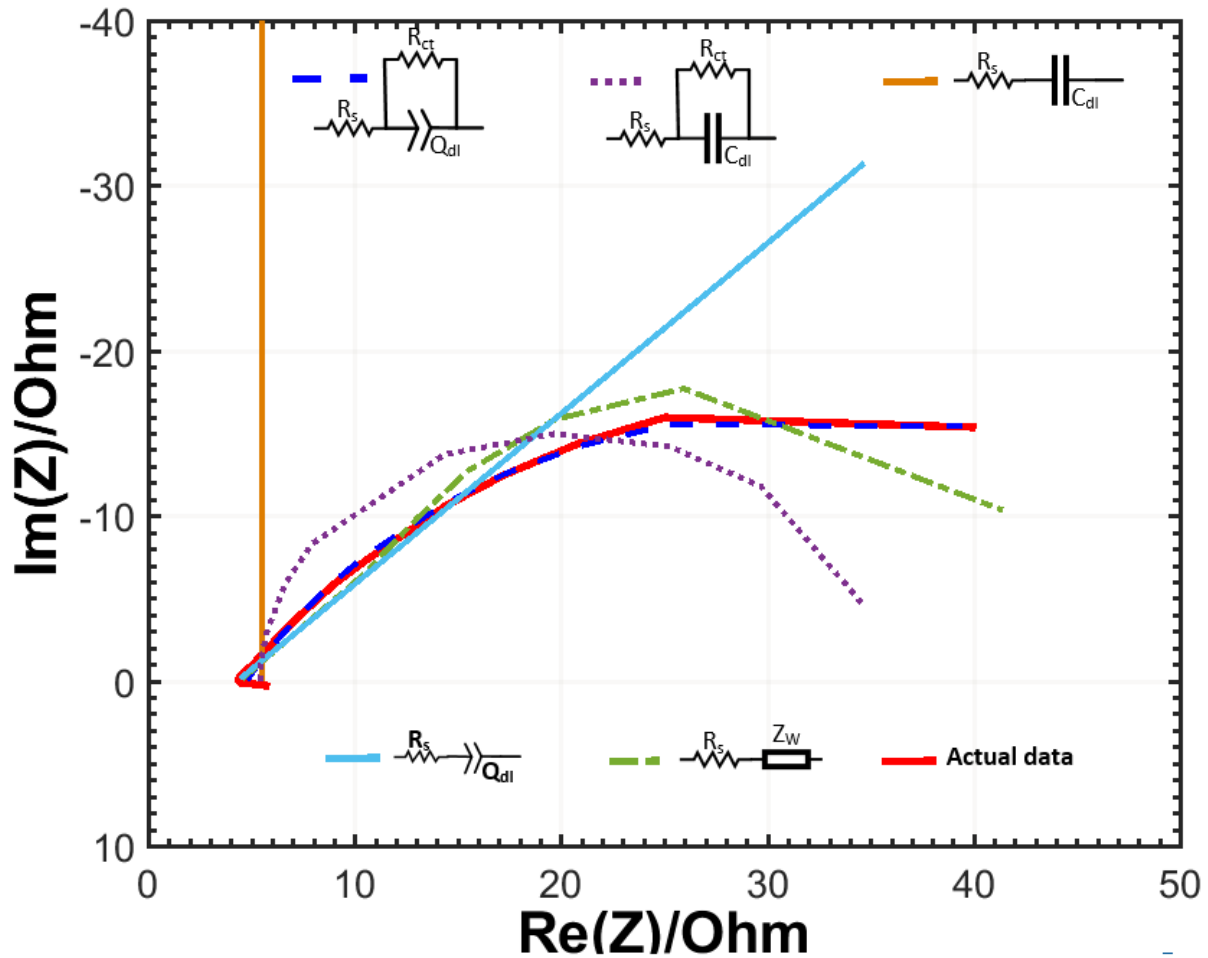


Figure 13: Fitting of different li-ion battery models to measured EIS data using Nyquist

shows the curve fitting of modified Randles equivalent circuit using Levenberg-Marquardt curve fitting algorithm to extract parameter values. The values are shown in Table 3.

Understanding the fundamentals of internal battery chemical reactions and battery modelling is paramount to designing battery charging systems that improve charge and energy efficiencies while reducing charge time. By taking the diffusion and kinetic processes in the battery into

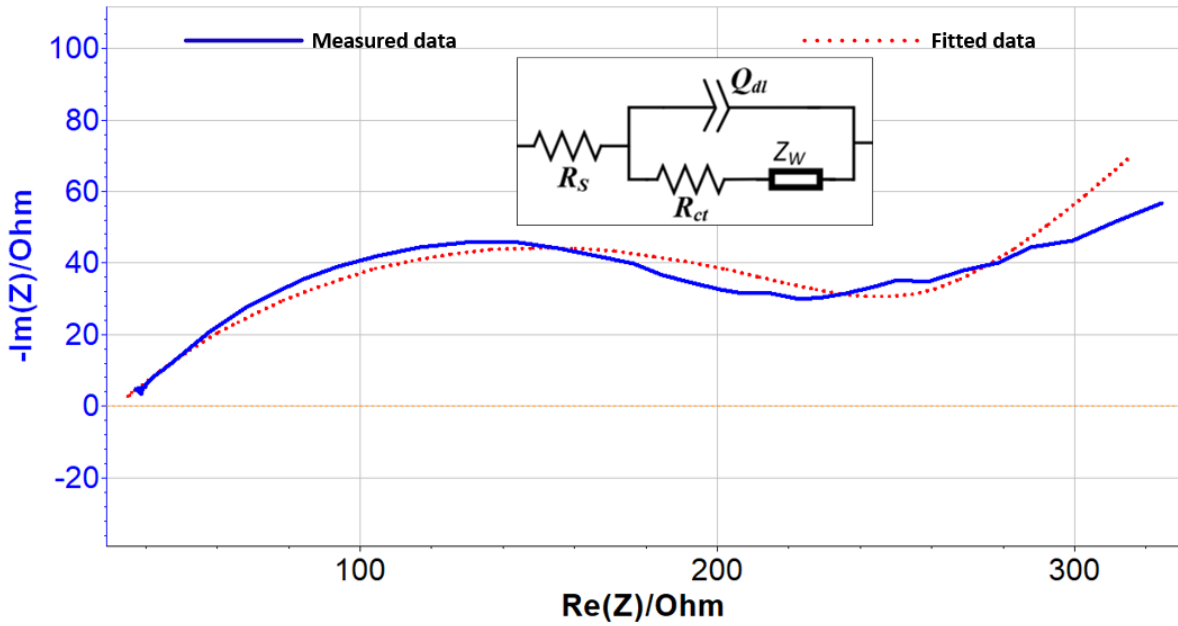


Figure 14: Fitting a modified Randles equivalent circuit to measured li-ion battery data

Table 3: Extracted battery parameter values from fitted curve using Levenberg-Marquardt

R_s	Q_{dl}	α	R_{ct}	Z_w
31.76 Ω	0.183 $mFs^{\alpha-1}$	0.4604	230.2 Ω	52.64 $\Omega s^{-\frac{1}{2}}$

account during the battery charger design process, the appropriate charge voltage and current across the entire battery charging profile can be carefully selected. Battery chargers are therefore important systems that can increase battery life cycle, improve battery safety, and increase battery charge or energy efficiencies. The inappropriate design of a battery charger can have detrimental effects on the battery, device, and user.

3. BATTERY CHARGERS

The battery charger market is projected to exceed \$18.8 billion by 2022 [108]. This is driven by the portable electronics, automotive, and telecommunication industries. Battery chargers are needed to replenish the charge in a depleted battery. Depending on the battery, the charging algorithm might be different. Battery chargers perform critical functions, such as extracting power from the available power source, conditioning that power, using the power to replenish the battery in a safe and optimized way, and terminating the charging process to prevent overvoltage and other potential safety issues. A battery life cycle or health depends on the type of charger used. Charging incorrectly can lead to overvoltage, overcharging, overheating, increased polarization effects, and dendrite formation [109]. Lithium deposits on the surface of the electrodes result in dendrite formation [110]. The continuous growth of dendrites can result in the penetration of the separator, leading to a short circuit in the battery. This internal short circuit can cause a thermal runaway which can potentially lead to a fire or explosion [111]. Overcharging of a li-ion battery can lead to battery failure and overheating [112]. From Table 2, different types of li-ion batteries have different upper or cut-off voltages. Exceeding this recommended voltage leads to an overvoltage condition that tends to reduce the life cycle of the battery [113]. It is therefore necessary to select the right charging algorithm to prevent these undesirable conditions and also ensure safety.

3.1 Battery charging algorithms

There are several battery charging algorithms [114]-[118], some of which are discussed below.

- **Trickle charge:** This is when a small charge current is used to charge the battery, usually below a charge rate of $C/10$ [119]. This can either be for ‘top up’ purposes or for when the battery is deeply discharged. The application of a high charge current to a deeply

discharged li-ion battery can result in damage to the battery. This charging algorithm results in very long charge times due to the small charge currents used.

- **Constant voltage (CV):** This is when a constant voltage is applied to the battery during the charge process. This simple charging technique is good for lead acid batteries [120] and because of its simple design, constant voltage chargers are relatively cheap.
- **Constant current (CC):** This involves the application of a constant charge current to the battery. This is achieved by varying the applied charging voltage to maintain the specified charge current. Nickel chemistry based batteries use this charging technique [116].
- **Pulse charging:** This is the application of carefully controlled charge current pulses to the battery during the charging process.
- **Burp charging:** This is similar to the pulse charging algorithm, but a discharge pulse is applied during the rest periods of the pulses.
- **Constant voltage-constant current (CC-CV):** This charging technique involves applying a constant current at the beginning of charging and a constant voltage towards the end of charging.

Fig. 15 shows the macro models of the discussed charging algorithms. The CC-CV and pulse charging algorithms will be discussed in the upcoming sections.

3.2 Li-ion battery charging algorithms

One of the disadvantages of the li-ion battery is the complexity of its charging system and the protection circuits needed to ensure safe charging. Therefore, care must be taken when choosing a charging algorithm for the li-ion battery. Many charging algorithms have been proposed for li-ion batteries. These include fuzzy logic based algorithms [121]-[124], multi-stage constant current

charging algorithms [125], [126], and optimization algorithms [127]-[129]. The charging algorithm used in most commercial li-ion battery chargers and also considered as the benchmark charging algorithm is the CC-CV algorithm [130]. The CC-CV charging algorithm will be described in the following section.

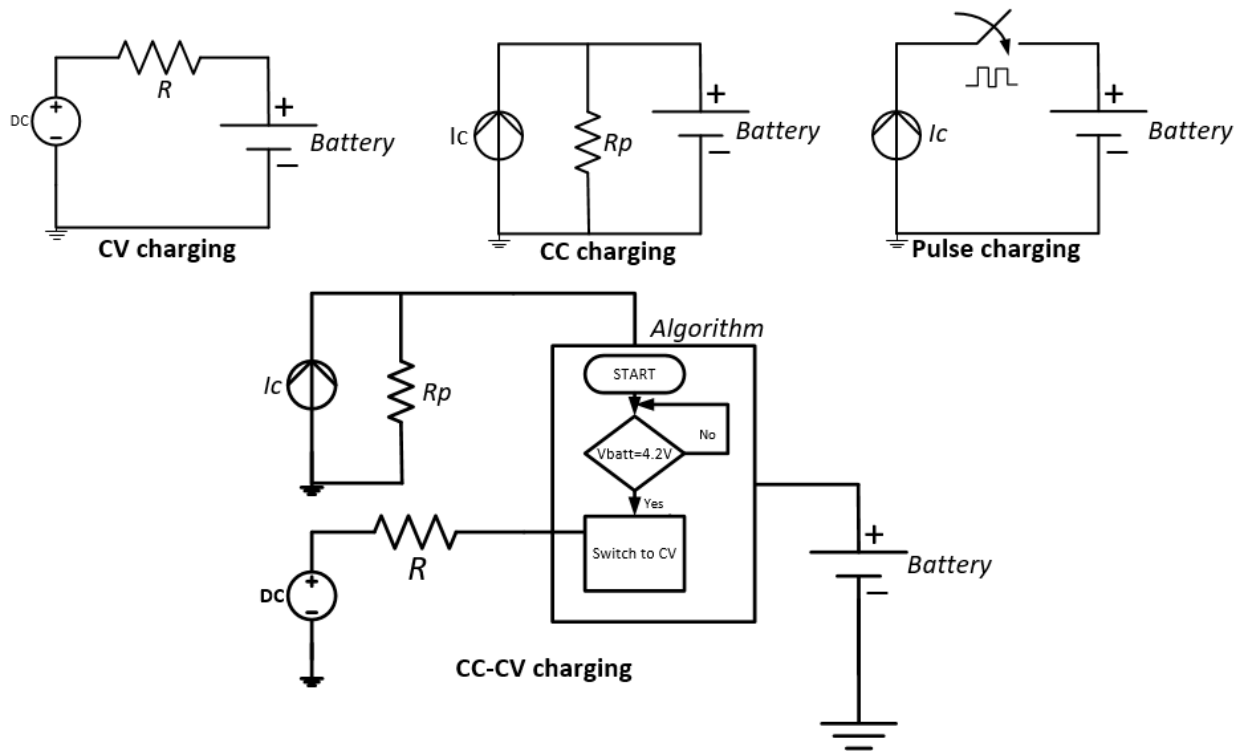


Figure 15: Macro model representation of different charging algorithms

3.2.1 Constant current - constant voltage charging algorithm

The CC-CV charging algorithm is the benchmark charging technique for li-ion batteries. It is used in most of today's li-ion battery chargers. The CC-CV charging algorithm consists of three charging phases shown in Fig. 16.

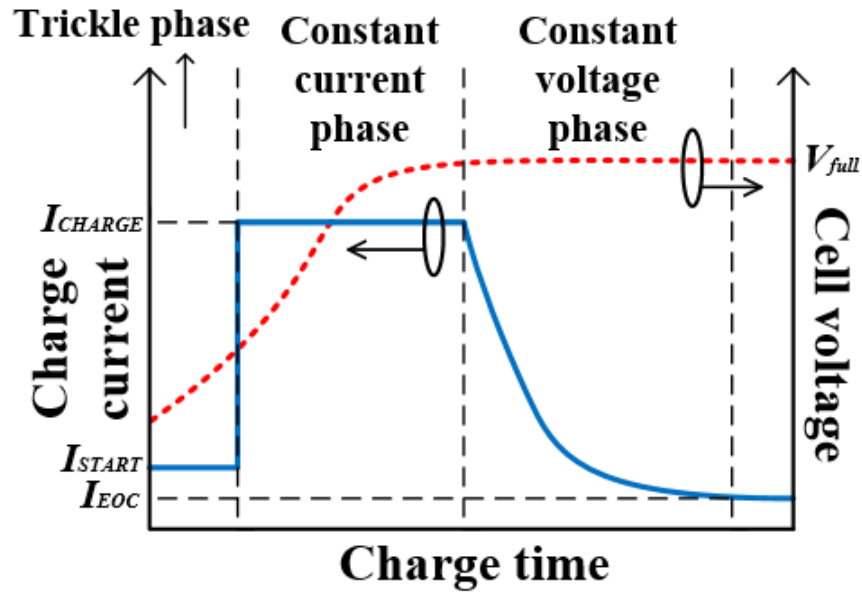


Figure 16: CC-CV charging algorithm

- **Trickle charge phase:** In this phase, a very small charge current (I_{START}) is used to precondition a deeply discharged li-ion battery. Usually, a charge current less than 0.1C is used in this phase.
- **Constant current charge phase:** Once the trickle charge phase ends or if preconditioning of the li-ion battery is not needed, the constant current charge phase is initiated. A constant charge current (I_{CHARGE}) is used to charge the battery. This charge current can range from 0.5C to 3.2C depending on the application and safety boundaries [131], [132].

The battery charges very fast in this region due to the high charge current. It approaches its full voltage (V_{full}) very quickly. During this phase, the Li^+ can easily intercalate in the negative electrode.

- **Constant voltage charge phase:** In the later stages of charging, once the battery voltage is approaching V_{full} , the charging phase switches to the constant voltage phase. In this phase, a constant voltage is applied and charging current is decreased. This decreasing charge current is needed to prevent overcharging and overvoltage conditions as the Li^+ find difficulty intercalating in the negative electrode towards the end of charging. With a decreasing charge current, the Li^+ can find time to intercalate and ensure that damage to the battery is averted. Charging is terminated when the charge current reaches I_{EOC} . Even though this decreasing charge current is needed because of the battery properties, i.e. limited diffusion of Li^+ at this stage of charging, it results in an extended charge time.

3.2.2 CC-CV based li-ion battery chargers

The CC-CV charging algorithm is usually implemented using switching converters [133]-[135] and linear regulators [133], [136]-[138], therefore, battery chargers can be categorized as switch mode chargers or linear chargers, respectively. Both types of chargers incorporate complex circuitry (indicated as battery management system (BMS) in Fig. 17) to obtain the CC-CV charging algorithm and ensure safety during charging.

3.2.2.1 Linear chargers

Linear chargers are usually implemented with low drop out (LDO) regulators. LDO regulators are typically composed of a pass transistor T_p and a feedback loop consisting of an operational amplifier and two feedback resistors, R_1 and R_2 . A linear charger is therefore a LDO regulator that has additionally circuitry to achieve the CC-CV charging algorithm. A typical linear charger is shown in Fig. 17. In order to achieve the CC-CV charging algorithm and also ensure safe charging, several control loops are needed. Control loops monitor the battery voltage V_{batt} and the charge

current I_{charge} to ensure that the right charge algorithm is achieved and V_{batt} and I_{charge} are within the set specifications. In order to handle multiple input sources, control loops are also needed to monitor the input voltage V_{IN} and input current I_{IN} . Die temperature monitoring is needed to prevent the linear charger IC from overheating. At high charge currents, the die temperature rises quickly, and therefore to prevent damage to the IC, the die temperature control can safely reduce the charge current to prevent any further heating and ensure the IC is operating within the safe operating temperature region.

Different variations of linear chargers have been proposed in literature. Some focus on the transition point between the CC and CV loops. This is important because transitioning early from CC to CV will prolong charge time and transitioning late can result in overcharging conditions. To ensure that the transition occurs at the optimal point, some works have proposed compensating for the internal resistance of the battery [139]-[142], which causes the battery charging voltage to be higher than the ideal battery voltage (Fig. 7). Others have also proposed using smooth transition circuits [143]-[145]. To improve the efficiency of the charging process, some works in literature have proposed using adaptive voltage and current sources [146]-[148]. There are also many commercial linear chargers on the market, from companies such as Maxim Integrated, Texas Instruments, Analog Devices, and Richtek Technology, that can be used for various applications.

3.2.2.2 Switch-mode chargers

Switch-mode chargers can be implemented with either buck, boost, or buck-boost converters. Fig. 17 shows a generalized implementation of a buck converter with multiple control loops for safe charging and attaining the CC-CV charging algorithm. Similar to the linear charger, these multiple control loops are needed to ensure V_{batt} , I_{charge} , V_{IN} , I_{IN} , and die temperature are within the

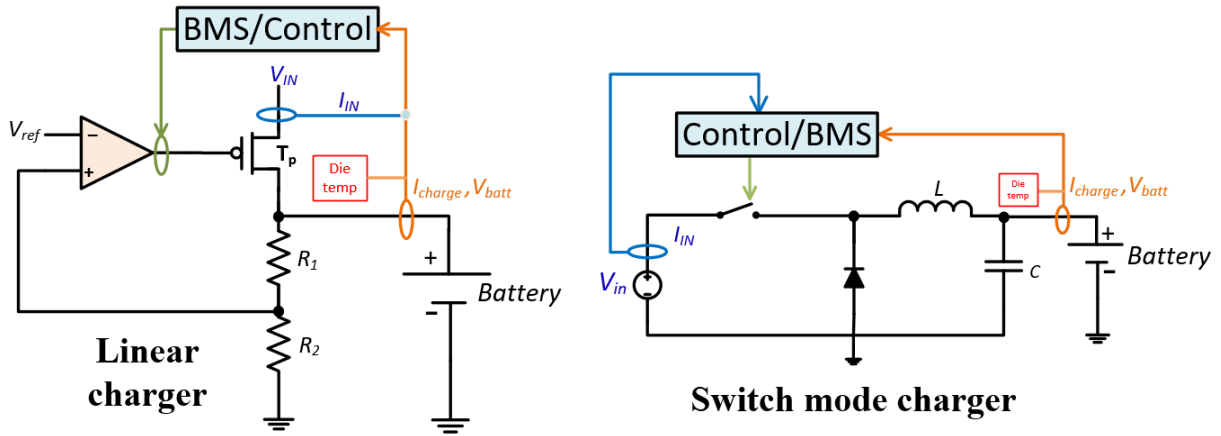


Figure 17: Linear and switch mode CC-CV li-ion battery charger

prescribed specifications. Buck converter based chargers are usually used in applications where the input voltage will never exceed the output voltage, e.g. mobile phone applications. Boost converter based chargers are used in applications like energy harvesting where the input voltage is not enough to power the electrical load, while buck-boost converter based chargers can be used in either scenario. There are other types of switch-mode chargers that have been presented in literature. These include resonant converter based chargers [149]-[151], full-bridge converter charger [152], and flyback converter chargers [153], [154]. These chargers all implement the CC-CV charging algorithm.

Similar to the linear chargers, previous work in literature seek ways to ensure a smooth transition between the CC and CV regions [155], [156]. Others target specific applications, and high efficiency and minimum power consumption metrics [153], [157]-[161]. Commercial switch-mode chargers are also available on the market from companies such as Richtek Technology, Texas Instruments, Maxim Integrated, and STMicroelectronics.

Table 4 summarizes the advantages and disadvantages of these two different chargers.

Table 4: Advantages and disadvantages of switch mode and linear chargers

Charger type	Advantages	Disadvantages
Linear	<ul style="list-style-type: none"> • Less complexity 	<ul style="list-style-type: none"> • Higher power consumption
Switch mode	<ul style="list-style-type: none"> • Minimal power consumption • High efficiency 	<ul style="list-style-type: none"> • Complex • Consumes large board area

Both linear and switch-mode battery charger require complex circuitry to implement the CC-CV charging algorithm. In all, li-ion battery chargers must be able to provide safe charging without compromising charge time, prevent deterioration of the battery, increase battery charge and energy efficiencies, and terminate charging when needed. The main drawback of the CC-CV charging algorithm, in addition to the complex circuitry, is the extended charge time due to the constant voltage charge phase. In order to reduce charge time without compromising the safety of the battery and the user, while increasing the battery energy and charge efficiencies, and at the same time use simple circuitry, the pulse charging algorithm is used in this work and will be elaborated on in the next section

4. PULSE CHARGING¹

Pulse charging is the application of carefully controlled charge current pulses to charge a battery. It is another technique to achieve fast charging and better battery charge efficiency without increased cost and complicated charge algorithms. The art of pulse charging can be traced back to the 1900s, when David H. Wilson proposed a method to reduce the time needed to store energy in a battery [162]. Pulse charging has slowly caught the attention of OEMs, with a few products on the market today. It had been used for primarily lead acid batteries [163], [164], where it was also used to eliminate sulfation [165]. Recently, pulse charging has been applied to li-ion batteries [166]-[171]. These pulse charge current pulses have the following parameters: frequency, duty cycle, and amplitude, which must be carefully chosen to ensure safe and fast charging with improved charge and energy efficiencies.

4.1 Basics and benefits of pulse charging

The use of current pulses to charge a li-ion battery is effective to increase battery charge and energy efficiencies and also decrease charge time. During charging, if the rate at which the Li^+ are electrochemically reduced at the graphite electrode is higher than the rate at which Li^+ are intercalated into the graphite (in the case of a high charge rate or approaching the end of charge), then, a buildup will occur at the graphite-electrode interface, increasing concentration polarization [33], [172] and the potential for dendritic growth. Due to decreasing concentration and, hence, limited diffusion of Li^+ during the later stage of charging, the constant voltage phase of a CC-CV

¹ Part of this section is reprinted with permission from "An Efficient and Fast Li-Ion Battery Charging System Using Energy Harvesting or Conventional Sources," J. M. Amanor-Boadu, M. A. Abouzied and E. Sánchez-Sinencio. IEEE Transactions on Industrial Electronics, vol. 65, no. 9, pp. 7383-7394. Copyright [2018] by IEEE.

charge technique uses decreasing charge current, thereby increasing charge time. However, this problem of prolonged charge time is avoided in pulse charging due to the relaxation periods in between pulses. This eliminates concentration polarization [171], which interferes with ion movement, and ensures equilibrium between the electrodes, i.e. charge reactions are able to stabilize. In that regard, the next charge pulse is efficiently absorbed, thereby increasing power rate transfer, and hence decreasing charge time [33]. It also allows for the battery to be charged at high charge rates, since the relaxation periods in between the pulses allow time for the ions to intercalate in the electrode. Pulse charging is also an effective method for increasing the life cycle of a battery [173], i.e., incomplete chemical reactions which increase the internal impedance of the battery are eliminated [171], thereby improving battery health. The pulse charging algorithm is therefore, a good charging technique for safe, fast, and efficient battery charging.

Every pulse charge current has the following characteristics:

- **Duty cycle, D** : This refers to the width of the charge current pulses, t_{on} as a function of the period, T_p , where $T_p = t_{on} + t_{off}$, with t_{off} being the rest periods.

$$D = \frac{t_{on}}{T_p} \quad (16)$$

- **Frequency, f** : This can be described as the inverse of T_p . Therefore, $f = \frac{1}{T_p}$.
- **Amplitude, I_{pk}** : This is the peak value of the current pulses. It can be derived as a function of duty cycle and average charge current, I_{avg} .

$$I_{avg} = I_{pk} \cdot D \quad (17)$$

Fig. 18 shows the characteristics of these pulses. In this work, unipolar pulses will be used.

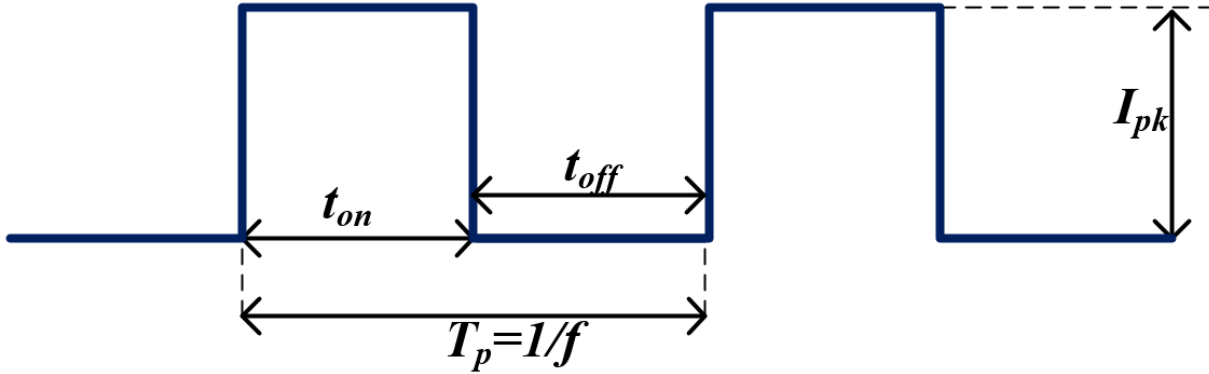


Figure 18: Pulse charge current characteristics

The different combinations of duty cycle, amplitude, and frequency of a pulse charge current will result in different battery output performance metrics, i.e. charge time, battery charge and energy efficiencies, and life cycle. It is therefore important to select the right values to ensure optimal performance of the pulse charging circuit and battery.

The frequency selection of the pulses is important since the response of the battery will vary depending on the chosen frequency. At low frequencies, the mass transport effects are dominant [95] as seen from the Nyquist plot in Fig. 10. In this region of operation, Z_w dominates and becomes larger as frequency decreases. This is because, in this region, the diffusions of ions into the electrode is limited. As frequency increases, the parallel combination of the double layer capacitor and charge transfer resistance begin to have an impact. The energy transfer is due to the surface charges on the electrodes. In this medium frequency range, the C_{dl} and R_{ct} can also act as a low pass filter such that when a pulse charge current is applied, the chemical charge reactions in the battery only experience the average current, hence the battery surface temperature behavior is

comparable to CC-CV charging technique [95]. As mentioned in section 2, these battery parameters vary with SoC, SoH, and temperature, hence the diameter of the semi-circle in the Nyquist plot can change depending on the current state of the battery. At higher frequencies, C_{dl} begins to exhibit a low impedance and chemical reactions in the battery begin to slow down, hence, the effect of R_{ct} reduces, and the ohmic resistance R_s dominates. The inductance also begins to have an impact, as shown in Fig. 10. The behavior of the battery across frequency shows that the impedance of the battery is dependent on the frequency. On examining the battery impedance across frequency, there is a point on the impedance magnitude plot at which a local minima occurs, as shown in Fig. 19. This minimum impedance, Z_{intmin} , occurs at a frequency, f_{zmin} , which can be derived from (11). Even though the Warburg impedance, Z_w , is dependent on frequency, at high frequencies, Z_w is small and negligible due to the depth of diffusion reactants being shallow. Lower frequencies ($< 1 \text{ Hz}$) cause diffusion reactants depth to increase, thereby increasing Z_w .

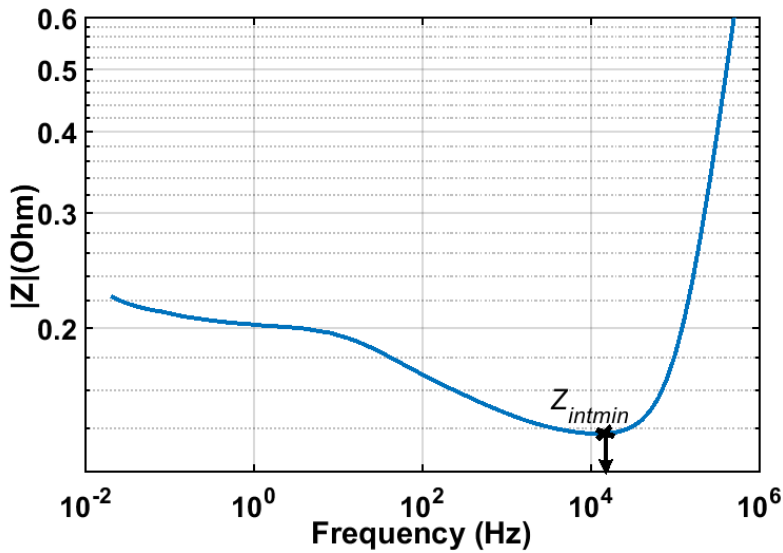


Figure 19: Bode impedance magnitude plot showing minimum impedance occurrence

If the pulse frequency is above 1Hz, Z_w is negligible, and f_{zmin} can be found from (11) by $d|Z_{int}(\omega)|^2/d\omega = 0$.

$$\frac{d|Z_{int}(\omega)|^2}{d\omega} = 2\omega \left(L^2 - \frac{C_{dl}R_{ct}^2(2L + C_{dl}R_{ct}(R_{ct} + 2R_s))}{(1 + C_{dl}^2R_{ct}^2\omega^2)^2} \right) \quad (18)$$

Therefore,

$$f_{zmin} = \frac{1}{2\pi} \cdot \left(-\frac{1}{C_{dl}^2R_{ct}^2} + \frac{\sqrt{A \cdot B}}{C_{dl}^4L^2R_{ct}^4} \right)^{\frac{1}{2}} \quad (19)$$

where $A = C_{dl}^5L^2R_{ct}^6$ and $B = 2L + C_{dl}R_{ct}^2 + 2C_{dl}R_{ct}R_s$ [32]. It is important to perform pulse charging at a frequency where the battery impedance is minimized to reduce energy losses in the battery.

The duty cycle of the pulses should also be taken into consideration. A higher duty cycle will result in faster charging (approaching the CC charge phase of the CC-CV charge algorithm) but will cause the battery to be prone to overcharging and overvoltage conditions due to an increase in concentration polarization, which limits the movement of the ions. Li-ion batteries cannot absorb overcharge, so an overcharging condition can lead to increasing temperature and an eventual thermal runaway [174], [175]. A lower duty cycle will result in a longer charge time, but it also gives better battery charge efficiency, since elongated rest periods give time for the ions to intercalate in the electrode. Mayers *et al* [176] discovered that short pulses with longer periods reduced the propensity for dendrite formation, but that results in an extended charge time. Purushothaman *et al* [177] also concluded from their work that by varying the width of pulses, the concentration overpotential can be reduced. The duty cycle of the pulse charge current can also impact the discharge capacity of the li-ion battery as demonstrated in [178], [179].

The peak current amplitude can impact safety, as high peak currents can result in fast charging, but the risk of overvoltage and increasing temperature is high. The use of high current amplitudes necessitates the incorporation of longer rest periods to prevent accumulation of ions at the electrode interface. The longer rest periods will allow the ions time to intercalate in the electrode, but this extends charge time. Smaller current amplitudes require shorter rest periods, but can also result in extended charge time.

It is therefore necessary to select the pulse charging parameters that will improve safety, reduce concentration potential, increase battery charge and energy efficiencies, and also reduce charge time.

4.2 Previous works on li-ion pulse charging

Several chargers using pulse charging algorithms have been proposed. Other studies have also been conducted on the use of pulse charging with li-ion batteries. Different ways of implementing the pulse algorithm have been proposed, and this has resulted in different charge times, charge efficiencies, and life cycle results. These previous works vary in their degrees of complexity. Yin *et al* [180] proposes a pulse charging technique based on optimal search mode for duty cycle and frequency for distributed multiple cells. The frequency was searched by setting an initial frequency at a duty cycle of 50% and by using a step process. The current can be calculated at each step by an algorithm and updated accordingly. After obtaining this optimal frequency, the search for duty cycle began from an initialized value, then charging was performed for five seconds, after which the average current was determined. Per the proposed algorithm, if the average current was below a certain predefined limit, the duty cycle was increased by 10%. This kept updating until the duty cycle reached 90% or the SoC reached 80%. The algorithms were implemented in software and

the pulses were generated by a microcontroller. The proposed method, when charging from 0% to 80% SoC, resulted in 18.6% reduction in charge time when compared to the CC-CV charging algorithm.

Chen [166] proposed a variable frequency pulse charging algorithm by measuring average current at fixed amplitude pulses at different frequencies. The frequency at which the maximum current occurred was considered the optimal frequency. This proposed algorithm was implemented using a microprocessor, voltage regulator, and a pair of transistors. Through software, the search and charge modes were implemented to find the optimal frequency at which to charge the li-ion battery. A charge time improvement of 24% was recorded when compared with the CC-CV charging algorithm.

Chen [167] proposed a charging system with an optimal duty cycle searching algorithm. By implementing the search for optimal duty cycle, which is based on sequentially charging the battery by using pulses with different duty cycles and measuring the average current to determine if the applied duty cycle resulted in better electrochemical reactions, the optimal duty cycle could be found. This algorithm was implemented on a microprocessor and used in conjunction with a voltage regulator, current sensing resistor, operational amplifier, and a transistor to charge a battery. This resulted in a charge time and battery charge efficiency improvement of 14% and 3.4%, respectively, when compared with the CC-CV charging algorithm.

Purushothaman *et al* [181] tested various pulse charging algorithms through a modelling process. A li-ion battery model based on the macro homogenous analysis of how lithium ions diffuse into

the graphite electrode was used to analyze both CC-CV and pulse charging algorithms. Based on the developed model, different waveforms of varying pulse widths, rest periods, and amplitudes were tested and simulation results analyzed. They concluded that fast charging could be obtained without any detrimental effects by using the pulse charging algorithm.

From the discussed previous works, pulse charging algorithms provides good benefits if the pulse charge current parameters are chosen properly. Some of the drawbacks of these previous works are the large form factors of the systems that have been designed. They have increased complexity when it comes to the implementation of the algorithms and need microcontrollers or microprocessors that consume extra power and board space. It is necessary to design a battery charging system that addresses these drawbacks, taking into account reduced charge time, increased battery charge and energy efficiencies, safety, and small form factor design.

4.3 Design of a pulse-based charger for IoT applications

A charger design incorporating a pulse charging algorithm is proposed in this work that addresses the aforementioned drawbacks and also takes into account battery polarization across the entire charging cycle. This proposed charger is targeting applications from the Internet of Things (IoTs), such as smart thermostats, windows shades, and door sensors, to wearables, such as smart glasses, fitness bands, and digital pens. With IoTs projected to hit \$561.04 billion by 2022 [182], there is a need for the fast charging of these devices that are always connected to the internet and constantly consuming power. A failure in the battery or charging system of an IoT device can be catastrophic, therefore there is a need to have small form factor charger circuits that are simple, cost effective, easily integrated, and are able to charge batteries in a fast, safe, and reliable manner. These small

devices sometimes make use of batteries in coin or button formats [183]. Therefore, the pulse charger designed in this work will target li-ion coin cells. This work has been presented in [32]

4.3.1 Proposed pulse charger system level overview

The proposed pulse charger can take its input $V_{in,PS}$ from a dc voltage source and pulse the charge current at different duty cycles into the battery to improve charge efficiency and at the same time reduce charge time. Previous works incorporating pulse charging algorithms do not include a pre-charge phase in the design to account for deeply discharged batteries. This proposed pulse charger incorporates pre-charge phase for deeply discharged cells and preconditioning purposes, fast/slow charge phase to improve battery charge efficiency and reduction of charge time, and termination phase to prevent overcharge and overvoltage conditions. All these phases are user programmable. It further incorporates safety mechanisms, such as external battery temperature sensing and an overvoltage circuit, to protect both the user and the battery during charging.

A flow chart describing the operation of the proposed pulse charger is shown in Fig. 20. The proposed pulse charger operates in three charge phases: trickle charge (pre-charge), fast charge, and slow charge. A charge phase is selected based on the battery state during charge. If the battery is determined to be deeply discharged, the trickle charge phase is initiated. The fast charge phase is initiated once the battery is out of the deeply discharged state but less than the nominal voltage V_{nom} . As the battery approaches full charge voltage, where full charge denotes a SoC of 100%, the slow charge phase is initiated. With the battery approaching its full charge, it is necessary for the battery to absorb charge efficiently to prevent it from overcharging due to increased concentration of lithium ions Li^+ at the electrodes during this phase. Fig. 21 shows the battery polarization across SoC. Jiang *et al* [184] determined that the SoC of a li-ion battery will

have an effect on the polarization of the battery. Polarization is initially high at low SoC due to nucleation, and as SoC increases, polarization decreases as shown in Fig. 21. As SoC exceeds 80%, due to the difficulty of intercalation of Li^+ , polarization increases again. Therefore, by varying duty cycles across the charge process, concentration polarization can be minimized to ensure proper intercalation.

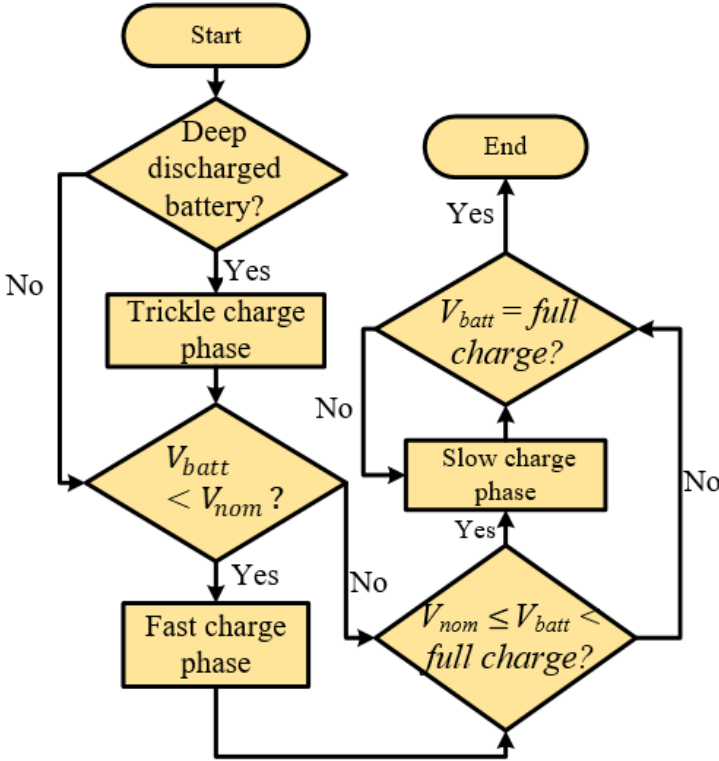


Figure 20: Flow chart of proposed pulse charger for IoT applications

The fast and slow charge phases seek to combine fast charging with increased battery charge efficiency, and also account for the battery polarization characteristics across charging.

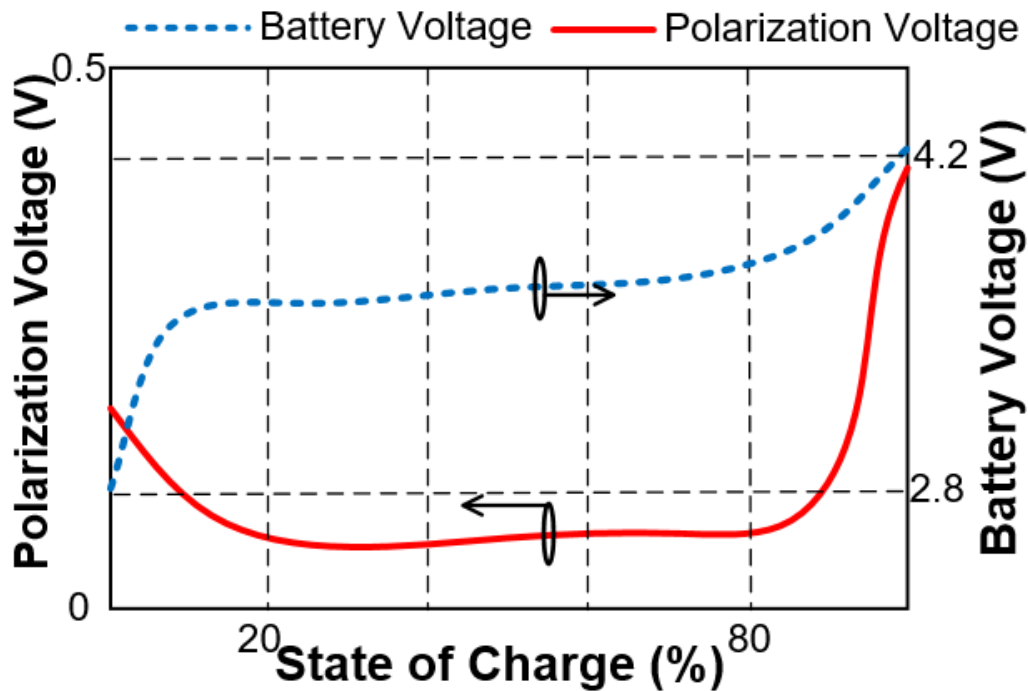


Figure 21: Changes in battery polarization with respect to SoC

The charger should operate at a frequency at which the li-ion battery impedance is minimum to reduce energy losses in the battery and improve battery charge and energy efficiencies. The selection of the duty cycle of the pulse charge current should also be taken into consideration. At the early stages of charging, the Li^+ are easily intercalated into the electrodes, but as the battery starts approaching full capacity, as shown in Fig. 21, polarization is much higher since it takes a longer time for the Li^+ to intercalate in the anode. If higher duty cycles are used at this stage, the Li^+ are going to collect at the surface of the electrode which can cause the growth of dendrites. Thus, a method is proposed where faster charging and improved battery charge and energy efficiencies can be achieved without entering overvoltage or overcharge conditions. Battery health and battery life cycle consequently improve. The charging phase is divided into two parts: one part

provides fast charging time using a higher duty cycle, when battery polarization is low, and the other part using a lower duty cycle to allow better battery charging efficiency and account for the high battery polarization. Due to the stringent charging requirements of a li-ion battery, a duty cycle of 70% or higher is appropriate for the initial charging stage. The duty cycle is then reduced as the battery approaches full charge.

A system level block diagram of the proposed pulse charger detailing the major blocks which control the charge phases is shown in Fig. 22. A decision block will produce the necessary pulse voltages to operate the switch, SW_{p1} , at the correct duty cycle and frequency based on the current state of the battery that is sensed through $V_{batt\ detect}$. SW_{p1} will then pulse the charge current from $V_{in,PS}$ into the battery to charge it. Depending on the value of V_{batt} , which is detected by a voltage detector circuit, $V_{batt\ detect}$, the trickle charge phase, fast charge phase, or slow charge phase will be initiated. Safety circuits, such as battery temperature sense and overvoltage protection, are required to ensure the battery charges within its safety limits. A system level simulation was performed using the CAD system Cadence [185]. The duty cycle for the fast charge phase in Fig. 21 was varied from 10% to 90% and the power consumption and charge time measured. In this simulation, the battery was modeled as a 100F capacitor in series with a 100m Ω resistor. The power consumption and charge time versus the fast charge duty cycle was obtained and shown in Fig. 23. In order to obtain fast charging at relatively low power consumption, the duty cycle for fast charge has to be set below 75%. Purushothaman *et al* [181] suggested that using a duty cycle of 75% was sufficient for fast charging while preventing lithium saturation on the electrodes. To account for the high battery polarization toward the end of charging, the duty cycle was reduced to 25% to achieve improved charge efficiency.

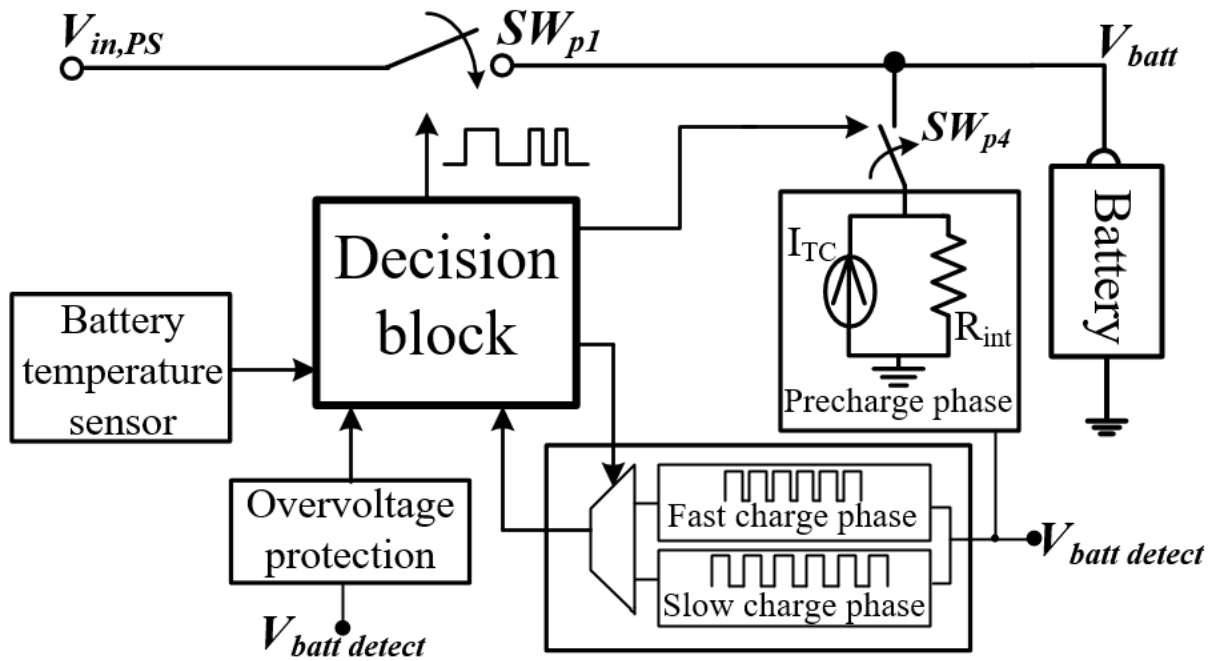


Figure 22: Block level diagram of proposed pulse charger for IoT applications

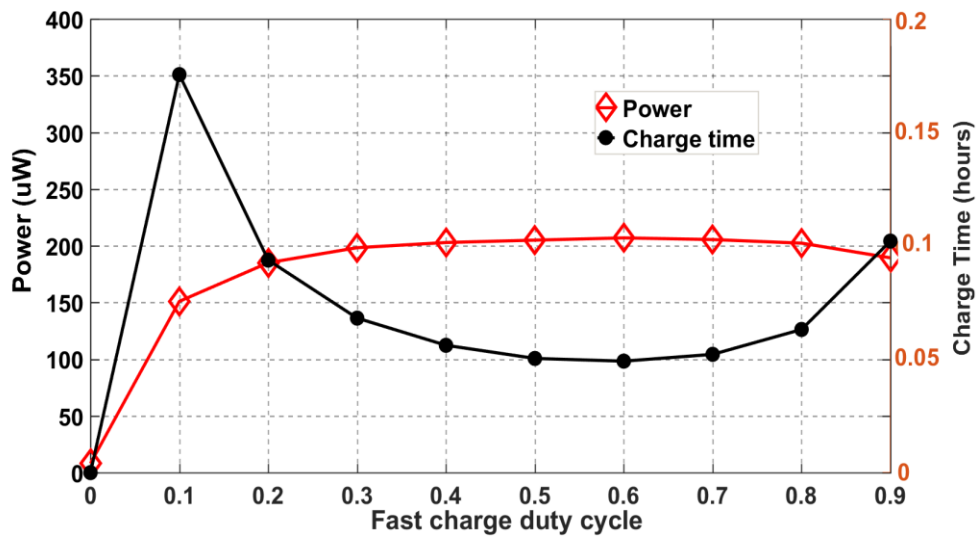


Figure 23: Simulation results showing variation of power consumption and charge time versus fast charge phase duty cycle of proposed pulse charger

This proposed approach of using duty cycles of 75% and 25% was implemented by using a duty cycle selector (DCS).

4.3.2 Implementation of proposed pulse charger for IoT applications

The top-level implementation of the proposed pulse charger is shown in Fig. 24.

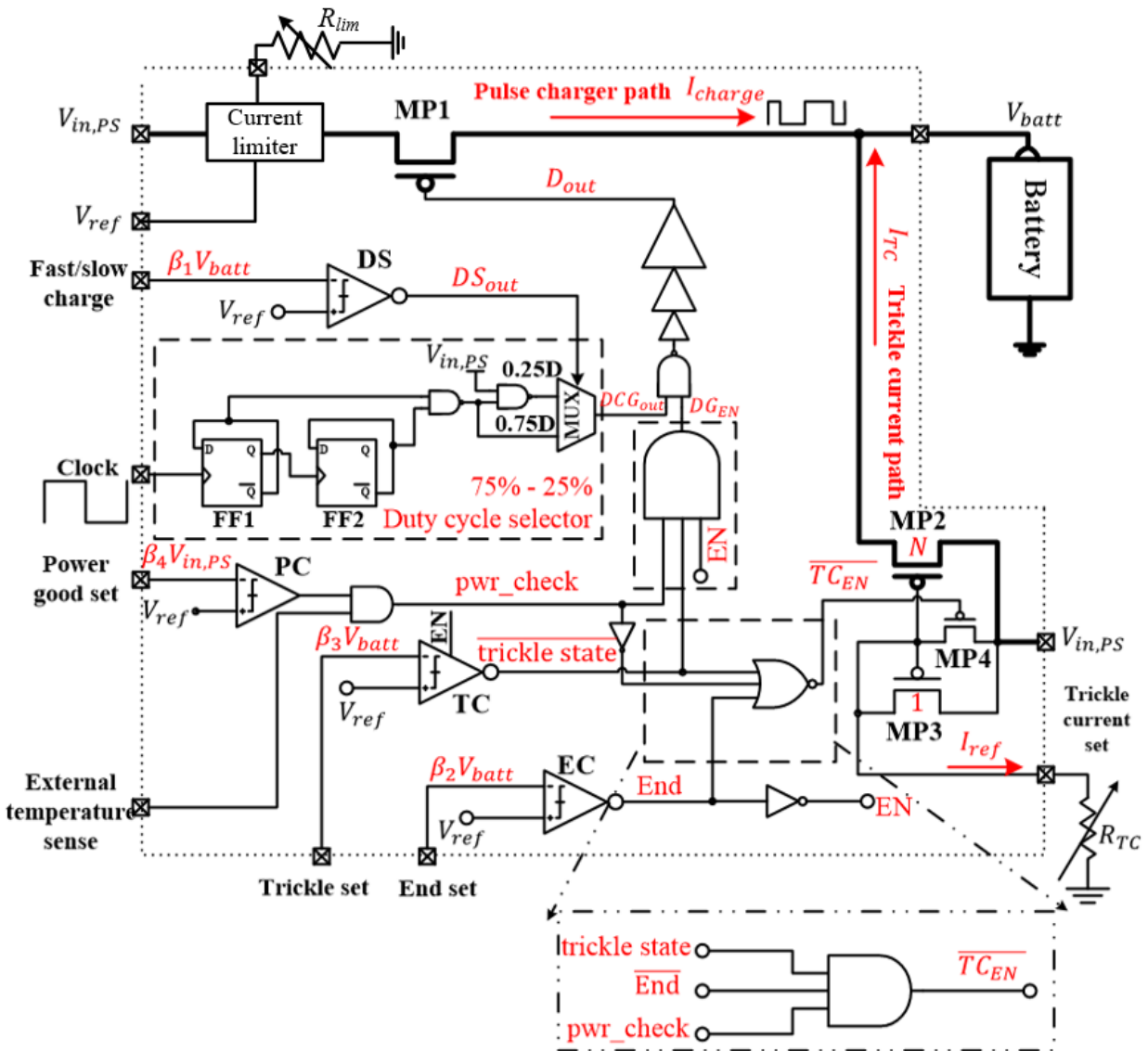


Figure 24: Implementation of proposed pulse charger

The proposed pulse charger operates as follows:

- Verification:** The charger must always ensure the dc source is at the right power level and within safety limits. Operation outside the designed limit is avoided to protect the user, device, and battery. This is achieved through the PC comparator. The PC comparator ensures that $V_{in,PS}$ is ideal for charging at all times. It sends logic signals to all charging phases to either proceed with charging or not depending on whether the input voltage meets the required specifications. The dc input voltage level specification is set by V_{ref}/β_4 , where β_4 is the resistive feedback gain from $V_{in,PS}$, and V_{ref} is the reference voltage. Some batteries have temperature sensors to monitor their temperatures while charging. The signal from that sensor can be used as an input (external temperature sense) to disable charging when battery temperature is not suitable for charging. If the battery does not have an embedded temperature sensor, a temperature IC, such as the MAX31875 [186], can be used.
- Trickle charge phase:** This charge phase is implemented by comparator TC to compare the battery voltage with the deep discharged voltage threshold V_{ref}/β_3 , where β_3 is the resistive feedback gain from V_{batt} . If it is determined that the battery is deeply discharged, an internal high output impedance current source, implemented by $MP2$, $MP3$ and $MP4$, controlled by a variable resistor R_{TC} is enabled to begin trickle charging. The current source is enabled when the gate of $MP4$ $\overline{TC_{EN}}$ attains a logic high, accomplished by the NOR gate according to (20).

$$\overline{TC_{EN}} = pwr_{check} \cdot \overline{End} \cdot trickle\ state. \quad (20)$$

If $\overline{TC_{EN}}$ is logic high, i.e., $MP4$ is off, then

$$\frac{I_{TC}}{I_{ref}} = \frac{K_{p2}}{K_{p3}} \cdot \frac{W_2 L_3}{W_3 L_2} \cdot \left(\frac{V_{gs2} - V_t}{V_{gs3} - V_t} \right)^2 \quad (21)$$

where I_{TC} is the trickle charge current, $I_{ref} \cong \frac{V_{in} - V_t}{R_{TC}}$ is the reference current set by R_{TC} , $K_{p2,3}$ is the process transconductance parameter, $V_{gs2,3}$ is the gate-source voltage of $MP2$ and $MP3$, V_t is the threshold voltage of the transistor, and W and L are the dimensions of the PMOS transistors. Since the battery capacity is huge, and in effect its capacitance is large, the error in I_{TC} due to the mismatch and process variations between $MP3$ and $MP2$ is negligible. Therefore, if $L_3 = L_2$, $K_{p2} = K_{p3}$, $V_{gs2} - V_t = V_{gs3} - V_t$, then (21) yields

$$I_{TC} = \frac{W_2 L_3}{W_3 L_2} I_{ref}. \quad (22)$$

To obtain an I_{TC} ranging from 1 mA to 4 mA when I_{ref} varies from 20 μ A to 80 μ A, $W_2 = 50W_3$. At the end of the trickle phase, $MP2$ and $MP3$ are shut off when their gates are pulled to V_{in} , i.e. TC_{EN} is logic low according to (20). I_{TC} is disconnected and the trickle charge phase is no longer in operation.

- **Fast and slow charge phases:** Once the battery voltage exceeds V_{ref}/β_3 , charging can transition into the fast charge phase. At this point, $\overline{TC_{EN}}$ is at logic low. The two positive edge flip flops are part of the duty cycle selector (DCS). The first flip flop $FF1$ divides the frequency of the clock by two which is then divided again by modulo two using the second flip flop $FF2$. The NAND gates will then generate pulses with duty cycles of 25% and 75%. As soon as the trickle charge phase ends, the main pass transistor $MP1$ is pulsed at a duty cycle of 75% to achieve faster charging when battery polarization is low. Once the battery voltage starts approaching a SoC of a 100% and battery polarization starts increasing, $MP1$ starts pulsing charge current into the battery at a duty cycle of 25% to

achieve better battery charge efficiency. This also ensures maximum charge absorption, with the increased rest time in between pulses allowing ions to properly intercalate in the anode. The transition is achieved by comparator DS , which compares the battery voltage to a changeover voltage threshold. This voltage threshold, based on SoC, is set by V_{ref}/β_1 , where β_1 is the resistive feedback gain from V_{batt} . The output of this comparator DS_{out} serves as the select signal to the multiplexer which outputs either a 75% or 25% duty cycle depending on the battery voltage. The following equations summarize the operation of the fast charge/slow charge phase in Fig. 24.

$$(pwr_check \cdot \overline{trickle\ state} \cdot EN) = DG_{EN}. \quad (23)$$

$$\overline{DS_{out}} \cdot 0.25D + DS_{out} \cdot 0.75D = DCG_{out}. \quad (24)$$

$$DG_{EN} \cdot DCG_{out} = D_{out}. \quad (25)$$

where DCG_{out} is the output of the DCS and D_{out} drives $MP1$. The charge rate for both the fast and slow charge phases is dependent on the specifications of the battery. This can be set by effectively tuning the charge current which is controlled by R_{lim} . The peak pulse charge current (I_p) can be limited by using (26)

$$I_p = \frac{V_{ref}}{R_{lim}}. \quad (26)$$

During charging, the charge rate will differ across the two phases since battery polarization voltage changes drastically towards the end of charging. The change in charge rate is due to the difference in duty cycles and a constant I_p . For a selected I_p , the effective charge current in the fast charge phase, $I_{chargefast}$, is

$$I_{chargefast} = I_p \cdot \sqrt{D_{fast}} \quad (27)$$

and the effective charge current in the slow charge phase, $I_{chargeslow}$, is

$$I_{chargeslow} = I_{chargefast} \cdot \sqrt{\frac{D_{slow}}{D_{fast}}} \quad (28)$$

where D_{fast} and D_{slow} are the duty cycles for the fast and slow charge phases respectively. The slow charge phase charge rate will be about 58% of the fast charge phase. This reduced constant charge rate in addition to the relaxation periods in the pulses enable increased charge efficiency and reduction of accumulation of lithium ions on the surface of the electrode. The frequency at which *MP1* operates should be equal to f_{Zmin} . This frequency can be generated from the IoT system frequency by using clock dividers.

To analyze the power losses in the pulse charger circuit, the conduction loss $P_{C_{rp1}}$ in *MP1* can be approximated as

$$P_{C_{rp1}} = I_{chargeex}^2 R_{p1} \frac{t_{on}}{T} \quad (29)$$

where $I_{chargeex}$ is the effective charge current; R_{p1} and t_{on} are the on-resistance and on time of *MP1*, respectively, and T is the switching time period. There is a high conduction loss during the fast charge phase compared to the slow charge phase. With this varying power loss over the whole charging process, a lower average power loss can be achieved in the overall charging process. Switching loss $P_{S_{rp1}}$ in *MP1* varies linearly with switching frequency f_s according to (30).

$$P_{S_{rp1}} = C_{g1} V_x^2 f_s \quad (30)$$

where C_{g1} is the gate capacitance of *MP1* and V_x (D_{out} in Fig. 24) is the *MP1* drive voltage.

- **Termination:** The charging process terminates once the battery attains full voltage. A comparator *EC* (shown in Fig. 24) ensures the battery does not go into an overvoltage state

by sending logic signals to the appropriate blocks to discontinue charging. The TC and DS comparators are both shut down using the EN signal from the EC comparator output to save quiescent power. The end charge voltage threshold is set by V_{ref}/β_2 , where β_2 is the resistive feedback gain from V_{batt} . During the entire charging process, battery voltage, input power, and battery temperature (external temperature sense) are monitored. If at any time, any of these parameters fall outside of their specifications, charging is terminated.

4.3.3 Testing setup and experimental results

The proposed pulse charging system was designed using $0.18\ \mu\text{m}$ $3.3\ \text{V}$ CMOS standard IC technology and fabricated through the MOSIS educational program [187]. The fabricated circuit was packaged in a 8mm by 8mm Quad Flat No Lead (QFN) package. The actual silicon area consumed by the pulse charger was 2mm by 1mm . Fig. 25(a) shows the micrograph of the designed pulse charger and Fig. 25 (b) shows the IC in a QFN package on a PCB.

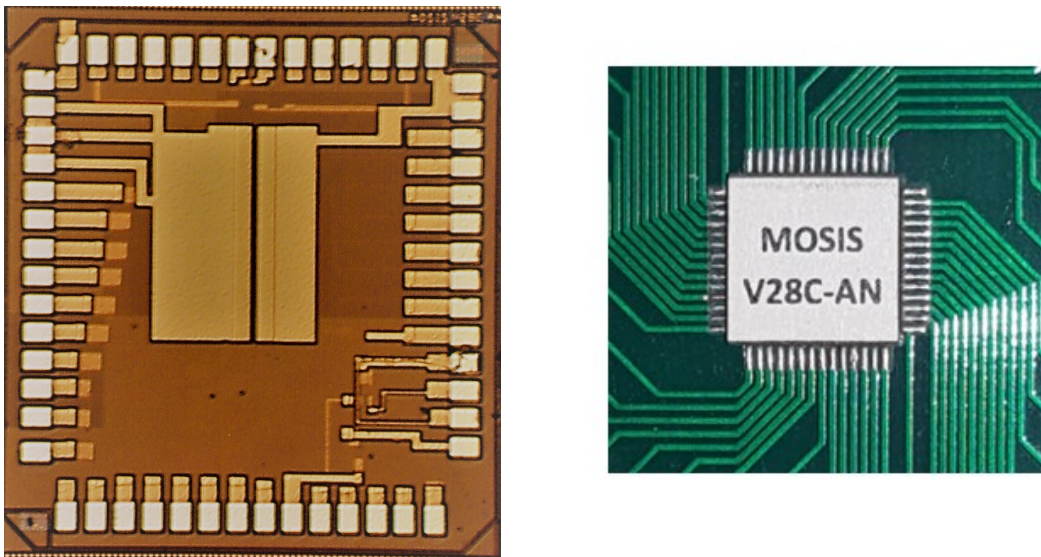


Figure 25: (a) Micrograph of designed pulse charger (*Left*) (b) Packaged IC (*Right*)

Before proceeding with the testing of the pulse charger IC, it is important to characterize the batteries to evaluate their properties and determine the frequency at which their impedance is minimum. Different li-ion batteries capacities with different cathode chemistries in coin format were characterized by using an ac impedance analyzer, VersaSTAT potentiostat [188]. The different cathode chemistries were lithium manganese composite oxide (Li_xMnO_y) and vanadium pentoxide (V_2O_5). f_{Zmin} of the batteries could be obtained by performing an ac impedance analysis. Fig. 26 shows the measured ac impedance spectrum of the different batteries capacities. From Fig. 26, there is a point on the ac impedance spectrum at which the ac impedance is minimum. This impedance is plotted against the frequency at which it occurs in Fig. 27.

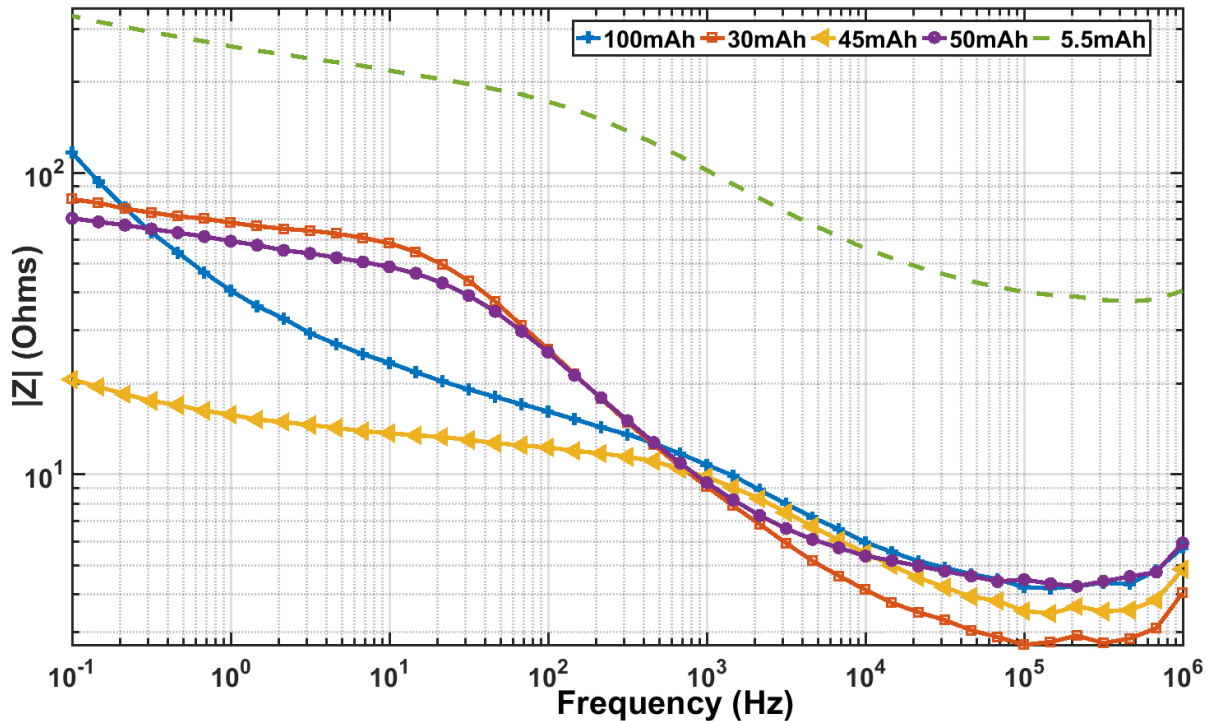


Figure 26: Bode impedance magnitude plot for different li-ion batteries under test

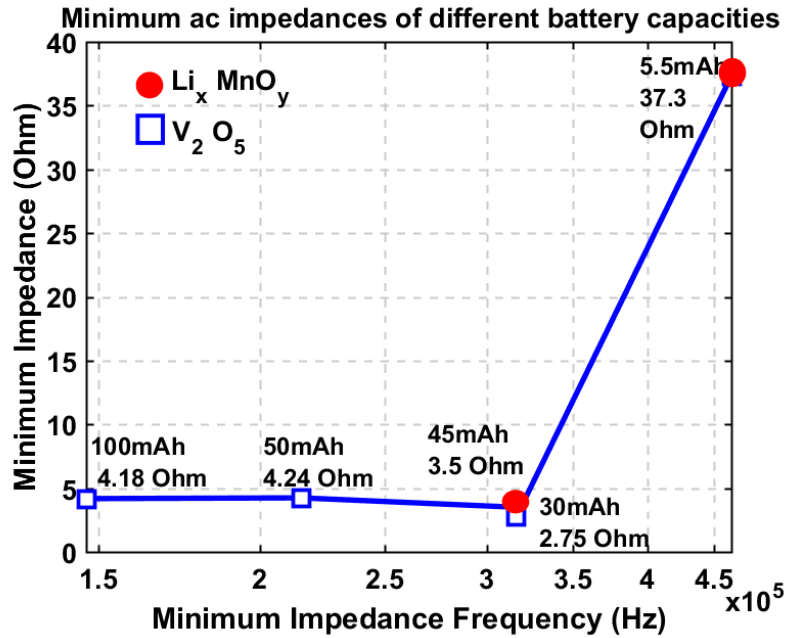


Figure 27: Measured minimum impedance vs the frequency at which it occurs for different battery capacities

From Fig. 27, it is important to note that as battery capacities increased, the frequency at which the minimum impedance occurred decreased across the same cathode material. The volumetric capacity of the battery, which depends on the crystal structure of the materials used and the size of the battery [81], therefore, has impact on the impedance and the frequency at which the minimum impedance occurs.

Fig. 28 shows the Nyquist plots for the different batteries. The battery impedance parameters can be extracted from these plots by fitting the Randles equivalent circuit model to the measured data and using curve fitting algorithms. Batch fitting operations [189] were performed to fit the model to the measured data and the battery parameters extracted and shown in Table. 5.

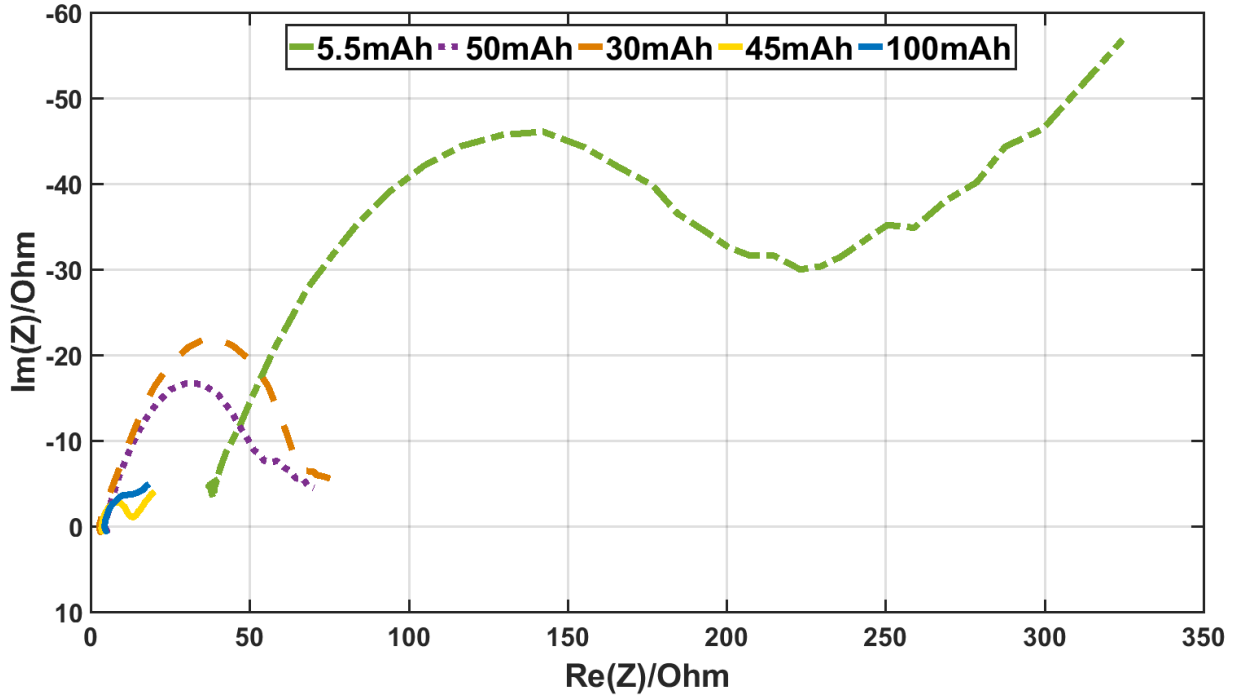


Figure 28: Nyquist plots for different li-ion batteries in coin format under test

Table 5: Impedance parameters of characterized li-ion batteries

Battery capacity (mAh)	L (nH)	R_s (Ω)	C_{dl} (μF)	R_{ct} (Ω)	f_z (kHz)	Z_{int_min} (Ω)	Cathode chemistry
100	93.9	4.64	17.7	6.53	146.78	4.18	V_2O_5
50	78.0	4.69	13.7	5.12	215.44	4.24	V_2O_5
45	56.7	4.01	6.35	7.29	316.23	3.50	Li_xMnO_y
30	73.1	3.49	4.71	5.95	316.23	2.75	V_2O_5
5.5	74.9	47.22	1.79	176.20	464.16	37.32	Li_xMnO_y

It is seen from Table 5 that the battery with the smallest capacity had the largest ohmic and charge transfer resistances. As expected, C_{dl} is also small due to smaller electrode area. C_{dl} increases as battery capacity increases.

The experimental test setup is shown in Fig. 29. The proposed pulse charging algorithm and the benchmark CC-CV charging method were used to charge a Panasonic VL series 3 V 100 mAh li-ion battery with a chemical composition of vanadium oxide for cathode and lithium alloy for anode with a non-aqueous solvent for electrolyte [190]. The two charging techniques were also used to charge a Panasonic ML series 3 V 45 mAh li-ion battery with a chemical composition of manganese composite oxide as cathode and lithium aluminum alloy as anode with a non-aqueous solvent for electrolyte [190].

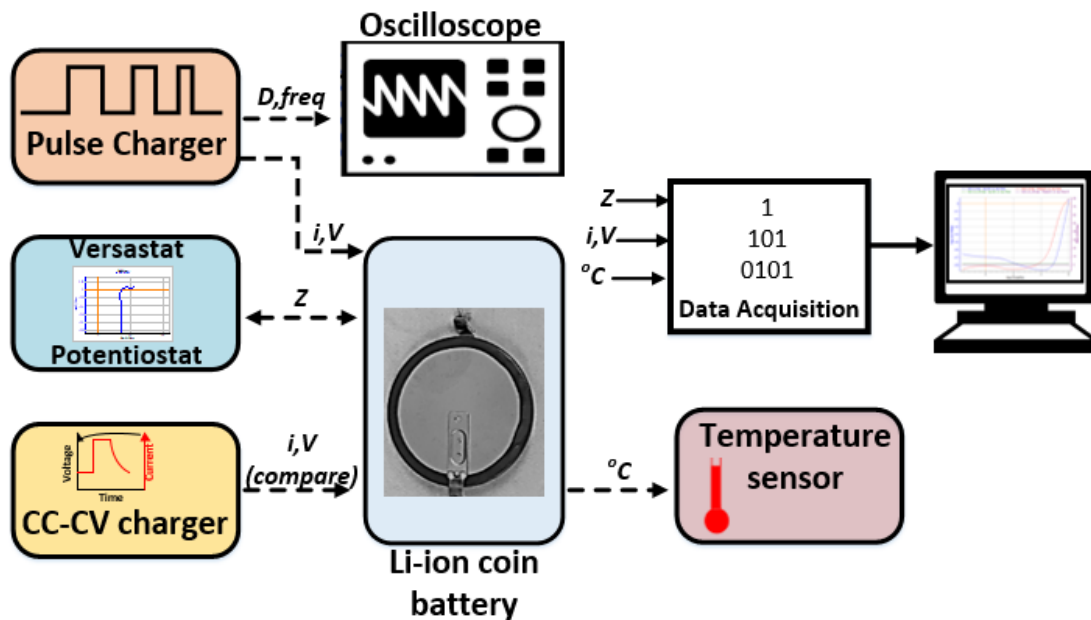


Figure 29: Experimental setup for testing designed pulse charger

Both batteries were charged at a charge rate of 0.1 C based on their specifications. For the 100 mAh and 45 mAh li-ion batteries, the charge current for the constant current stage in the CC-CV charging technique and the effective pulse charging current was 10 mA and 4.5 mA respectively. The batteries were then subjected to a depth of discharge (DoD) of 100% at a discharge rate of 0.1C, i.e. 10 mA for the 100 mAh li-ion battery and 4.5 mA for the 45 mAh li-ion battery, after resting for an hour. The rest period is needed to ensure chemical reactions in the battery reach equilibrium. For a fair comparison, these charge and discharge currents were used for all experiments.

Charging at f_{Zmin} will decrease energy losses in the battery and improve battery charge efficiency. From Table 5 and Fig. 27, the f_{Zmin} of the 100 mAh and 45 mAh li-ion batteries was determined to be 146.8 kHz and 316.2 kHz, respectively. The minimum impedance Z_{int_min} at these frequencies were 4.18 Ω and 3.50 Ω , respectively. With these frequencies obtained, the battery could then be subjected to the proposed pulse charging algorithm, i.e. charge phases switching from fast to slow charge duty cycles of 75% and 25%, respectively. Fig. 30 shows the 100 mAh li-ion battery charge voltage vs charge time for different pulse frequencies, including f_{Zmin} . This was compared with the CC-CV charging algorithm. Fig. 31 shows the 45 mAh li-ion battery charge voltage vs charge time for different pulse frequencies, including f_{Zmin} . This was also compared with the CC-CV charging algorithm.

100 mAh Li-ion battery charging: Pulse vs CC-CV

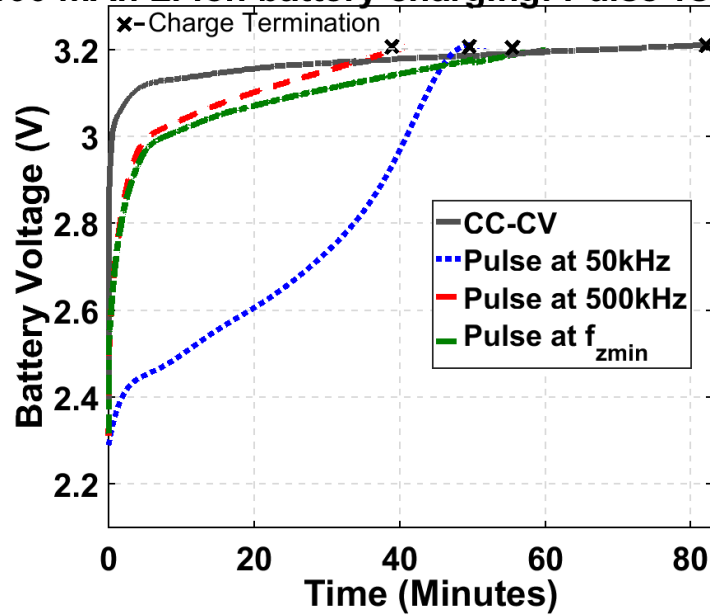


Figure 30: Proposed pulse charging algorithm vs CC-CV for a 100 mAh li-ion battery

45 mAh Li-ion battery charging: Pulse vs CC-CV

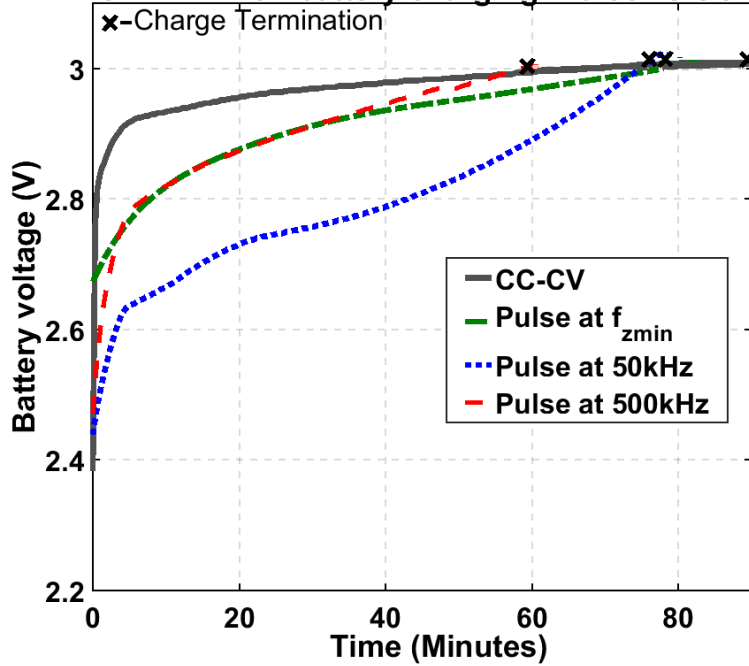


Figure 31: Proposed pulse charging algorithm vs CC-CV for a 45 mAh li-ion battery

In terms of charge time, the proposed pulse charging algorithm reduced charge time by 37% and 16% for the 100 mAh and 45 mAh li-ion batteries, respectively. Charge efficiency was improved by 3.2% in each case when the proposed pulse algorithm was used. The pulse charging algorithm was tested at other frequencies, 50 kHz and 500 kHz, other than f_{zmin} to determine the impact of charging frequencies on battery charging time and efficiency. The battery ac impedance at 50 kHz and 500 kHz were, 3.8 Ω and 3.6 Ω , and 4.5 Ω and 4.4 Ω for the 45 mAh and 100 mAh Li-ion batteries, respectively and results recorded in Tables 6 and 7. It is clear from these tables that using the proposed pulse charging algorithm operating at the frequency at which the battery ac impedance is minimum produced the best battery charge efficiency.

Table 6: Summary of experimental results for 100 mAh li-ion battery

Parameter	100 mAh			
	CC-CV	Pulse		
Charge profile				
Charge frequency (kHz)	n/a	50	f_{zmin}	500
Charge time (min)	83	47	52	38
Charge efficiency (%)	89.24	89.15	92.39	89.98
Charging battery surface temperature change ($^{\circ}$ C)	+0.31	-0.81	-0.37	+0.44

Table 7: Summary of experimental results for 45 mAh li-ion battery

Parameter	45 mAh			
	CC-CV	Pulse		
Charge profile				
Charge frequency (kHz)	n/a	50	f_{zmin}	500
Charge time (min)	90	74	76	56
Charge efficiency (%)	94.59	83.91	97.86	85.88
Charging battery surface temperature change (°C)	+0.5	-0.38	-0.5	+0.38

The battery surface temperature during charging was monitored using a high accuracy temperature sensor placed in direct contact with the battery as demonstrated in the approach described in [191]. The change in battery temperature was evaluated based on the maximum and minimum surface temperatures attained by the battery during charge. It is also important to note that in terms of battery surface temperatures during charging, a higher temperature rise was observed during the CC-CV charging. Both charging techniques exhibited a decrease in battery surface temperature during the initial stages of charging but it was more profound when using the proposed pulse charging algorithm as shown in Fig. 32 and Fig. 33. This decrease in temperature was due to the endothermic chemical reactions in the battery [192], [193]. In CC-CV charging, the continuous increase in surface battery temperature was due to an increase in concentration polarization [193], but in the case of using the proposed pulse charging algorithm, the battery initially cooled down during the fast phase of charging.

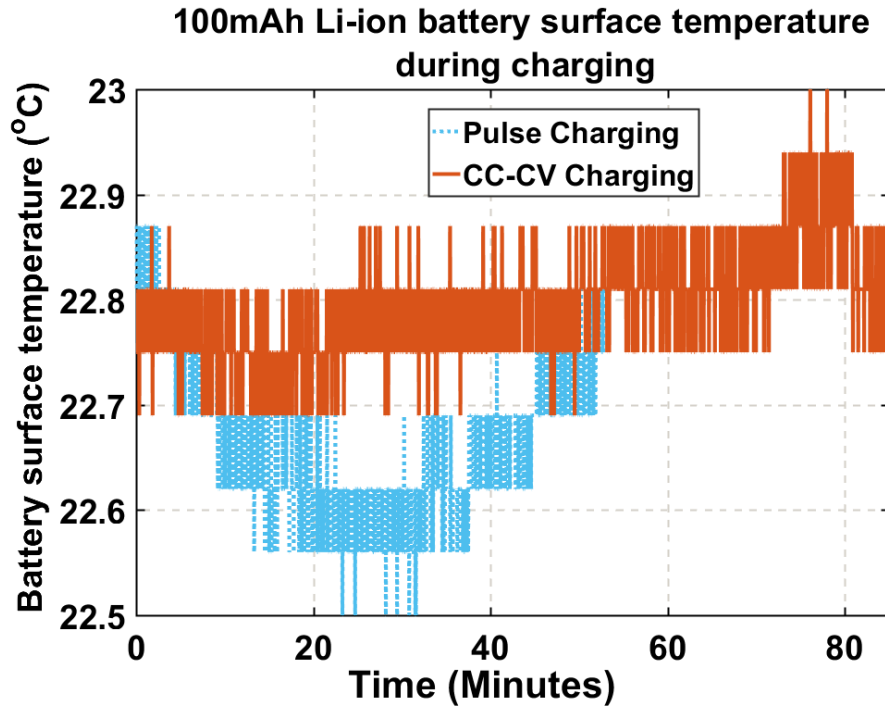


Figure 32: 100 mAh battery surface temperature for both pulse charging at f_{Zmin} vs CC-CV

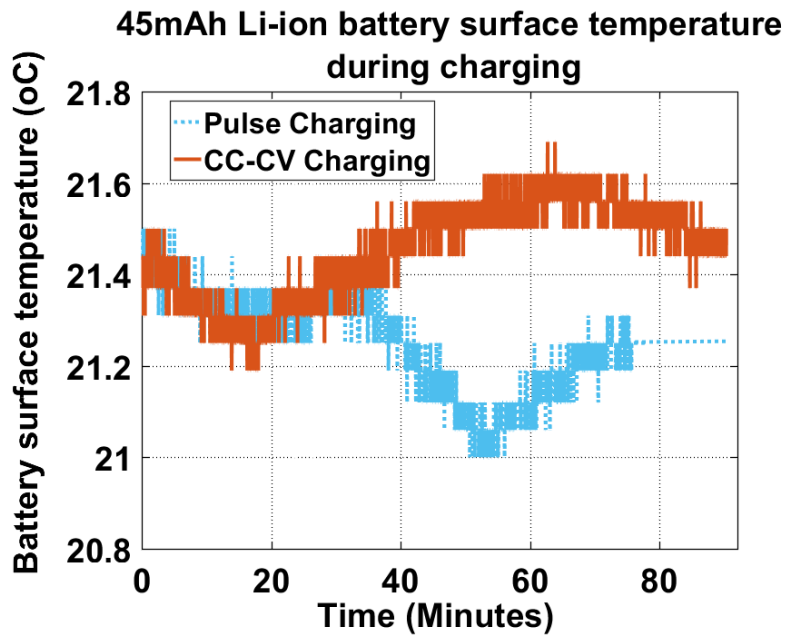


Figure 33: 45 mAh battery surface temperature for both pulse charging at f_{Zmin} vs CC-CV

4.3.3.1 Summary of experimental results

Tables 5 and 6 have summarized the experimental results comparing both the proposed pulse charging algorithm and the benchmark CC-CV charging algorithm. From these experimental results, it has been shown that the proposed pulse charging algorithm, which switches from a high duty cycle (fast charge phase), to a low duty cycle (slow charge phase) to account for increased battery polarization voltage, performs much better than the CC-CV charging, when charging at f_{Zmin} . In terms of charge time, the proposed pulse charging algorithm charged 100 mAh and 45 mAh li-ion batteries in 52 and 76 minutes, respectively, when compared to the CC-CV charging algorithm, which charged the batteries in 83 minutes and 90 minutes, respectively. This represented a charge time reduction of 37.35% and 15.56% for the 100 mAh and 45 mAh batteries, respectively. Battery charge efficiencies were also improved by 3.15% and 3.27%, respectively, when compared with the proposed charging algorithm.

Charging at frequencies other than f_{Zmin} , resulted in poor charging efficiencies, especially for the 45 mAh battery. Since impedance is minimum at f_{Zmin} and increased at all other frequencies, it can be deduced that there are much greater energy losses in the battery at other frequencies, other than f_{Zmin} . At 50 kHz and 500 kHz, the battery charge efficiency reduction was 13.95% and 11.98%, respectively, for the 45 mAh li-ion battery. Thus, the frequency at which pulse charging is performed is important and must be carefully chosen.

In terms of charge time, the proposed pulse charging algorithm produced faster charge times when compared to the CC-CV charging algorithm across the measured frequencies. This suggests that in order to perform fast charging, one can use the pulse charging algorithm, as the rest periods in

between the pulses allows effective ion movement, and prevention of dendrite formation. However, for better battery charge efficiency, the pulse charging algorithm has to operate at f_{zmin} .

The proposed pulse charging algorithm implemented on an IC has been verified through experiments and compared with the benchmark CC-CV charging algorithm. The proposed charging system produced better battery charge efficiencies and charge times, and hence its application in an IoT device will ensure the faster charging of device li-ion batteries and much better battery charge efficiency.

4.4 The need for searching for optimal pulse charging parameters

Many previous pulse chargers, including the proposed pulse charger discussed in the preceding sections, have used varying pulse charge current parameters, i.e. duty cycle, frequency, and amplitude. Depending on the I_{pk} , D , and f used, and also the temperature at which the battery is charged at, the output performance metrics, battery energy and charge efficiencies and charge time, will vary. This was experienced in Tables 6 and 7 with different frequencies giving different results. The battery impedance parameters can even vary depending on the level of the pulse charge current parameters, and this impacts the life cycle of the battery. It is therefore important to find the pulse charge current parameters and parameter levels that has the greatest impact on the aforementioned output performance metrics. To determine this will provide circuit designers the options to maximize or minimize one output performance metric with respect to the other, or seek a way to optimize all output performance metrics within a reasonable performance range depending on the application. For example, in applications where fast charging is of utmost importance and charge efficiency is not a performance metric that is really needed, circuit designers can choose the I_{pk} , D , and f that will result in the fastest charge time. Therefore, by

knowing these pulse charge current parameters and their impact on output performance metrics, optimum battery performances can be achieved.

In order to obtain these optimal pulse charge current parameters and also determine their impact on battery performance, optimization techniques will have to be used. One way to determine these optimal parameters is to test all possible combinations, but this will increase manufacturing costs and consume time. It is, therefore, important to use these optimization techniques to determine which pulse charging current parameters and levels have the greatest impact on output performance metrics, such as η_{BE} , η_{BC} , and t_c , and at the same time predict the performance of the pulse charger when dealing with manufacturing quality variability across batteries.

This work proposes the use of a partial factorial design of experiments (DoE) method to determine the optimal pulse charging parameters to maximize battery charge and energy efficiencies while reducing charge time. This technique can be applied to different battery capacities to obtain optimal charge parameters. This search for optimal pulse charging conditions was rendered manageable by employing design of experimental approaches and the Taguchi orthogonal arrays (OA) specifically. Section 5 will therefore introduce the concept of DoE and the Taguchi OA design process.

5. TAGUCHI ORTHOGONAL ARRAYS

Experiments are conducted to investigate the performance of systems, determine the effects of certain parameters, test a hypothesis, or even analyze certain parameter variables effect on the system. Every experiment will have input factors, output responses, control factors, and uncontrollable factors. This is shown in Fig. 34.

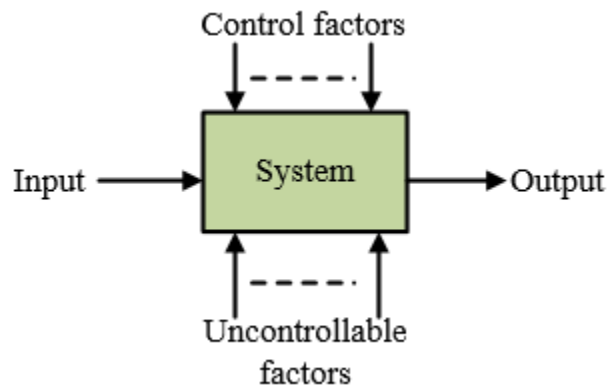


Figure 34: A typical system undergoing an experiment

Input factors are variables that can be controlled to impact the output performance of a system. Input factors could have various levels or values and are independent of the output response. The output responses, however, are dependent on the input, control factors, and uncontrollable factors, such as process variations, system noise, and manufacturing variabilities. It is sometimes needed to determine how the output responses are impacted by the input, control factor levels, and uncontrollable factors.

Statistical design of experiment are therefore different methods that can be used to evaluate how different factors or parameters at different levels influence the output of a system simultaneously. DoE was first introduced in the 1920s by Sir. R. Fisher to determine the optimum conditions to produce the best crops [194]. By using statistical methods, predictive information about systems can be obtained. By using DoE methods, minimal experimental runs are needed leading to a reduction in cost and time.

Each experiment can be visualized as a one-dimensional (1-D), two-dimensional (2-D), three-dimensional (3-D), or 4-onwards (hypercube) depending on the number of input factors in the system. Fig. 35 shows a pictorial representation of a system, undergoing a factorial design, with 3 inputs factors. The corners of the cube each represent an experimental run, taking into account the input factor levels. By using statistical DoEs, the number of runs, order of runs, and levels of factors can be optimized.

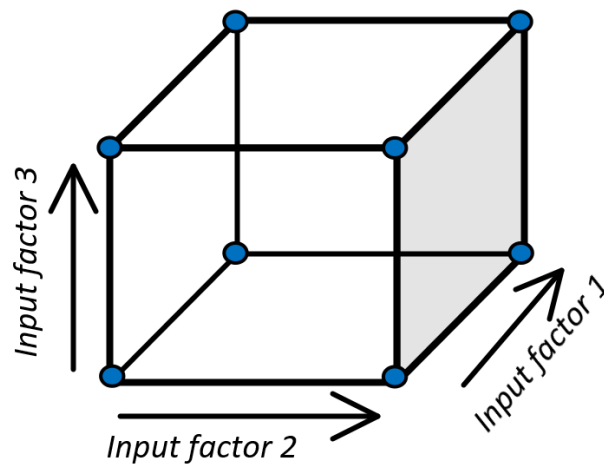


Figure 35: Pictorial representation of an experimental system with three input factors

DoE can be classified into three groups [195]. They are

- **Interaction or factorial designs:** With factorial design, all possible combinations of the control factors and levels are accounted for. This can result in a large number of experimental runs. There are sometimes interactions between factors and interaction designs seeks to quantify and analyze the extent of these interactions.
- **Screening designs:** These are used to eliminated system factors and levels that are insignificant to the output response of a system.
- **Response surface designs:** These are used to optimize the output responses based on input factors and their levels. The curvature effects of these inputs are also measured and can be used to determine what factors and levels can maximize or minimize a certain output response variable.

DoE generally follow the flow chart shown in Fig. 36. The objective of the experiment must first be clearly defined, i.e. maximization or minimization of a certain output response. Input factors and their levels must be carefully chosen to meet the objective of the experiment. Uncontrollable factors should also be identified and incorporated into the design such that they are accounted for. An appropriate DoE method that matches with the objective of the experiment should be chosen. Experiments are then run according to the designed DoE and results recorded. Software packages could then be used to analyze these results and conclusions can be drawn after interpretation of the results to determine if the chosen DoE method met the objectives of the experiment. The common types of DoE methods are: full factorial design, fractional factorial design, Plackett-Burman, Taguchi orthogonal array (OA), and Box-Behnken. Taguchi OA will be used in this work to find

optimal factor levels for pulse charge current and determine the impact of pulse charging parameters on the output performance metrics, η_{BE} , η_{BC} , and t_c .

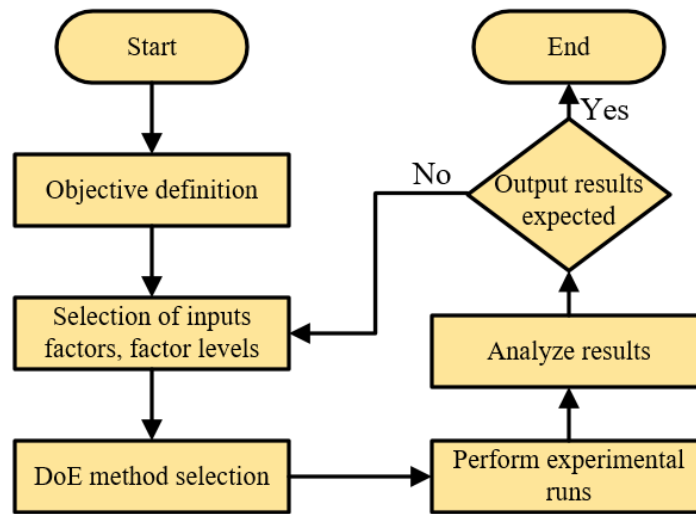


Figure 36: General procedure for a DoE flow chart

5.1 Overview of Taguchi orthogonal arrays

Taguchi OA is one of the DoE methods for a robust experimental design named after Genichi Taguchi [196]. Taguchi OA focuses on achieving optimal settings for a series of control factors by the implementation of a limited number of experiments. It produces a balanced experiment where different levels of different factors are given an equal chance during the experiment's design and hence are weighted equally. This method is used to test how sensitive the output response of a system is to a set of control factors at different levels. Taguchi OA uses a balanced partial factorial design method to reduce the number of experiments needed. Even though the number of

experiments are reduced, it has been proven that results from OA designs are comparable to that of full factorial designs [197], [198].

Taguchi OA has been successfully applied in the field of RF [199], electromagnetics [198], packaging [200], and power electronics [201]. Dudhe *et al* used Taguchi OA design process to optimize the parameters involved in designing a bulk acoustic wave (BAW) resonator for wireless applications [199]. Weng *et al* also demonstrated the use of Taguchi OA in the field of electromagnetics to design a linear antenna array. By employing Taguchi OA design process, they were able to obtain the optimal antenna pattern and frequency response of the microstrip band stop filter used in their work [198]. Kim *et al* [201] used the robustness property of the Taguchi OA to reduce the effects of manufacturing tolerances on the cogging torque for permanent synchronous motors.

5.2 Design and analysis of Taguchi OA

Taguchi OA design process is a three-step approach consisting of system design, parameter design, and tolerance design [202]. System design refers to the design of a model, machine, process, circuit, or prototype by understanding what is needed and what is expected; parameter design is recognizing the different variables or factors that will impact the design of the system and reduce the impact of disturbances on the system; and tolerance design refers to taking into account unpredictable parameters which can impact the design of the system.

Taguchi OA takes into account the factors that can be controlled, which are referred to as the inner array factors, and that which cannot be controlled, i.e. outer array factors. Fig. 37 shows the pictorial cube representation from Fig. 35 with a three-factor inner array and a two-factor outer

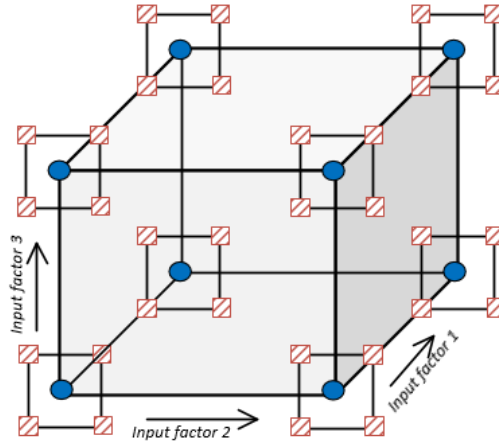


Figure 37: Pictorial representation of a Taguchi OA with 3 factor inner array and 2 factor outer array

array. The three factor inner array results in 2^3 experimental runs (corners of the cube) and at each corner, the outer arrays are considered [203]. This results in a total of 32 experiments.

A typical OA is shown in Table 8 where Y is the output response of the system. The OA can be expressed in the format $L_x A^z$, where L stands for Latin square, x is the number of rows in the array, corresponding to the number of experiments, A corresponds to the columns which represent the different levels of each factor, and z is the number of factors, i.e., control variables. Mixed level designs consisting of an additional Y factor at B levels can be expressed as $L_x(A^z B^Y)$. Standard Taguchi OAs have been described in [204] and shown in Table 9. The designed array is always orthogonal, indicating the number of factor levels in each column occur the same number of times, therefore it is balanced. To evaluate the results obtained by running experiments according to the OA design, Genichi Taguchi recommended the use of signal-to-noise ratios (S/N) [202]. These signal-to-noise ratios are

Table 8: Typical orthogonal array

L	Factors				Y		
	F_1	F_2	-----	F_n	Y_a	-----	Y_m
1	A_n				Y_{a1}		Y_{m1}
2					Y_{a2}	-----	Y_{m2}
⋮					⋮		⋮
x					Y_{ax}		Y_{mx}

$$\frac{S}{N} = \begin{cases} -10 \log \left(n^{-1} \sum_i Y_{ij}^{-2} \right) & \text{larger - the - better} \\ -10 \log \left(n^{-1} \sum_i Y_{ij}^2 \right) & \text{smaller - the - better} \\ -10 \log \left(\frac{\bar{Y}^2}{v^2} \right) & \text{Nominal is the best} \end{cases} \quad (31)$$

where $\bar{Y} = n^{-1} \sum_i Y_{ij}$ and $v^2 = (n - 1)^{-1} \sum_i (Y_{ij} - \bar{Y})^2$; i and j refer to the output response in the i_{th} row and j_{th} column, and n is the number of experiments. The larger-the-better S/N is used when the maximization of the output response is preferred. The smaller-the-better S/N is for when the output response should be minimized and the nominal-the-best S/N is when a fixed or target value is desired.

Table 9: Standard Taguchi orthogonal arrays [204]

OA size	Number of rows	Maximum number of factors	Maximum number of columns at levels shown			
			2	3	4	5
L_4	4	3	3	–	–	–
L_8	8	7	7	–	–	–
L_9	9	4	–	4	–	–
L_{12}	12	11	11	–	–	–
L_{16}	16	15	15	–	–	–
L_{16}'	16	5	–	–	5	–
L_{18}	18	8	1	7	–	–
L_{25}	25	6	–	–	–	6
L_{27}	27	13	31	13	–	–
L_{32}	32	31	1	–	9	–
L_{32}'	32	10	11	–	–	–
L_{36}	36	23	3	12	–	–
L_{36}'	36	16	1	13	–	–
L_{50}	50	12	1	–	–	11
L_{54}	54	26	63	25	–	–
L_{64}	64	63	–	–	21	–
L_{64}'	64	21	–	–	–	–
L_{81}	81	40	–	40	–	–

5.3 Design example using Taguchi OA

The discussed Taguchi OA design will be applied to an arbitrary example. Suppose it is needed to determine the impact of certain factors, type of deposition, time, and temperature, on the yield of ICs in an IC fabrication center. The objective is to find the factor levels that will maximize this yield. Table 10 can be constructed to show the factors and the factor levels.

Table 10: Design scenario example factors and factor levels

Factors	Factor levels	
	1	2
A. Deposition type	Scattering	Electroplating
B. Temperature(°C)	25	45
C. Time (min)	1	4

From Table 10, there are three factors with each factor at two levels. Using the standard arrays table in [204] and summarized in Table 9, the best OA is L_4 . This design can thus be expressed as L_42^3 . The experimental table is shown in Table 11. A, B, and C are the input factors shown in Table 10. The different levels have been coded as 1 and 2 per Table 10. The output response that is recorded is yield and the objective is to determine the impact of the factors on the yield of ICs in the fabrication center. It can be seen from Table 11 that the array is balanced since the number of factor levels occur the same number of times.

Table 11: L_4 OA showing experimental runs

Experiment number	A	B	C	Output (Yield)
1	1	1	1	95%
2	1	2	2	90%
3	2	1	2	98%
4	2	2	1	91%

Analysis of means (ANOM) can also be used to determine the factor level effects. This is achieved by calculating the mean of the yield due to each level of the factors investigated. For example, the mean yield due to the factor deposition type at level 1, i.e. scattering, A_1 , is

$$A_1 = \frac{1}{2}(95 + 90) = 92.5\% \quad (32)$$

The mean yield due to the factor temperature at level 1, i.e. 25°C, B_1 , is

$$B_1 = \frac{1}{2}(95 + 98) = 96.5\% \quad (33)$$

The rest of the means can be calculated and plotted in Fig. 38. The signal-to-noise ratio, the larger-the-better, shown in (31) can also be used to determine the impact of a factor level on the yield. The larger-the-better S/N is used since the objective is to maximize the yield. The S/N is shown in Fig. 39. From Fig. 38 and Fig. 39, it can be seen that electroplating, $temperature = 25^\circ C$, and $time = 4 minutes$, have the most impact on the yield.

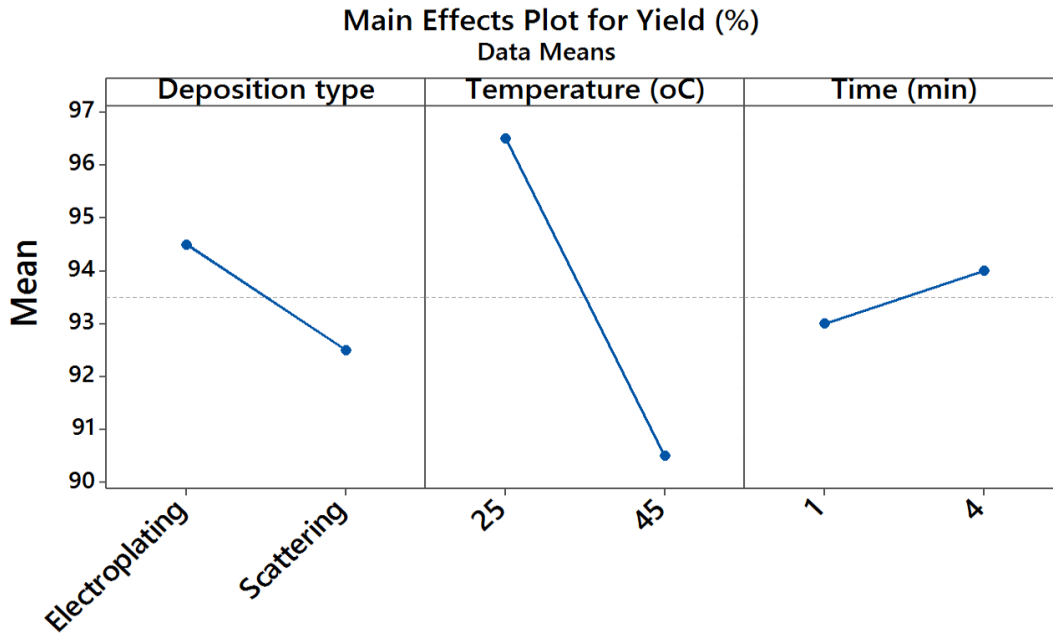


Figure 38: Main effects plot for yield

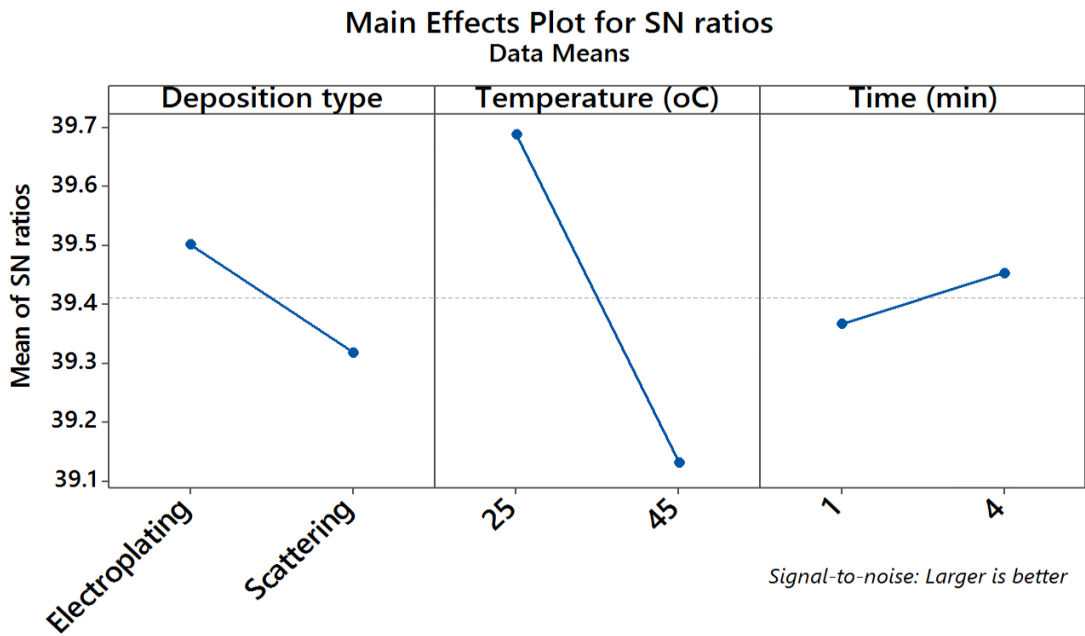


Figure 39: S/N (larger-the-better) for factor levels

By using Taguchi OA design, there is no need to perform a full factorial design as the analyzed results from the OA is comparable to a full factorial design. It has been demonstrated that by using Taguchi OA DoE method, the impact of factor levels on an output response can be determined. Further analysis, such as the analysis of variance, can also be performed to determine which factor has the most impact on an output response. The Taguchi OA design approach will be used in determining the optimal pulse charge current parameters that will result in a reduced charge time and increased battery charge and energy efficiencies.

6. THE SEARCH FOR OPTIMAL PULSE CHARGING PARAMETERS²

To get the benefits of pulse charging, the pulse charge current characteristics, duty cycle, amplitude, and frequency, must be properly selected. Depending on the selected values of these characteristics, the output performance metrics, battery charge and energy efficiencies, charge time, and life cycle will be different. From section 4.2, previous pulse chargers used varying levels of frequency and duty cycles. Chen [166] used charge frequencies equal to the frequency at which the impedance is at minimum and 50% duty cycles [168]. Other works have also used varying duty cycles [167], [180] and frequencies [180] during pulse charging. Purushothaman and Landau [181] proposed charging at 75% duty cycle because any additional rest time of the charge pulses will contribute to increased charge time. It is apparent that there is a need to find the optimal charge parameters for pulse charging based on an optimization method in order to maximize charging efficiency and reduce charge time. It is also important to determine which factors and factor levels have the most impact on certain output responses and using this information can tune output responses to fit particular applications. Taguchi OAs will be used to determine optimal pulse charge current parameters for different application specific optimized output responses. The proposed technique can be applied to different battery capacities to obtain optimal charge parameters for different applications.

6.1 Previous li-ion battery charging works using Taguchi OA

Taguchi OAs have been used in the field of li-ion battery charging [205], [206]. Wang *et al* [205]

² Part of this section is reprinted with permission from "Search for Optimal Pulse Charging Parameters for Li-ion Polymer Batteries Using Taguchi Orthogonal Arrays," J. M. Amanor BOADU, A. Guiseppi-Elie and E. Sanchez-Sinencio, IEEE Transactions on Industrial Electronics (Early access), pp. 1-1. Copyright [2018] by IEEE.

proposed a fuzzy based Taguchi method to search for an optimal rapid charging pattern based on a multi stage constant current (MSCC) method for Li-ion batteries. The MSCC method is based on the premise that the charge current reduces progressively from one stage to another. By using the measured S/N , larger-the-better for discharged capacity and smaller-the-better for charge time, as inputs to the fuzzy algorithm, the cost-benefit function of the li-ion batteries could be determined and the parameters that result in the maximization of this function can be determined. A five-stage constant current charging algorithm is used and current in each stage is used as the input factor for the Taguchi OA. Each of these five factors had three levels, therefore $L_{18}(2^1 * 3^7)$ OA was selected for the experiments. The output responses were evaluated and optimal charging pattern obtained. By using the optimal charging pattern for the five-stage constant current, battery charge efficiency was increased by 0.58% when compared to the CC-CV method. Liu and Luo [206] proposed a global optimization technique based on Taguchi OA to search for optimal charging patterns for li-ion batteries. They also proposed a five-stage constant current charging pattern and used each stage current as the control factor, similar to Wang *et al* [205]. Each control factor was evaluated at three levels. The output responses from the Taguchi OA experimental runs were evaluated and the optimal charging pattern determined. By using these optimal settings, the battery charge efficiency was increased by an average of 0.83% when compared with the CC-CV charging algorithm. These previous works using Taguchi OA to determine the optimal settings for the MSCC charging method will be compared with the results from using pulse charging operating with the optimal pulse charge current parameters that is obtained using Taguchi OA.

6.2 Search for optimal pulse charging parameters

A Taguchi design process involves the design of the system, the parameter design, and tolerance design. In this work, the system is the charger, the design parameters are i) the duty cycle of the

pulses, ii) the frequency at which the pulse charger operates, and iii) the ambient temperature at which the li-ion battery is charged. Tolerance design could refer to statistical deviations in battery impedance parameters across different batteries. This work has been presented in [33]. Fig. 40 shows the flow chart of the proposed method for searching for the optimal parameters for pulse charging using Taguchi OA modeling and analysis.

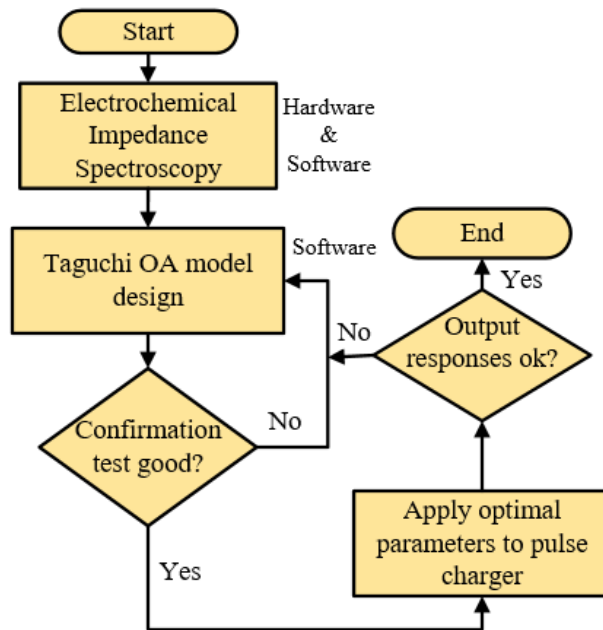


Figure 40: Proposed method for search of pulse charging optimal parameters

6.2.1 Characterization of li-ion polymer batteries

Before the Taguchi OA is designed, it is important to characterize the batteries under test. This can be done by performing EIS. The ac impedance spectrum of the batteries under test must first be determined. In this work, EIS was performed on 18 new 600 mAh 3.7 V batteries with similar

electrochemical properties to determine the frequency at which battery impedance is minimized. The chemical composition of the batteries consisted of a graphite anode, lithium cobalt oxide cathode, lithium hexafluorophosphate electrolyte, and a microporous film blend of polypropylene and polyethylene for the separator [207]. These batteries were used for all experiments, i.e. both CC-CV and pulse charging techniques. The Bode and Nyquist impedance plot of LiPo batteries under test is shown in Fig. 41. By fitting the Randles equivalent circuit with inductance and constant phase element, the battery impedance parameters can be extracted from the Nyquist plots and the probability density function (PDF) of these parameters plotted to show manufacturing variabilities. The statistical deviations of L , Q_{dl} , R_{ct} , R_s , and α across the population size, i.e. batteries under test, were fitted using probability distributions and plotted in Fig. 42. The extracted mean values of the impedance parameters of the batteries under test are shown in Table 12.

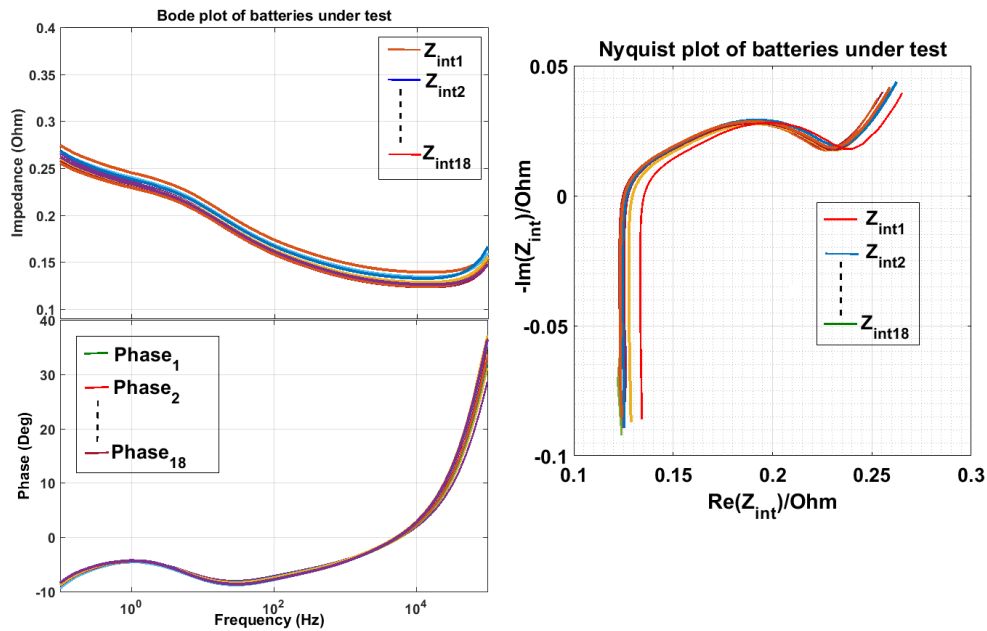


Figure 41: Bode and Nyquist impedance plot of LiPo batteries under test

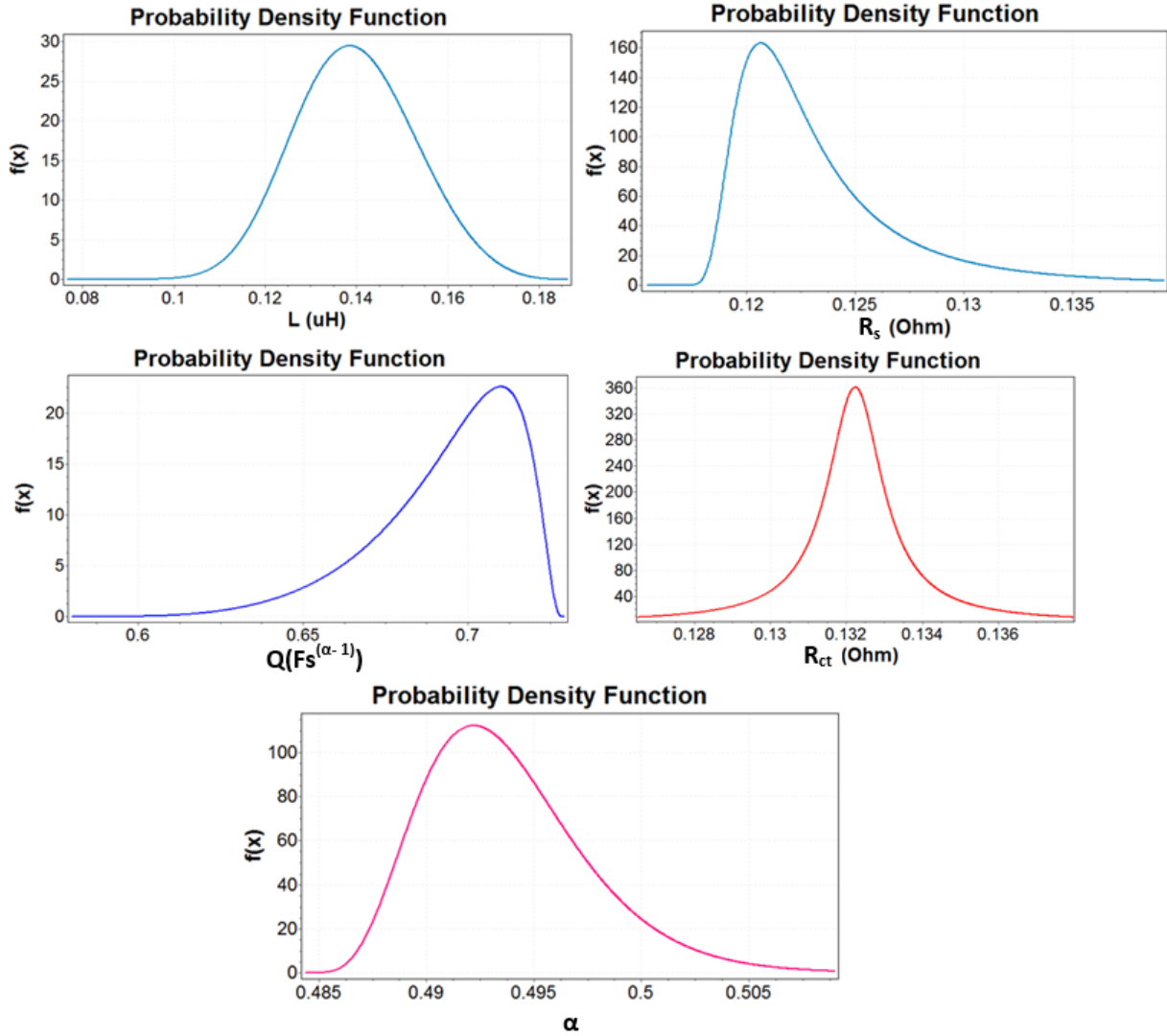


Figure 42: PDFs for extracted LiPo batteries under test impedance parameters

Table 12: Extracted mean values of the impedance parameters of the batteries under test

$R_s(\Omega)$	$Q_{dl}(Fs^{\alpha-1})$	α	$R_{ct}(\Omega)$	$L(\mu H)$
0.124	0.696	0.494	0.133	0.139

6.2.2 Taguchi OA model design

After the characterization of the batteries, the Taguchi OA model design was then initiated to determine the optimal parameters for charging. Fig. 43 illustrates the following steps involved in the model design.

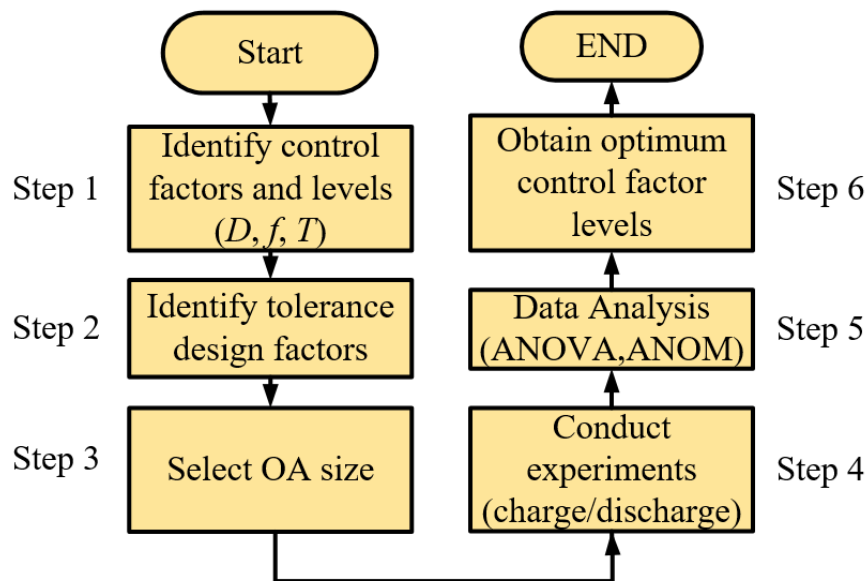


Figure 43: Taguchi OA model design procedure

6.2.2.1 Control factors identification and level determination

Different pulse charging parameters or factors will result in different battery charger performances. For parameter design, it is important to select the factors and factor levels that will impact the output responses. The factors that can be controlled during pulse charging are duty cycle, D , frequency, f , of the charge current pulses, the amplitude of the charge current, and the ambient temperature at which the battery is charged, T . For a fair comparison to the CC-CV charging

method, a charge current of 0.5C was used for all charging methods, hence the amplitude of the pulse charge current is not used as a control factor. The amplitude will be examined when comparing different charge rates and its effects on the battery η_{BE} , η_{BC} , and t_c will be evaluated. The duty cycle levels were selected based on the pulse charger circuit, which had duty cycles ranging from 20% to 80%. Therefore, the maximum, minimum, and midpoint of the pulse charger duty cycle range was chosen, and hence the levels for the duty cycle were chosen to be 20%, 50%, and 80%. Selection of frequency levels was based on the change in Z_{int} across the EIS spectrum. As frequency reduced, there was much more significant change in Z_{int} compared to frequencies above the f_{Zmin} . This is evident in Fig. 41. Six frequency levels, 0.1 kHz, 1 kHz, 6 kHz, f_{Zmin_a} , 50 kHz, and 100 kHz, were chosen based on the change in impedance of 100 m Ω across the measurement frequency range as shown in Fig. 41. Taguchi OA is beneficial in this case as all factor levels do not need to be evaluated to determine which factor level has the most impact. The statistical methods from Taguchi OA analysis is comparable to full factorial designs [198]. The ambient temperature at which the battery is charged also has an impact on η_{BE} , η_{BC} , and t_c . To evaluate the extent of this impact, the temperature levels were set at 0 °C, 23 °C, and 45 °C. The factors and their levels are shown in Table 13. Level 4 of f is f_{Zmin_a} , the mean value of f_{Zmin} of the batteries under test. The OA design is described in step 3, section 6.2.2.3.

6.2.2.2 Tolerance design

Tolerance design parameters were determined to be the impact of process parameters during manufacturing on battery impedance parameters. Fig. 44 shows the PDF for the minimum ac battery impedance Z_{int} and the f_{Zmin} of the batteries under test. Since these manufacturing differences cannot be controlled in the experimental design, the search for optimal values must be able to account for and accommodate these variations.

Table 13: Factors levels under test

Factor	Levels					
	1	2	3	4	5	6
D	0.2	0.5	0.8	–	–	–
$T(^{\circ}\text{C})$	0	23	45	–	–	–
f (kHz)	0.1	1	6	12.6	50	100

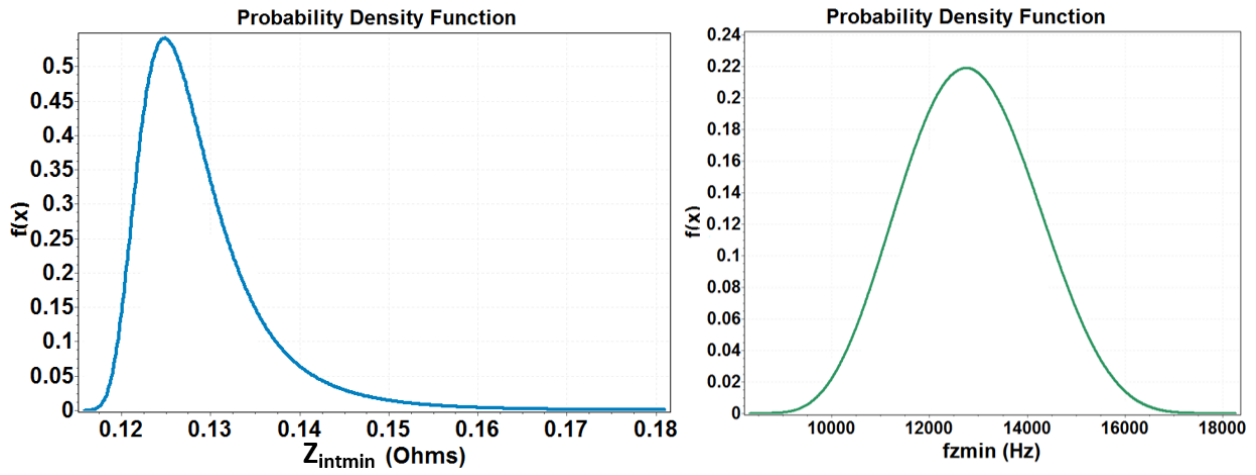


Figure 44: PDF for $|Z_{intmin}|$ and f_{zmin} of batteries under test

6.2.2.3 OA size selection

Based on three control factors, with two factors at three levels, i.e. duty cycle and the temperature at which the battery is charged at, and the last factor, frequency, at six levels, the mixed level OA was chosen to be $L_{36}(3^2 \times 6^1)$ and shown in Table 14. The OA was designed such that it was balanced, i.e., all the factor levels appear in the array for an equal number of times.

Table 14: $L_{36}(3^2 \times 6^1)$ Orthogonal array

Factors			
No	<i>T</i>	<i>D</i>	<i>f</i>
1	2	1	4
2	3	3	1
3	3	1	5
4	3	1	3
5	3	2	6
6	1	3	4
7	1	1	1
8	3	3	2
9	2	2	2
10	1	1	2
11	1	2	5
12	3	2	4
13	2	3	5
14	3	2	4
15	3	3	2
16	3	3	1
17	2	2	1
18	2	1	4
19	1	3	4
20	1	2	3
21	1	1	2
22	1	1	1
23	2	1	6
24	1	2	3
25	3	2	6
26	2	1	6
27	2	3	5
28	3	1	5
29	2	3	3
30	2	2	1
31	1	2	5
32	1	3	6
33	3	1	3
34	2	2	2
35	2	3	3
36	1	3	6

6.2.2.4 Conduction of experiments

The OA design resulted in the total number of experiments being equal to 36. The charging and discharging of the LiPo batteries were both performed at charge/discharge rate of 0.5C in a controlled temperature chamber. The charging pulse parameters were applied at the specific temperatures per Table 14. The battery energy and charge efficiencies were evaluated using (1) and (2) and charge time was recorded.

6.2.2.5 Data analysis

Analysis of the evaluated results were used to determine the optimal factor levels to maximize battery charge and energy efficiencies while minimizing charge time. By using the objective function, the optimal factors that minimize battery charge time and maximize battery charge and energy efficiencies can be determined. The effects of factor levels on the output responses, η_{BC} , η_{BE} , and t_c , can be evaluated from the differences of the average S/N for the output responses corresponding to these levels and the overall mean. Effects of factor level, n , can be calculated using (34).

$$A_{L_n} = \left(\frac{1}{n_{L_n}} \sum_{i_{L_n}} Y_{i_{L_n}j} \right) - \bar{Y} \quad (34)$$

where A_{L_n} is the effect of factor level n on the output response, Y_j , n_{L_n} is the number of output responses corresponding to level n , and i_{L_n} refers to the rows corresponding to level n responses only. The effects of the factors on the output responses can also be determined by the decomposition of their variance and computation of sum of squares. Sum of squares due to factor n can be expressed as

$$SS_{F_n} = \sum_{L_n} \left(n_{L_n} \cdot \left(\frac{1}{n_{L_n}} \sum_{i_{L_n}} Y_{i_{L_n}j} - \bar{Y} \right)^2 \right) \quad (35)$$

6.2.2.6 Optimal parameters evaluation

Optimal parameters were then obtained from these analyses and used to run confirmation tests for verification and validation.

6.2.3 Pulse charger design

A pulse charger was designed such that the duty cycle could be changed without affecting frequency and vice versa. Fig. 45 shows the circuit diagram of the designed pulse charger. The pulse charger will take its voltage input from a current limited wall adapter, V_{in} , and pulse the charge current through the pass transistor, Mp , into the battery. The duty cycle and the frequency at which Mp is operated is controlled by the duty cycle-frequency adjuster circuit (DC-FAC). When a battery, serving as a device under test load, was placed in the circuit, the voltage detector and fuel gauge determine if the battery is fully charged or not. If it is fully charged, the pulse charger is switched off, otherwise, the DC-FAC is activated. The R input of the latch is low initially since $V_{1+} < (V_{1-} = 2/3V_{in})$ for $R1 = R2 = R3$. The output, Q , goes high for $V_{2+} > V_{2-}$. C_f charges through D_c with a timing resistance of $R_o + R_{d_right} + R_{xc} + R_{DC}$, where R_{d_right} is the resistance to the right of the variable resistor and R_{DC} is the resistance of the diode. When V_{Cf} reaches $2/3V_{in}$, the R input of the latch goes high, Q is reset to 0, starting the discharge phase of C_f through D_d , R_{xd} , R_{d_left} , and R_o , where R_{d_left} is the resistance to the left of the variable resistor. By varying the values of R_{d_left} and R_{d_right} , the duty cycle of the pulse charge current can be changed.

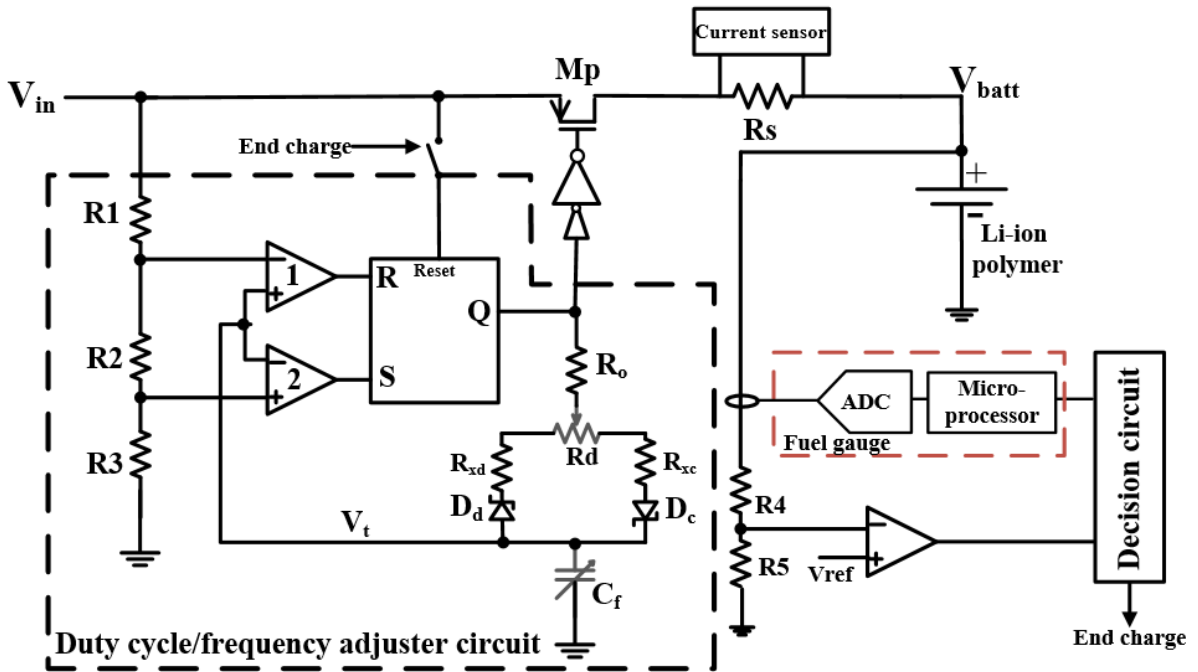


Figure 45: Pulse charger schematic

Since C_f is charged to only $2/3V_{in}$, the time constant during charging is $T_{charge} = 0.7 (R_o + 1/(2R_d) + R_{xc})C_f$ and the time constant during discharging is $T_{discharge} = 0.7 (R_o + 1/(2R_d) + R_{xd})C_f$. The frequency, f , is, therefore, equal to $1/1.4(R_o + 1/(2R_d) + R_{xd})C_f$. Mp will be pulsed at the set frequency and duty cycle. A simulation showing the pulse charger waveforms during operation is shown in Fig. 46. The *End charge* signal goes low when the battery voltage reaches 4.1V. LiPo batteries are sensitive to overcharge and any sort of overcharge can potentially damage the battery. To prevent overcharge and ensure safety, two methods of charge termination were implemented. A battery fuel gauge was used to track the state of charge (SoC) of the battery and a voltage detector to track the battery voltage to prevent battery overvoltage conditions. The fuel gauge terminates charging when SoC reaches 100%, while the

voltage detector was set at 4.1 V per battery data sheet specifications [207]. The current sensor was used to monitor the charge current.

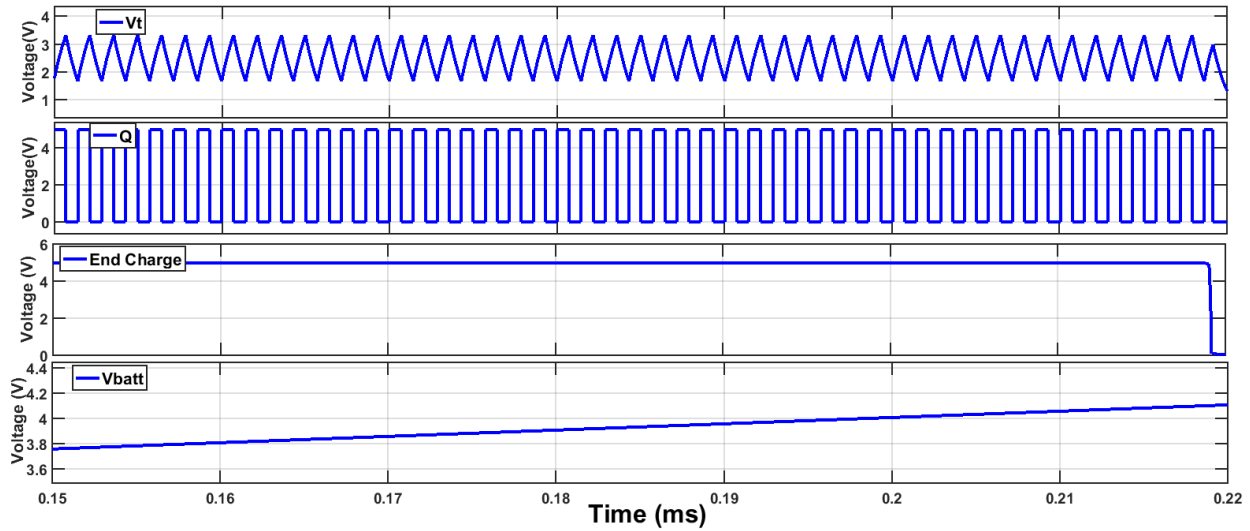


Figure 46: Designed pulse charger waveforms

6.3 Experimental results

The experimental setup is shown in Fig. 47. A Gamry Instruments Interface 1000E Potentiostat/Galvanostat/Zero Resistance Ammeter was used to determine the impedances of the batteries under test across a frequency range of 0.1 Hz to 100 kHz. This is shown in Fig. 41. The average Z_{intmin} was found to be 129 m Ω with an error margin of 0.18% across the minimum frequency range. The f_{zmin} of the batteries was determined to be at 12.6 kHz. The frequency information obtained from the EIS, together with the duty cycle of the pulse charger was used to select the levels of the factors to be used in the Taguchi OA design and analysis. The ambient temperature at which the battery was charged was also taken into consideration. Charge and

discharge cycles were performed per Table 14 and results recorded in Table 15.

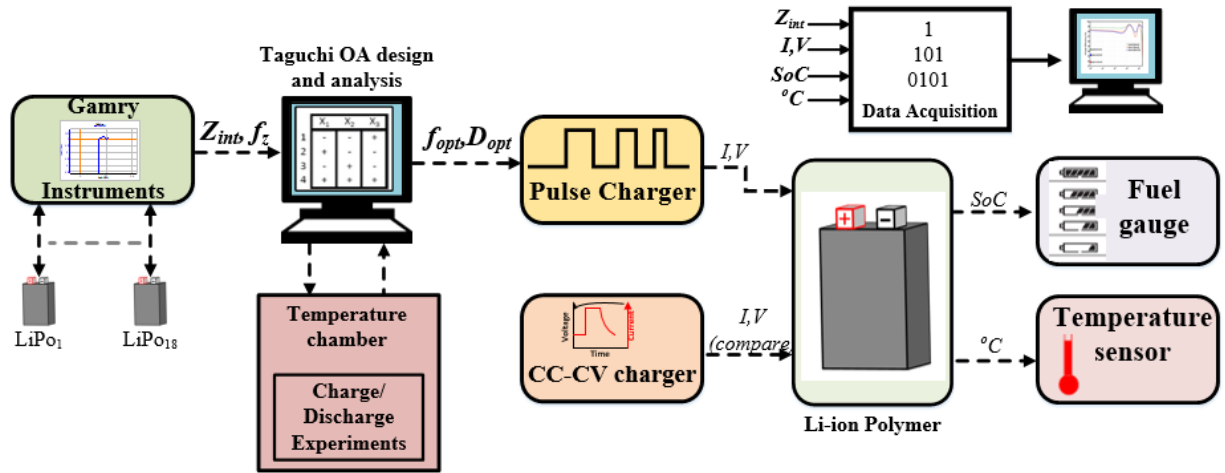


Figure 47: Experimental test setup for searching for optimal pulse charger parameters for LiPo batteries

Based on the results of the analysis, any output response can be maximized or minimized depending on the application. Depending on the application, charge time would be of much more concern than charge efficiency, hence appropriate optimal values to reduce charge time can be selected. The objective of this work was to determine the factor levels that maximize η_{BC} and η_{BE} and minimize t_c of LiPo when undergoing pulse charging. By evaluating the output responses shown in Table 15 using (35), ANOVA, the factor with the largest contribution to the total sum of squares can be determined. Duty cycle was found to make the largest contribution to all three output responses, 61.1% to η_{BE} , 61.8% to η_{BC} , and 68.0% to t_c . The frequency of operation of the pulse charger made the next largest contribution to t_c . The temperature at which the battery was

Table 15: Output responses of Taguchi OA experiment

Outputs				Outputs			
No	$\eta_{BC}(\%)$	$\eta_{BE}(\%)$	$t_c(\min)$	No	$\eta_{BC}(\%)$	$\eta_{BE}(\%)$	$t_c(\min)$
1	83.8	75.0	45.3	19	86.4	77.5	47.0
2	95.2	88.5	134.9	20	84.9	88.3	103.4
3	69.5	62.7	66.4	21	100.0	68.7	60.8
4	83.5	75.3	52.8	22	78.2	21.8	45.5
5	84.8	78.7	99.0	23	24.7	62.2	101.9
6	100.0	89.9	96.2	24	69.3	88.8	63.9
7	28.4	26.2	167.5	25	100.0	91.5	43.1
8	68.6	64.1	141.2	26	100.0	69.2	78.9
9	100.0	90.4	87.4	27	76.8	92.3	54.8
10	47.8	42.3	41.5	28	100.0	67.6	95.8
11	78.9	68.8	62.7	29	74.9	62.3	62.8
12	100.0	95.1	91.9	30	68.3	92.1	120.8
13	94.2	88.1	122.2	31	100.0	88.4	84.2
14	100.0	92.4	82.2	32	100.0	53.2	60.3
15	100.0	92.2	112.5	33	60.0	84.8	106.6
16	100.0	92.9	111.0	34	94.7	80.7	48.0
17	100.0	92.1	68.4	35	87.7	92.4	100.7
18	83.8	76.9	45.3	36	100.0	84.1	95.3

charged contributed 20.5%, 24.7%, and 2.2% to η_{BC} , η_{BE} , and t_c . These analyses help the designer with what factors to pay more attention to in relation to a specific output performance metric. Evaluating (31) and (34) using the output responses in Table 15, the optimal factor levels can be determined and plotted in Fig. 48 and Fig. 49.

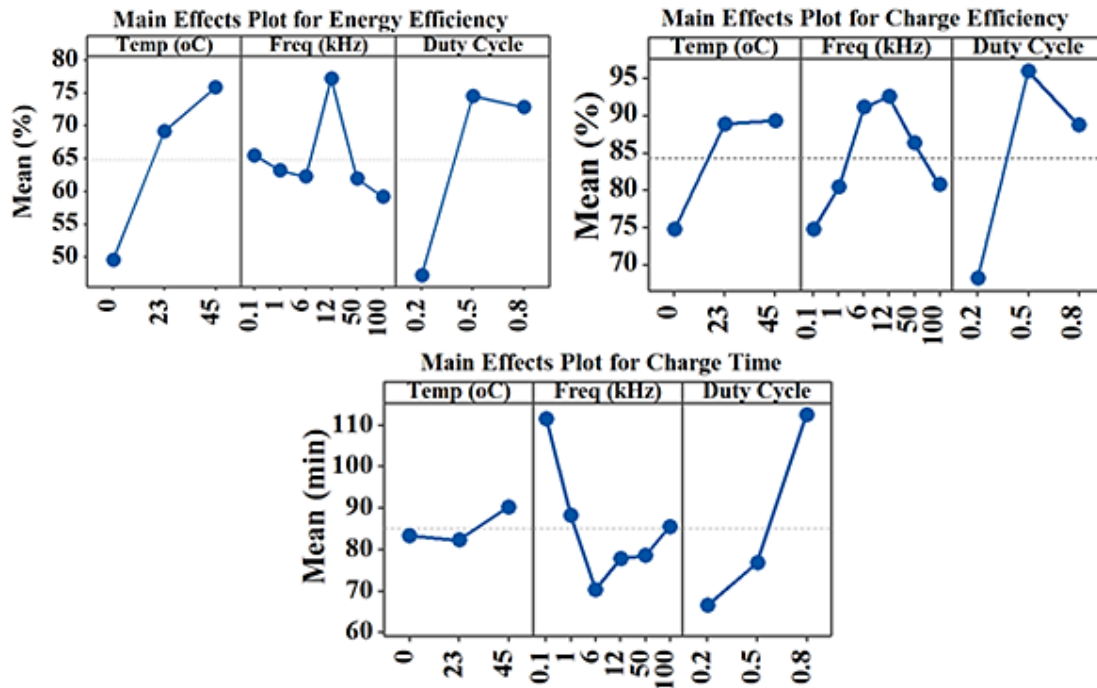


Figure 48: Main factor effects for output response using ANOM

From these figures, it is possible to see the behavior of the system across the different factors and their levels. Both ANOM and S/N evaluations produced similar trends. For example, analyzing the trend of charge time across temperature, using the smaller-the-better S/N , since the reduction in charge time is important, Fig. 49 produced a similar trend to Fig. 48.

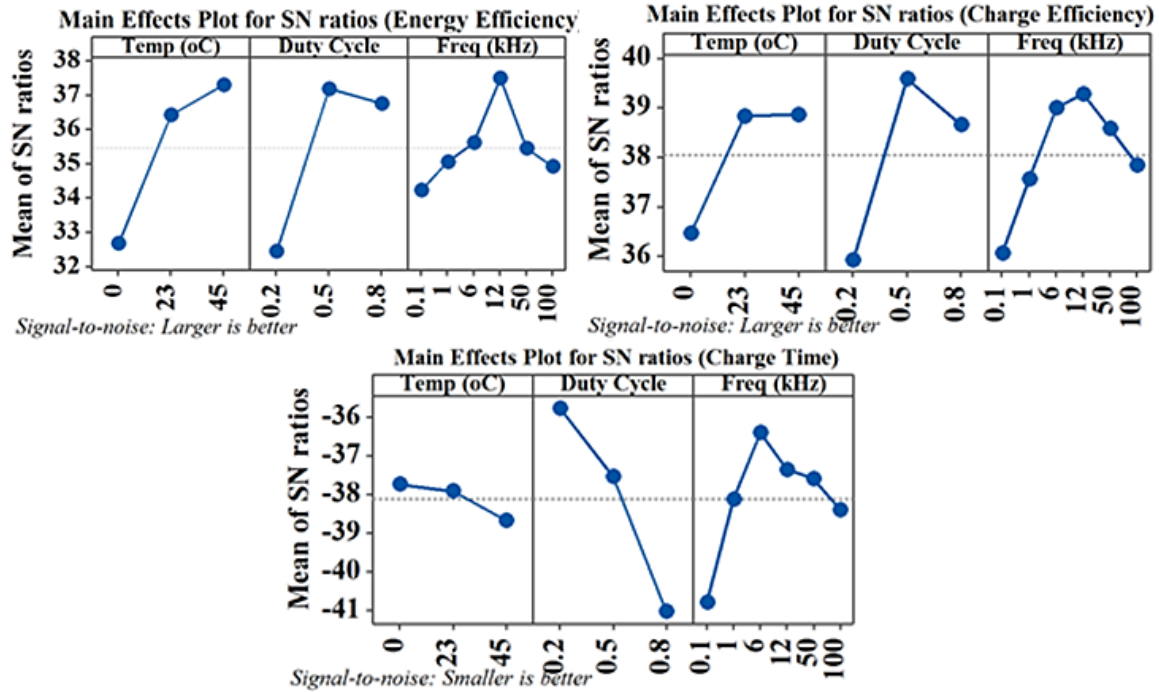


Figure 49: Main factor effects for output response using S/N

The factor levels that have the greatest impact on the LiPo battery output performance metrics can also be determined from these figures. The factor levels that correspond to the greatest impact on η_{BC} and η_{BE} are $f = 12.6\text{kHz}$ (f_{zmin}), $D = 0.5$, and $T = 45^\circ\text{C}$. Among these, f and D exhibit the greatest impact, also determined using ANOVA. Charging at f_{zmin} minimizes energy losses, thereby increasing η_{BC} and η_{BE} . In terms of the ambient temperature at which the battery was charged, as a general rule of thumb the rate of reaction doubles for every 10°C rise in temperature [208]. However, there was less than 3% change in η_{BC} and η_{BE} in going from 23°C to 45°C . The factor levels that had the greatest impact on t_c were $f = 6\text{kHz}$, $D = 0.2$, and $T = 23^\circ\text{C}$. It can definitely be seen that for only reduction in charge time, the optimized factor levels are different from that obtained if the objective is higher battery charge or energy efficiency. With battery

charge and energy efficiencies and charge time having different optimal factor level values, the user can determine which output responses are paramount and select that which is suitable for the application. In this work, high efficiency is important as the discharge of the battery, such as usage of a cell phone, can be prolonged after charging. Operating the pulse charge at 20% duty cycle and 6 kHz results in very poor η_{BE} . The difference in charge time is +10 minutes and + 15% for η_{BE} when comparing charging at $f = 6kHz$, $D = 0.2$, $T = 23\text{ }^\circ\text{C}$ to charging at $f = 12.6\text{ kHz}$ (f_{zmin}), $D = 0.5$, $T = 45\text{ }^\circ\text{C}$. Across frequency, f_{zmin} produced the best η_{BC} and η_{BE} . This is evident in Fig. 48 and 49. By using S/N ratios (31), the larger-the-better for η_{BC} and η_{BE} and the smaller-the-better for t_c , the factor level effects can also be seen in Fig. 49. Regarding the ambient temperature at which the battery is charged, charging at $0\text{ }^\circ\text{C}$ produced poor η_{BC} and η_{BE} and longer charge time. This is due to the reduced mobility of the Li^+ at that temperature.

A confirmation experiment was run at f_{zmin} across various duty cycles and is presented in Fig. 50. This confirms what was previously observed in Fig. 48, i.e., charge time increases with D , and maximum η_{BE} occurs at f_{zmin} . The increase in t_c as the duty cycle increased was due to the LiPo battery not having enough rest between pulses for effective ion redistribution, thereby contributing to concentration polarization and preventing the maximum charge from being absorbed.

Using the optimal factor levels of $f = 12.6\text{ kHz}$ (f_{zmin}) and $D = 0.5$ to maximize η_{BC} and η_{BE} , the pulse charge method was compared with the CC-CV charge method across temperature at a charge and discharge rate of 0.5C and results shown in Fig. 51. The batteries were allowed to rest for about an hour, to ensure equilibrium of chemical reactions, and then discharged at a rate of 0.5C. Across all output responses, pulse charging produced better results. These improvements are

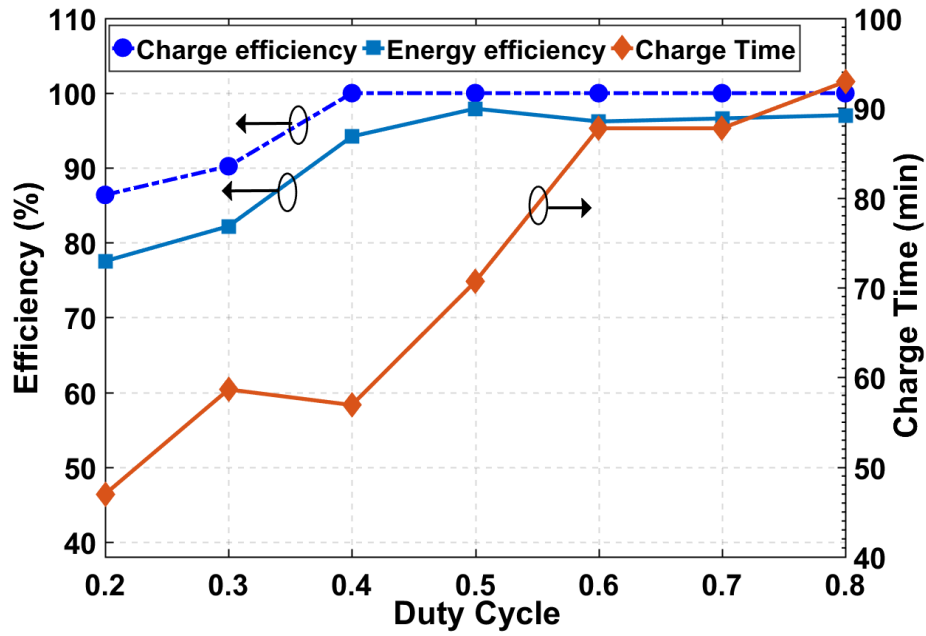


Figure 50: η_{BC} , η_{BE} , t_c vs D

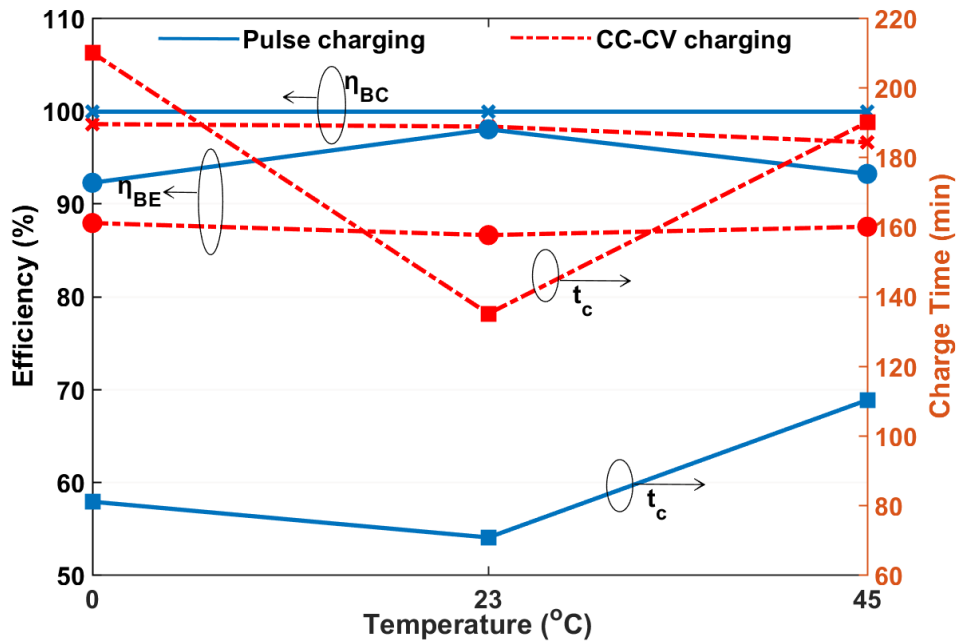


Figure 51: CC-CV charge method vs Pulse charge method (50% duty cycle, f_{zmin})

Table 16: Charge improvement - Pulse charge vs CC-CV at 0.5C charge rate

Output responses	Charge method		
	CC-CV	Pulse	Improvement
η_{BE} (%)	86.6	97.9	11.3% increase
η_{BC} (%)	98.4	99.9	1.5% increase
t_c (min)	135.0	70.7	47.6% reduction

summarized in Table 16 for a charge rate of 0.5C. The confirmation results were parsed out for $T = 23$ °C, since most portable devices are used at room temperature. These results are shown in Fig. 52. Fig. 51 and Fig. 52 confirm the trends indicated in Fig. 48, for example, concerning charge time, i.e. charging at room temperature produced the minimum charge time. The longer charge time of the CC-CV charge method is due to the CV stage where a decreasing charge current was used to prevent overcharging. It is observed that η_{BE} for both charging methods in Table 16 are lower than η_{BC} . This is attributed to the voltage efficiency of the battery, the ratio of the average battery discharge voltage to the average battery charge voltage [209], [210], which is affected by polarization and ohmic losses. From Fig. 7, V_{batt} will be higher during charging and lower during discharging. Using the proposed pulse charging method reduced these losses contributing to a much higher η_{BE} when compared to the benchmark method.

Compared with [205] and [206], where they used Taguchi based approach for MSCC, this work produced a better charge efficiency improvement when compared with the CC-CV charge method, a 1.5% increase compared to a 0.58% increase in [205] and 0.83% increase in [206].

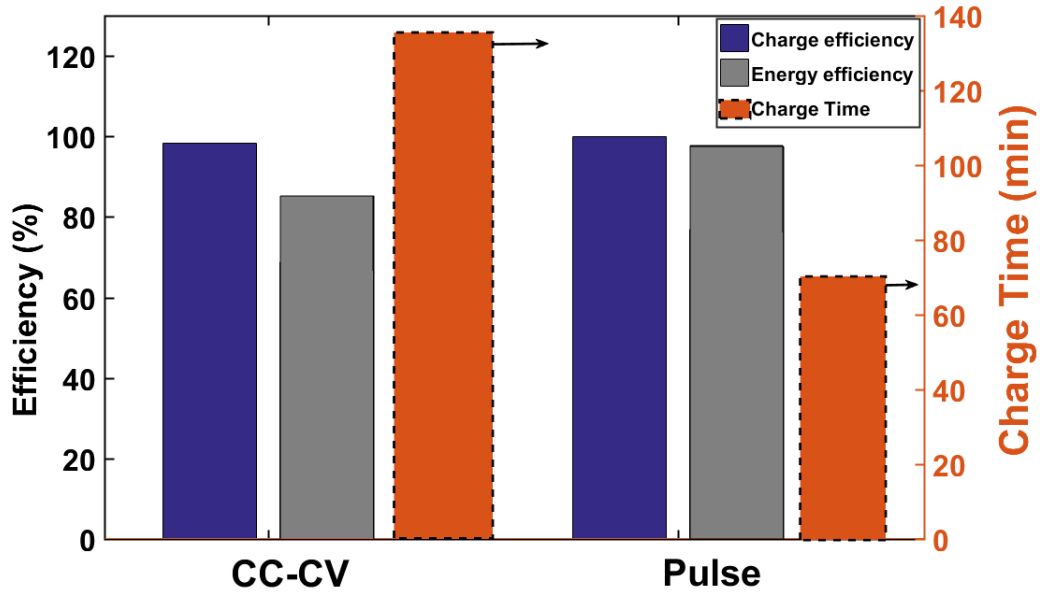


Figure 52: CC-CV vs Pulse at room temperature (23°C) at 0.5C charge rate

Table 17: Output responses at the different charge rates

Output responses	1C		2C	
	CC-CV	Pulse	CC-CV	Pulse
η_{BE} (%)	83.0	90.6	85.4	79.8
η_{BC} (%)	91.1	99.2	88.9	96.1
t_c (min)	79.7	33.5	66.8	19.8

The proposed pulse charging method operating at selected optimal parameters was also compared with the CC-CV charge method at the charge rates of 1C and 2C. In the CC-CV charging method, the CC phase charge current was 600 mA and 1200 mA with respect to the charge rates of 1C and

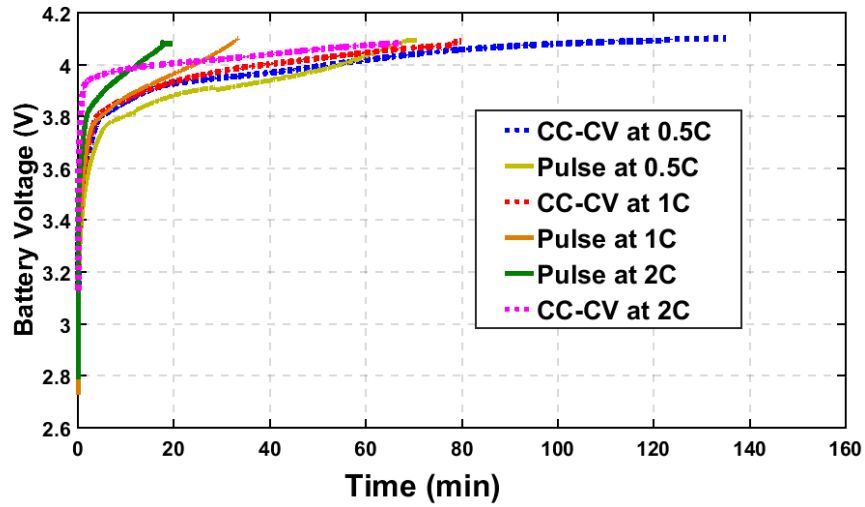


Figure 53: Battery charge curves at different charge rates

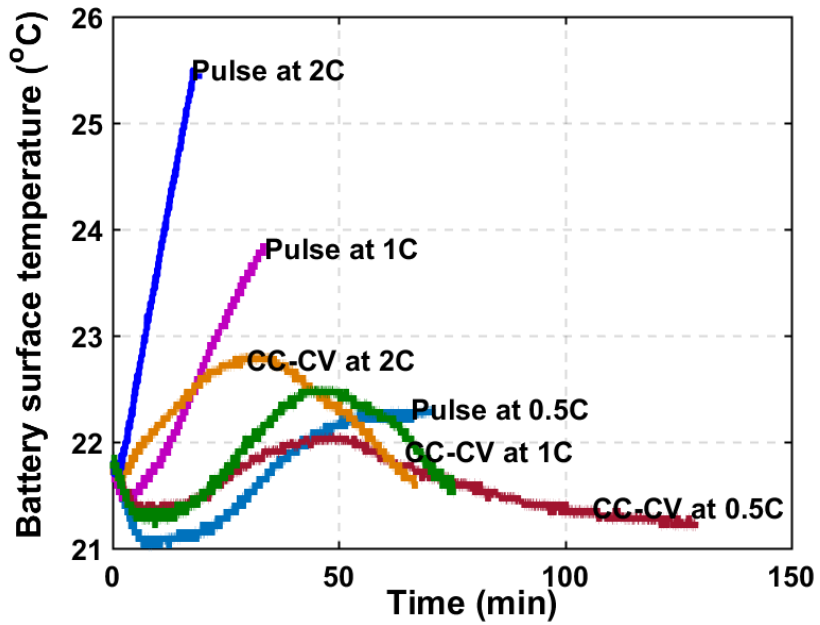


Figure 54: Battery surface temperature during charging at different charge rates

2C. Table 17 summarizes these results. Fig. 53 shows the battery charging voltage vs charge time curves at different charge rates. Fig. 54 shows the battery surface temperature characteristics during charging for the two charging methods at different charging rates. It is noticed that across all the different charge rates, the proposed pulse charging method produced a much faster charge time but at a slightly higher battery surface temperature when compared to the CC-CV method.

At a charge rate of 2C, the proposed pulse charger produced a charge time reduction of 70.4% but at a rapidly increasing battery surface temperature as shown in Fig. 54. Pulse charging at higher rates, 1C and above, means the battery is subjected to higher peak charge current amplitudes according to (17). At a 2C charge rate, the battery is subjected to a peak charge current of 2400mA, i.e. 4C in terms of charge rate. The battery can be subjected to overvoltage conditions which results in early charging termination to prevent damage to the battery. A consequence of this early charging termination is the reduced discharge capacity of the battery, i.e. limited usage time of the battery. At high charging rates, the life cycle of the battery can be negatively impacted [211] and drastically reduced. It is not advisable to subject the battery to such high peak currents, even though temperature rise is reasonable.

Observing the battery surface temperature during charging at the different charge rates, there was an initial drop in the battery surface temperature during charging. This was due to the endothermic reactions [193], [212] at the beginning of charging, which then becomes overwhelmed with other sources of heat as charging continues and hence, the increase in temperature. The higher temperature rise is more noticeable at the charge rates of 1C and 2C. Although this temperature rise is within the Japan Electronics and Information Technology Industries Association (JEITA)

guidelines for battery charging safety in the standard temperature range [213], shown in Fig. 55, the increased charge rate can lead to reduced battery life cycle [211].

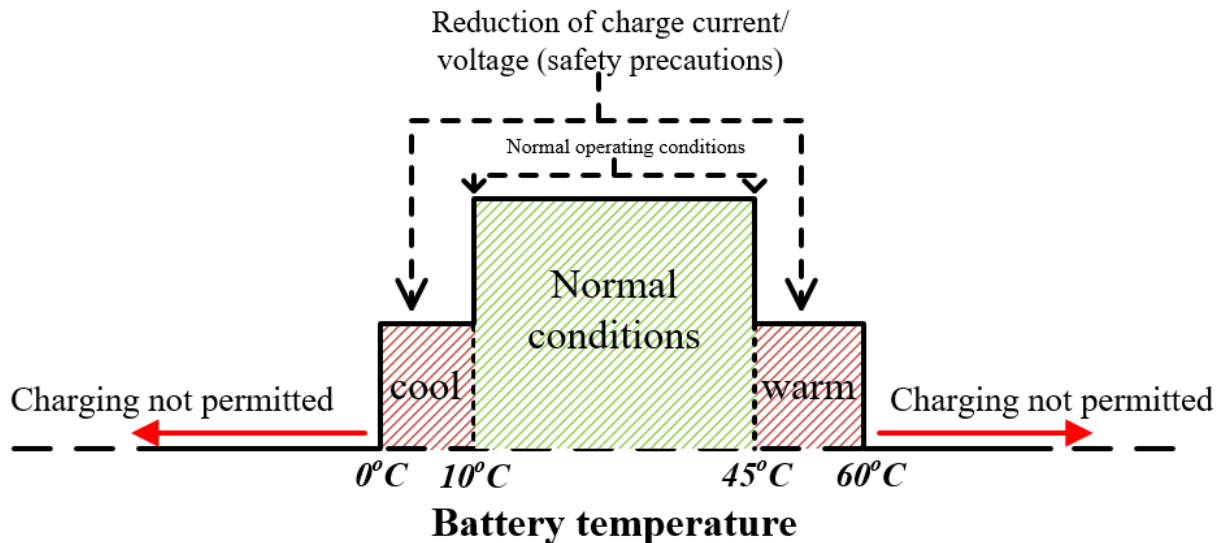


Figure 55: JEITA guidelines for li-ion battery charging

By using the pulse charger at the obtained optimal settings, η_{BC} and η_{BE} improved by 1.5% and 11.3% respectively, and charge time was reduced by 47.6% at a charge rate of 0.5C. Additionally, at a charge rate of 1C, η_{BC} and η_{BE} improved by 8.1% and 7.6% respectively, and charge time was reduced by 58.0%.

6.4 Summary

A new technique to experimentally search for the optimal parameters for the pulse charging of a LiPo battery by using Taguchi orthogonal arrays has been proposed [33]. This approach can be extended to both large battery capacities, such as those used in electric vehicles, and smaller battery

capacities, such as those used in portable electronic applications. This technique provides the optimal parameters that maximize battery charge and energy efficiencies while decreasing charge time. The approach can also be extended to select factors and factor levels that maximize or minimize any preferred output performance metric. The design of the Taguchi OA, the experimental procedure, the design of the pulse charger, and analysis of the output responses data have been presented in the preceding sections. The optimal parameters for the pulse charging of a 3.7V 600 mAh LiPo battery was determined to be 50% duty cycle, which gives an equal time for the battery to absorb and redistribute charge efficiently, a frequency equal to the frequency at which the minimum ac impedance of the battery occurs, which minimizes the energy losses in the battery, and room temperature, which is ideal for most applications. When compared with the benchmark CC-CV charge method, operating the pulse charger at these parameters increased battery energy and charge efficiencies by 11.3% and 1.5% respectively, and decreased charge time by 47.6%. This work has demonstrated that by using the methods presented herein, optimal parameter values of a pulse charger can be determined.

Determination of these relevant parameters is important for optimal operation of the charger. It is also important to determine the impact of the pulse charge current parameters on the battery impedance parameters over time and the battery life cycle. This can also be achieved by using the Taguchi OA design method.

7. THE IMPACT OF PULSE CHARGING PARAMETERS ON LI-ION POLYMER BATTERY LIFE CYCLE

The optimal parameters for obtaining a certain preferred output response have been determined by employing a DoE approach, Taguchi OA. This has been described in section 6 and also presented in [33]. After obtaining these optimal parameters, it is important to determine how they impact the battery characteristics, i.e. battery impedance parameters and life cycle. Determining the life cycle of batteries, which is impacted by battery impedance parameters, is important as it gives relevant information about whether using a particular charging system or algorithm results in a reduced life cycle. This information can help determine the cost (frequent replacement of batteries leads to increased cost), performance of systems being powered by the batteries, and necessary implementation of safe guards to ensure continued system operation.

7.1 Techniques for determining the impact of charging parameters on batteries

To determine the impact of charging parameters on the life cycle of the battery, it is important to use techniques that give relevant information about the battery characteristics. These techniques can be classified as destructive and non-destructive [214].

Destructive techniques involve disassembling the battery to investigate the current state of its internal components, in terms of structure, chemical composition, and morphology. These techniques can be used to determine how different charging methods have impacted SEI formation [215], electrode morphology and structure [216], [217], dendrite depositions [218], [219], separator [220], and electrolyte degradation [221], [222]. Investigation of these battery internal components can be performed using scanning electron microscopy (SEM) [214], [216], [217],

[219], [223], atomic force microscopy (AFM) [215], [221], X-ray diffraction (XRD) [223]-[226], Raman microscopy [221], [224], and electron probe microscopic analysis (EPMA) [227], of which SEM is the most popular.

Non-destructive techniques do not involve the disassembling of the battery and have been known to be popular ways for determining the battery impedance and performance across its life cycle. These techniques include cyclic voltammetry [94], [225], [227], impedance measurements, charge-discharge tests, and impedance spectroscopy [228], of which impedance spectroscopy is the most popular [229]. In this work, a combination of different non-destructive techniques will be used to characterize the battery aging, in effect its life cycle and the impact on battery impedance parameters.

By using the Taguchi OA design method described in section 6 in combination with regression analysis, the factors and factor levels that have the greatest impact on the life cycle of the battery can be determined. The impact of the pulse charge current duty cycles and the ambient temperature at which the battery is charged are also investigated. The results of these evaluations are compared with the benchmark CC-CV charging method.

7.2 Overall experimental test configuration

The overall system test setup is shown in Fig. 56. The batteries under test are placed in a temperature chamber, TestEquity model 107 [230], and experiments conducted according to Table 14. The recorded results were analyzed and the regression analysis performed. The pulse charging of the batteries was performed at 0.5C to ensure a fair comparison with the CC-CV charging algorithm, which was also performed at 0.5C. The pulse charger designed to conduct the

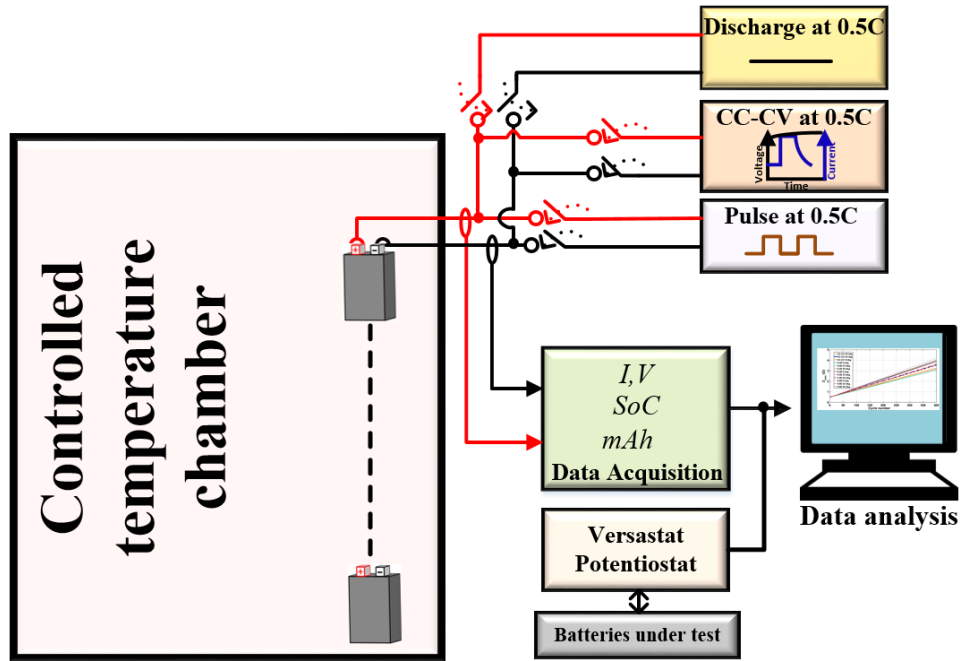


Figure 56: Experimental setup for determining impact of pulse charging parameters on LiPo batteries

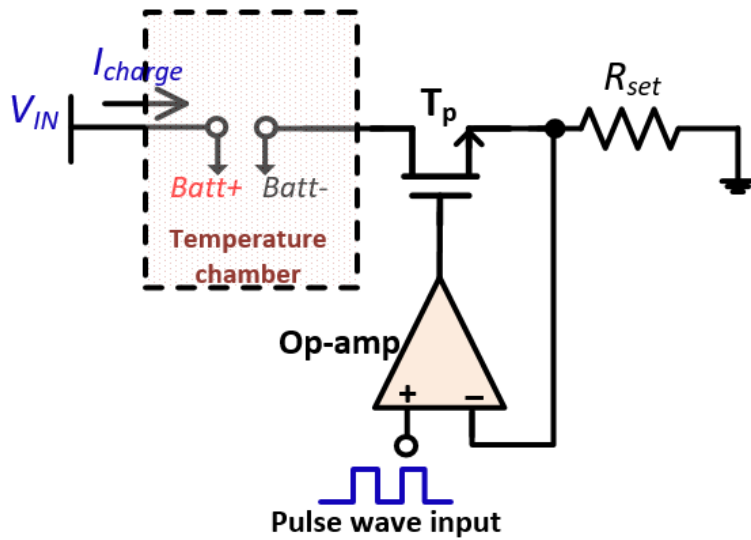


Figure 57: Pulse charger design for conducting experiments

experiments is shown in Fig. 57. The op-amp, through its negative feedback and characteristics, ensures that the applied unipolar pulse wave input is present at the source of the transistor, T_p , and hence a pulse current is generated whose average value will depend on R_{set} . This pulse charge current is then applied to the battery under test in the temperature chamber.

After each charging cycle, the batteries under test subsequently underwent a DOD of 100% after resting for an hour. 438 cycles were performed in total. Battery impedance characteristics were measured by performing an EIS using a Versastat Potentiostat [188] and the Nyquist plots analyzed by using the Simplex method [105] for curve fitting to obtain battery impedance parameters. Battery capacity measurements were also performed.

7.3 Experimental results and observations

The impact of pulse charge duty cycles and the ambient temperature at which the battery is charged on the battery impedance parameters will be investigated. The life cycle of batteries subjected to both pulse and CC-CV charging will be also be analyzed.

7.3.1 The impact of charging characteristics on battery impedance parameters

By fitting the Randles equivalent circuit with constant phase element to the obtained curves from the EIS, battery impedance parameters, Q_{dl} , R_{ct} , and R_s , of the batteries subjected to pulse charging were obtained. The trend of these parameters across the number of charge and discharge cycles was analyzed and plotted in Fig. 58 and Fig. 59. This trend was also compared with that obtained from batteries subjected to the CC-CV charging algorithm.

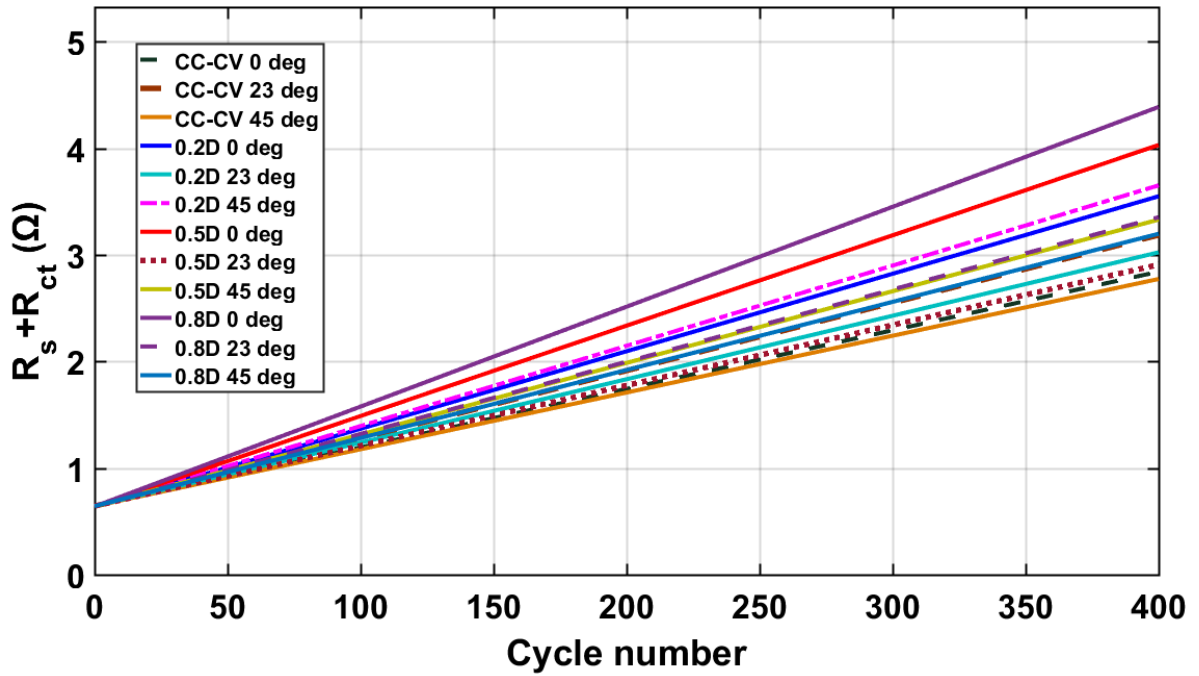


Figure 58: $R_s + R_{ct}$ vs number of charge and discharge cycles at 100% DoD

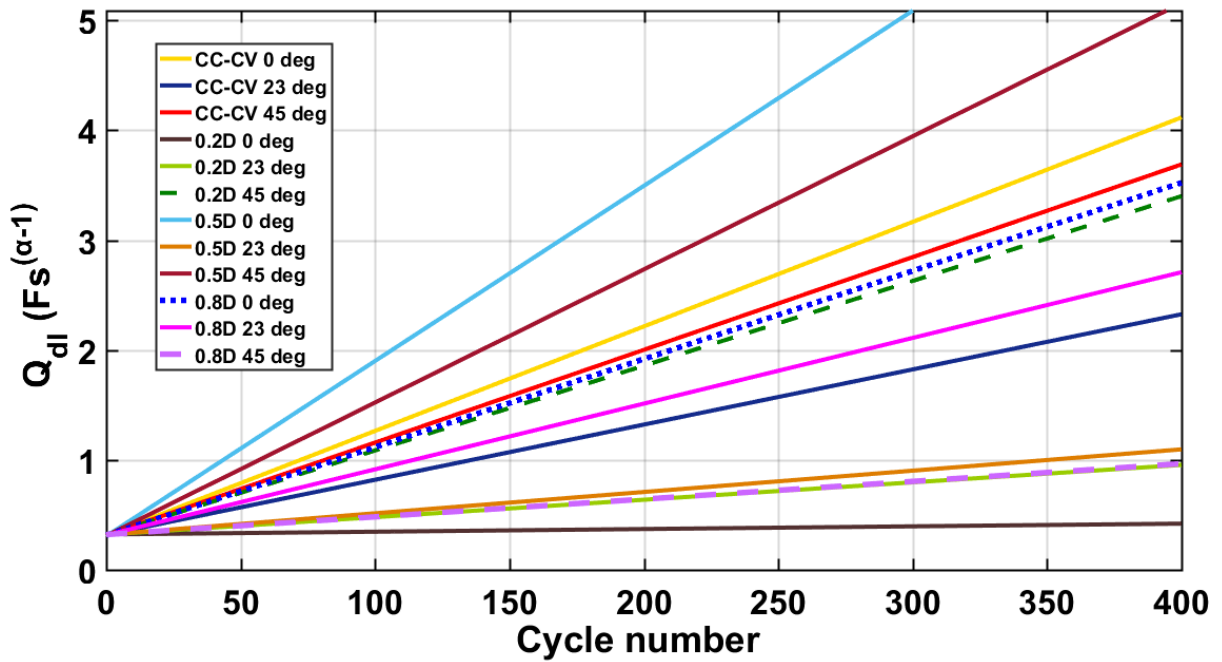


Figure 59: Q_{dl} vs number of charge and discharge cycles at 100% DoD

In general, battery impedance parameters increase as the number of charge and discharge cycles increase. This increase in impedance may be due to electrolyte decomposition, increase in surface film growth, reduction in active materials [225], [227], [229], [231], and other effects that are produced due to various side chemical reactions. These side reactions usually occur at the electrode/electrolyte interface [229]. These result in different degradations at the anode and cathode. Cathode degradation can arise from structural changes that occur during charge and discharge cycles while anode degradation can arise from increase in surface film growth (SEI) [232]. A combination of these degradation mechanisms can be examined using EIS, from which the battery impedance parameters can be obtained.

The battery impedance parameters, Q_{dl} , R_{ct} , and R_s , that were obtained from performing EIS, were observed to increase as the number of cycles increased for both charging algorithms. Fig. 58 and Fig. 59 are further separated using ambient temperature as a criterion and shown in Fig. 60 and Fig. 61. From Fig. 58 and Fig. 60, battery $R_{ct} + R_s$ values were much higher at 0 °C. This is due to the limited movement of Li^+ in the electrolyte and diffusion into the electrodes at that temperature. This also affects the capacity of the battery. LiPo batteries subjected to pulse charging at 0 °C demonstrated larger $R_{ct} + R_s$ values when compared to that of batteries subjected to CC-CV. At the 50th cycle mark, LiPo batteries subjected to pulse charging had impedances that were 15% higher than the batteries subjected to CC-CV. This difference became more profound as the cycle number increased. At room temperature, 23°C, the $R_{ct} + R_s$ was comparable across batteries subjected to both pulse and CC-CV charging algorithms. At 45°C, batteries subjected to CC-CV had much lower values of $R_{ct} + R_s$ than that subjected to pulse charging.

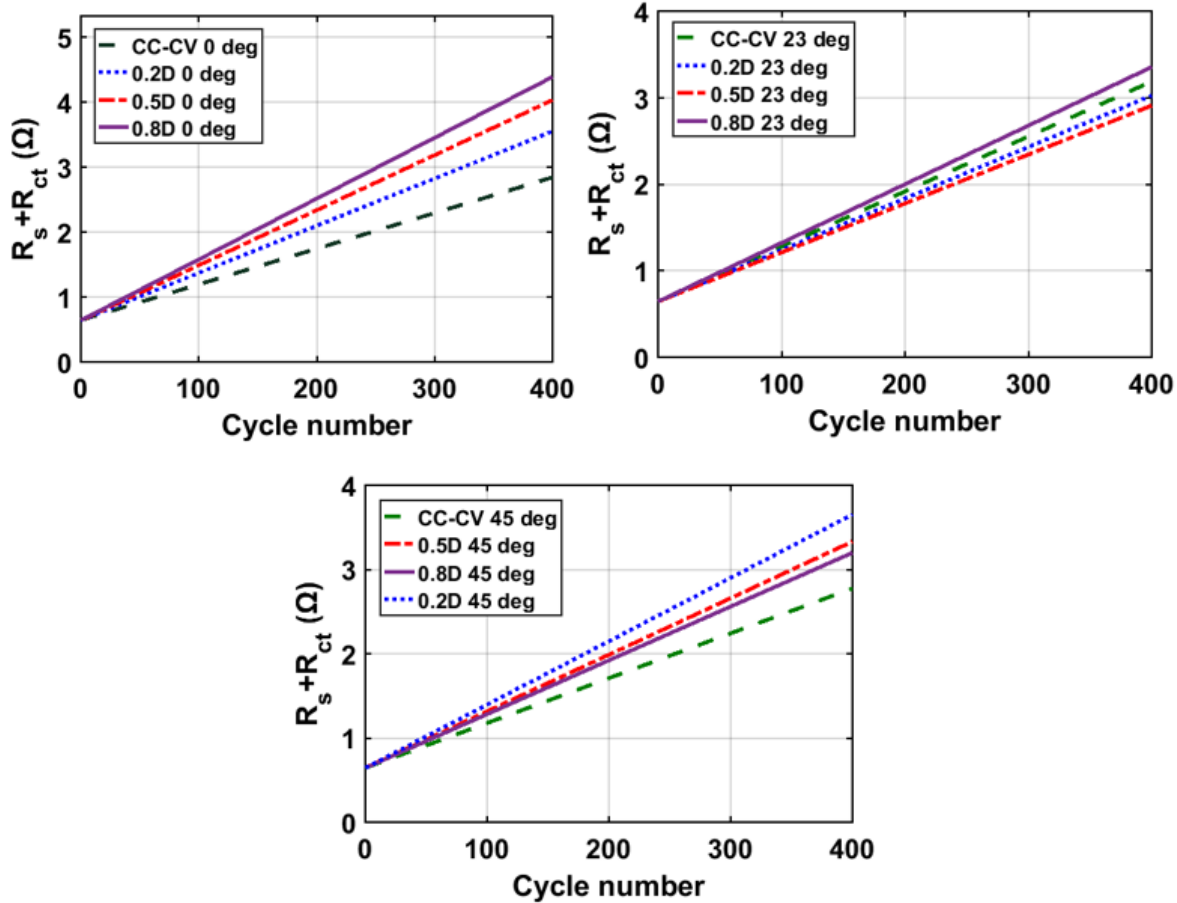


Figure 60: $R_s + R_{ct}$ vs number of charge and discharge cycles at 100% DoD separated at different temperatures

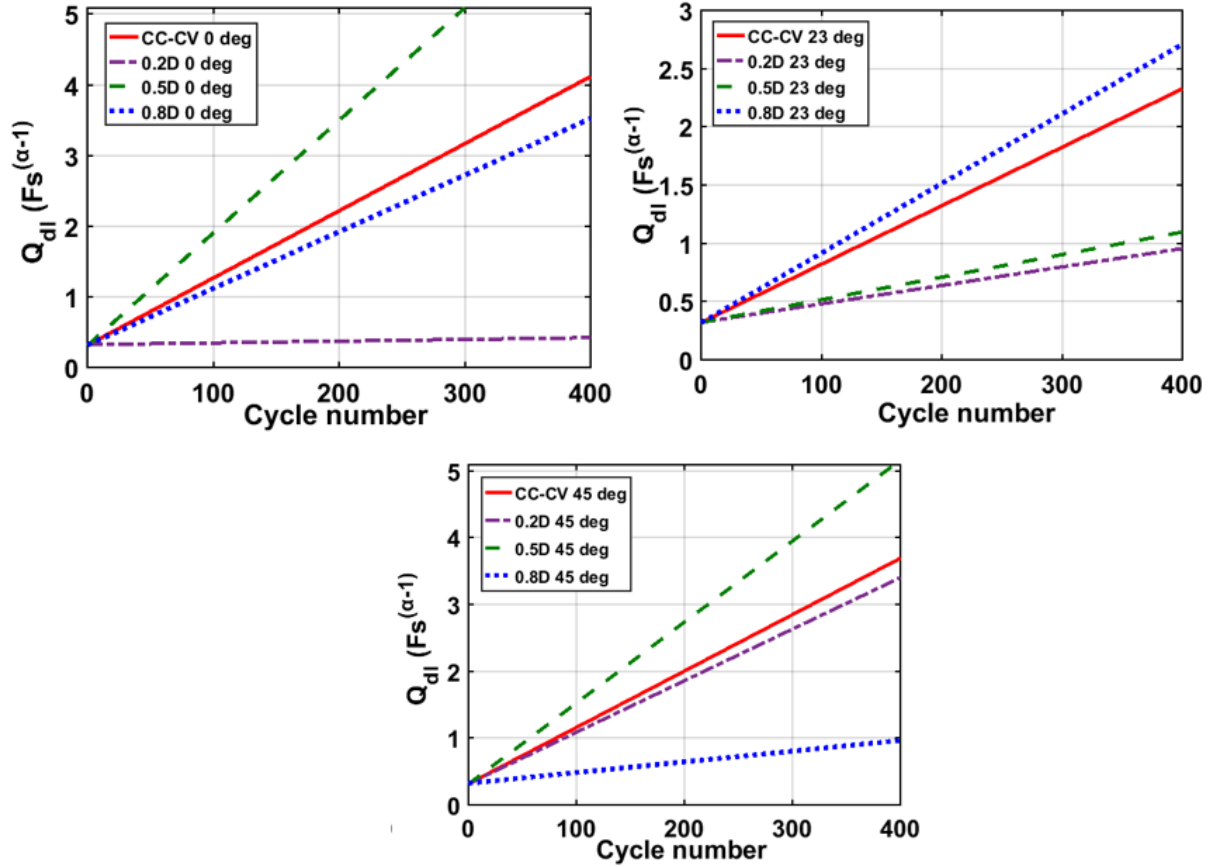


Figure 61: Q_{dl} vs number of charge and discharge cycles at 100% DoD separated at different temperatures

In comparing batteries subjected to pulse charging in terms of evaluating the impact of duty cycles on $R_{ct} + R_s$, pulsing at duty cycles of 20% and 80% resulted in increased resistance values. Batteries subjected to pulse charging at 50% duty cycles presented much lower $R_{ct} + R_s$ values and at 23°C; pulsing at 50% resulted in a much lower $R_{ct} + R_s$ when compared with batteries subjected to CC-CV at 23°C, a 3.6% reduction at the 50th cycle.

From Fig. 59 and Fig. 61, Q_{dl} also increased as cycle number increased. This increase is due to the continuous growth of the surface film, which results in higher dielectric constants [228]. Observing this parameter across temperature for batteries subjected to both charging algorithms, cycling at room temperature resulted in smaller Q_{dl} values.

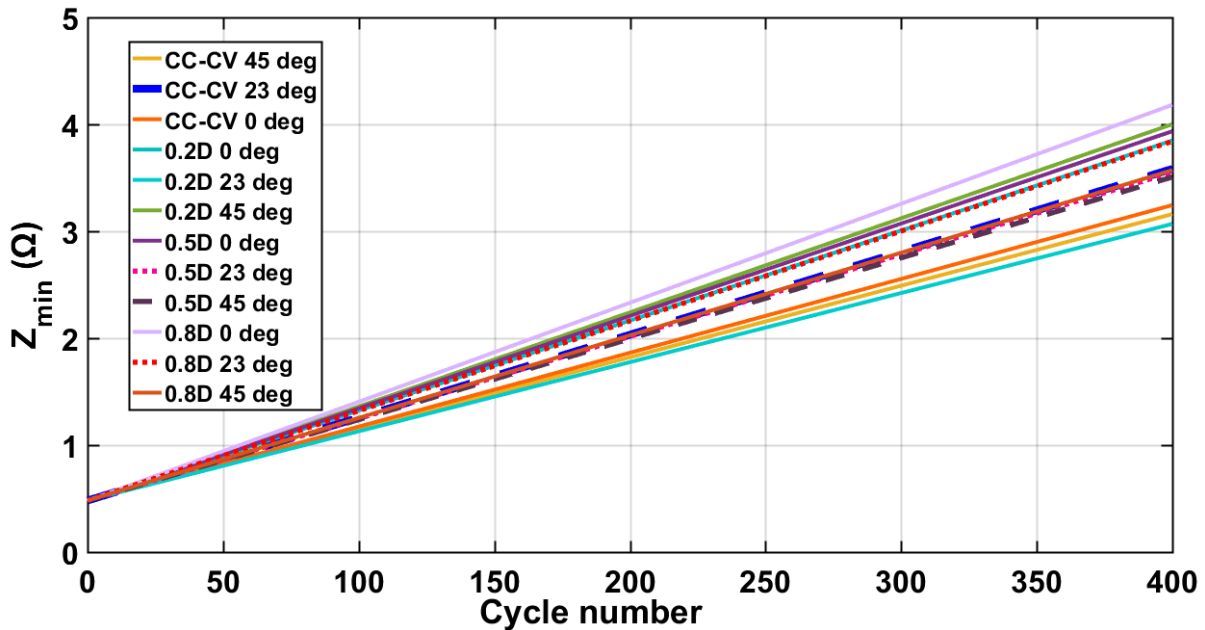


Figure 62: Z_{min} vs number of charge and discharge cycles at 100% DoD

To fully characterize the impact of charging parameters on the life cycle or aging of the LiPo battery, it is prudent to evaluate its impedance at one single frequency [228]. The battery impedance, Z_{min} , evaluated at f_{zmin} , obtained from section 6, was plotted across the number of charge and discharge cycles for batteries subjected to both pulse and CC-CV charging. This is shown in Fig. 62 and separated into three different groups according to temperature in Fig. 63. Similar to the previously discussed obtained battery parameters, Z_{min} increased with the number

of charge and discharge cycles. Batteries subjected to pulsing at a duty cycle of 50% at room temperature had similar Z_{min} values when compared to batteries subjected to CC-CV at that same temperature, a 4 m Ω difference at the 50th cycle. Z_{min} values at 0°C were generally higher. In terms of evaluating Z_{min} with respect to duty cycles, batteries subjected to 50% duty cycles mostly had lower Z_{min} values at 0°C and 45°C. CC-CV charged batteries had lower Z_{min} at 0°C and 45°C when compared with pulsed charged batteries.

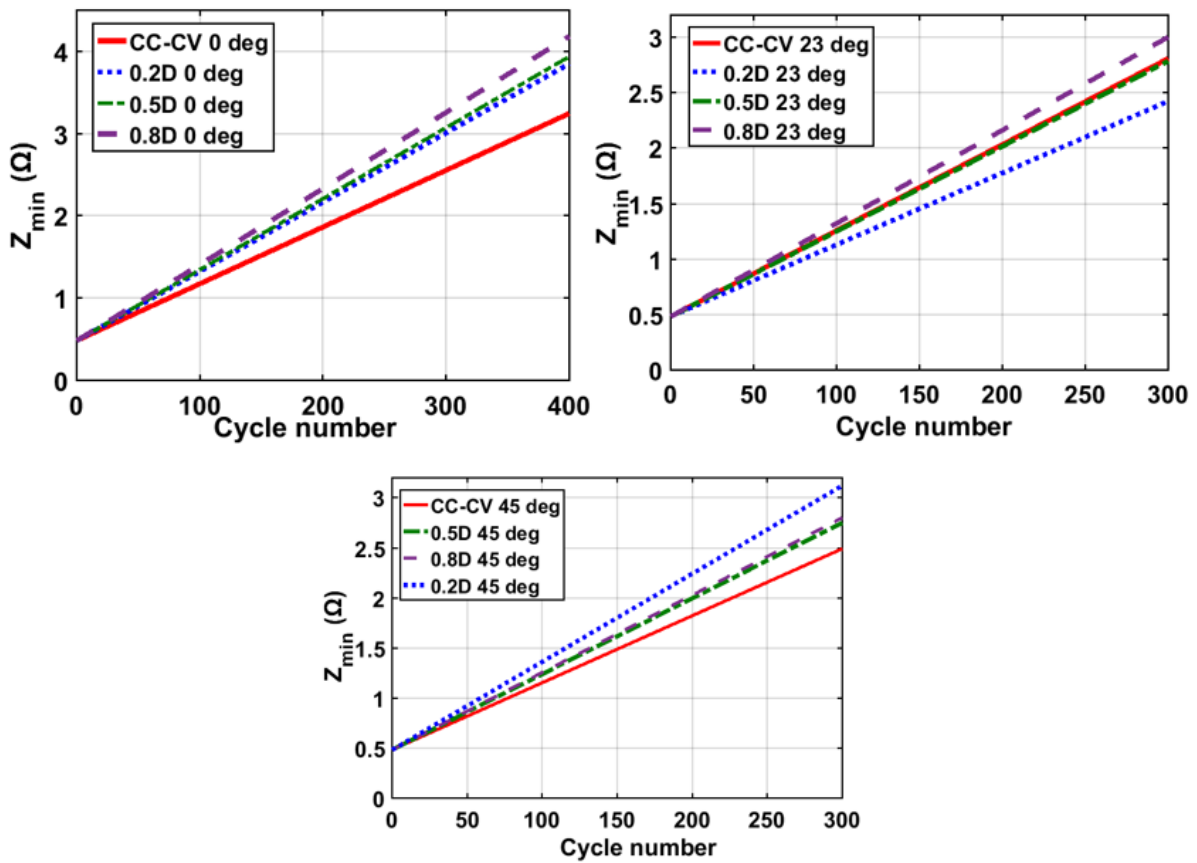


Figure 63: Z_{min} vs number of charge and discharge cycles at 100% DoD separated by temperature

7.3.2 The impact of charging characteristics on battery life cycle

In general, as the number of charge and discharge cycles increased, battery capacity decreased. The rate of decrease depends on the ambient temperature at which the battery is charged, charging voltage [233], charging and discharging current, and usage levels. It was observed from the experimental results that there was an initial increase in battery capacity at higher temperatures, i.e. 45°C, but that resulted in a corresponding decrease in life cycle. This increase in capacity is due to the enhanced kinetics of the intercalation and deintercalation of Li^+ [229]. Taking advantage of temperature, which affects battery life cycle noticeably, accelerated aging of the LiPo batteries was performed to compare the impact of the CC-CV charging algorithm and the pulse charging algorithm with optimal parameters (50% duty cycle and f_{zmin}) on the life cycles of the batteries. At higher temperatures, the batteries experienced capacity fade much faster [234] than lower temperatures. This accelerated degradation is due to changes in the morphology of the SEI, breakdown of the SEI, or growth of inorganic byproducts of side reactions that limit the kinetic movement of Li^+ [229]. This accelerated aging process for the LiPo batteries under test is plotted in Fig. 64. The expected behavior at room temperature can be estimated from how the batteries behave under an accelerated aging process. Pulsing at 50% and f_{zmin} resulted in about an extra 100 cycles when compared with CC-CV.

The impact of ambient temperature on the life cycle of batteries subjected to CC-CV was also investigated. This is shown in Fig. 65. Charging at 45°C resulted in a drastic decrease in capacity when compared to charging at 0°C and 23°C.

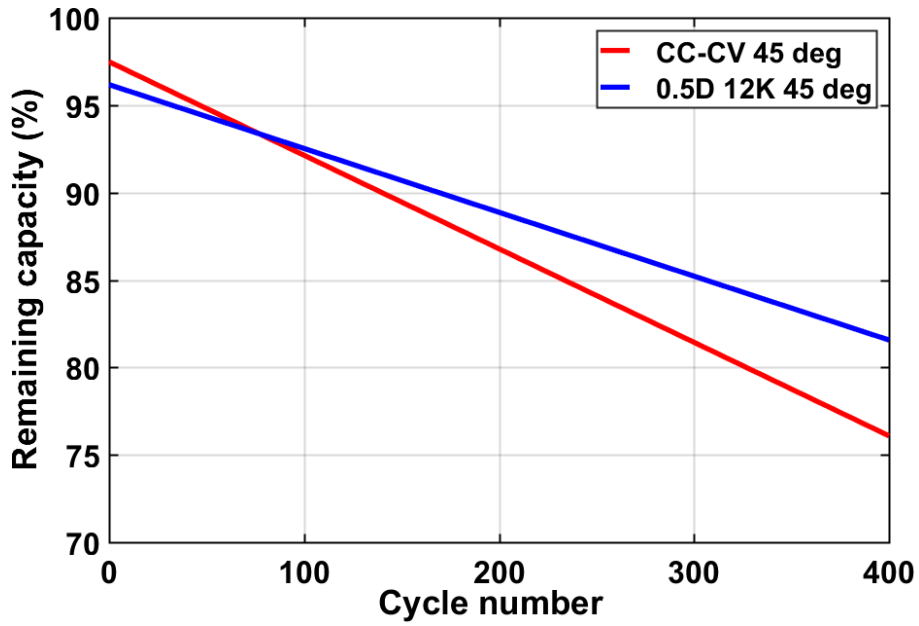


Figure 64: Accelerated aging of LiPo batteries subjected to pulsing at optimal parameters and conventional CC-CV algorithm

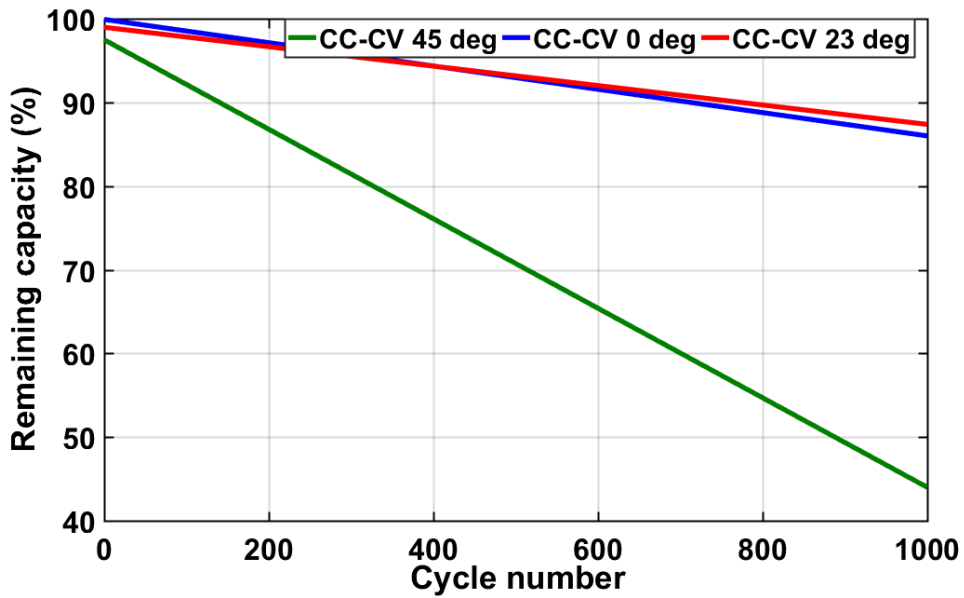


Figure 65: Life cycle of batteries subjected to CC-CV charging algorithm

Table 18: Output evaluated responses

	Factors			
No	LC	$R_s(\Omega)$	$R_{ct}(\Omega)$	$Q_{dl}(Fs^{a-1})$
1	583	0.8604	0.08091	0.4006
2	370	0.8680	0.09468	0.4020
3	239	0.9200	0.09845	0.7010
4	421	0.9200	0.09845	0.7010
5	763	0.8590	0.12000	0.9167
6	446	0.9420	0.16680	0.7160
7	213	0.9020	0.10390	0.3350
8	258	0.8680	0.09468	0.4020
9	545	0.8589	0.06816	0.4180
10	303	0.9020	0.10390	0.3350
11	512	0.9100	0.15500	1.1040
12	388	0.8590	0.12000	0.9167
13	309	0.9000	0.08174	0.6160
14	311	0.8590	0.12000	0.9167
15	215	0.8680	0.09468	0.4020
16	268	0.8680	0.09468	0.4020
17	434	0.8589	0.06816	0.4180
18	456	0.8604	0.08091	0.4006

	Factors			
No	LC	$R_s(\Omega)$	$R_{ct}(\Omega)$	$Q_{dl}(Fs^{a-1})$
19	873	0.9420	0.16680	0.7160
20	308	0.9100	0.15500	1.1040
21	438	0.9020	0.10390	0.3350
22	360	0.9020	0.10390	0.3350
23	295	0.8604	0.08091	0.4006
24	214	0.9100	0.15500	1.1040
25	755	0.8590	0.12000	0.9167
26	250	0.8604	0.08091	0.4006
27	486	0.9000	0.08174	0.6160
28	408	0.9200	0.09845	0.7010
29	377	0.9000	0.08174	0.6160
30	828	0.8589	0.06816	0.4180
31	871	0.9100	0.15500	1.1040
32	401	0.9420	0.16680	0.7160
33	593	0.9200	0.09845	0.7010
34	396	0.8589	0.06816	0.4180
35	393	0.9000	0.08174	0.6160
36	408	0.9420	0.16680	0.7160

7.3.3 Impact of pulse charge current factors and factor levels on battery characteristics

Having determined how the battery impedance parameters are affected by pulse and CC-CV charging algorithms, and also how batteries subjected to both algorithms perform under accelerated charging, it is important to determine the factors and factor levels, shown in Table 13, that impact the aging or life cycle of the battery. In order to determine this, the Taguchi OA approach is used. The same design approach detailed in section 6 is used and charge-discharge cycles are performed according to Table 14. The impedance parameters were reevaluated by using EIS and Simplex curve fitting algorithm after the aging process and the impedance parameters obtained are recorded in Table 18. Battery life cycles (LC) were also estimated by using regression analysis and recorded in Table 18. By using S/N ratios (31), the larger-the-better for life cycle tests, and the smaller-the-better for battery impedance parameters and ANOM, Fig. 66 and Fig. 67 can be obtained. It can be deduced from Fig. 66 that the factor levels that resulted in a longer battery life cycle were $f = 12.6kHz$ (f_{zmin}), $D = 0.5$, and $T = 23\text{ }^{\circ}C$.

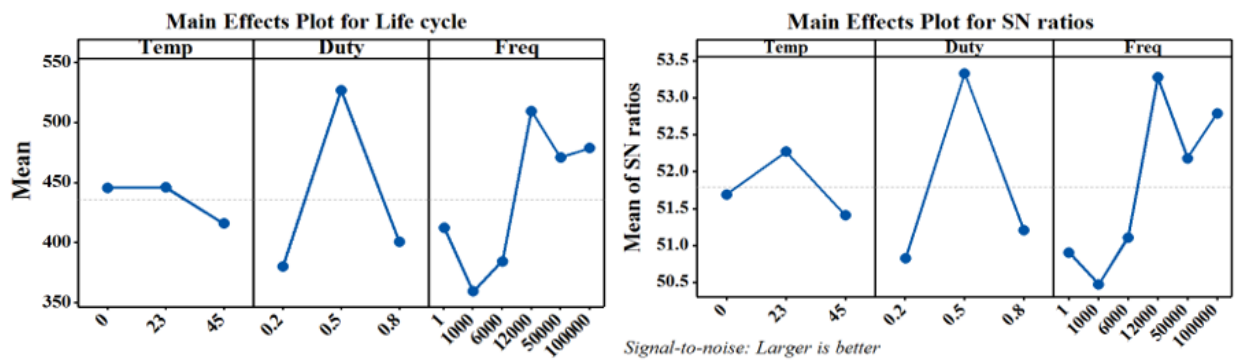
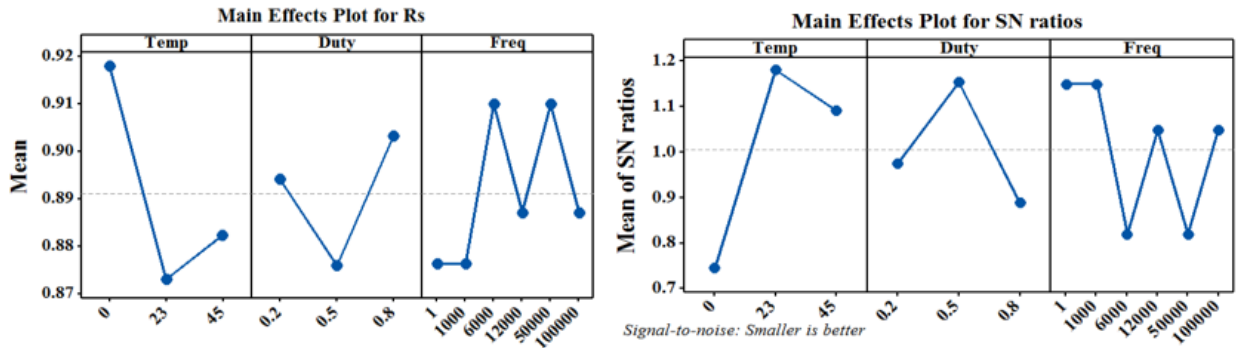
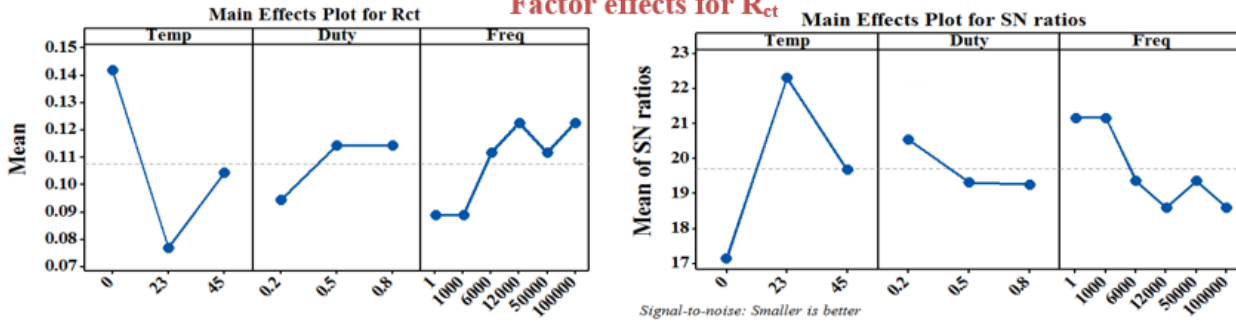


Figure 66: Pulse charging factors and factor level impact on battery life cycle

Factor effects for R_s



Factor effects for R_{ct}



Factor effects for Q_{dl}

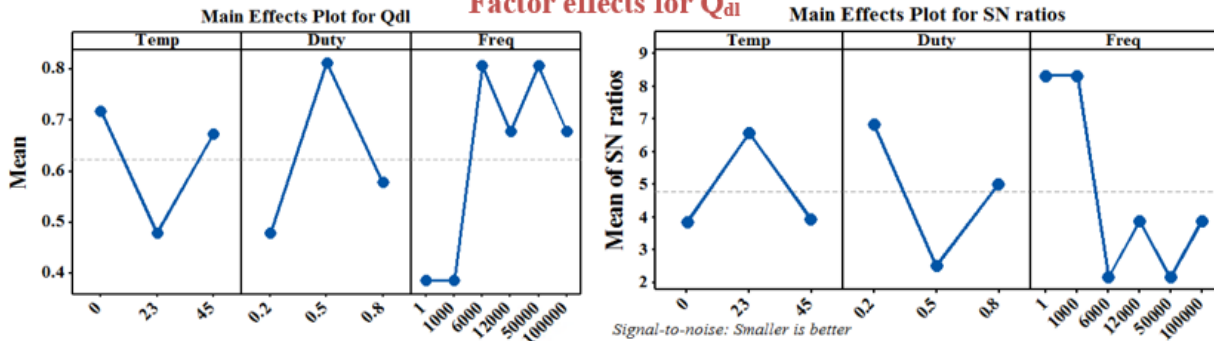


Figure 67: Pulse charge current factor effects on battery impedance parameters

Fig. 67 shows the main factor effects for the battery impedance parameters. Pulse charging at room temperature resulted in lower battery impedance parameters. In terms of pulse charge current duty cycles, the battery impedance parameters each behaved differently. For example, the duty cycle factor level that resulted in a lower R_s value was 50% while that for R_{ct} was 20%. To determine what factor has a significant impact on the battery life cycle and impedance parameters, the

ANOVA table has to be computed from Table 18 by using the sum of squares (SS) expressed in (35). The ANOVA tables are shown in Table 19 and Table 20.

Table 19: ANOVA table for battery life cycle

Life cycle				
Factor	DoF	Sum of squares	Mean square	Contribution to SS
<i>D</i>	2	152562	76281	57.52%
<i>f</i>	5	105460	21092	39.76%
<i>T</i>	2	7221	3611	2.72%
Total	-	265243	-	-

The degrees of freedom (DoF) associated with each factor is indicated in Table 19 and Table 20. The mean square (*sum of squares/DoF*) of each factor is also shown in the tables. From Table 19, it can be deduced that the duty cycle has the largest influence on the total sum of squares, contributing 57.52%. This means that the chosen duty cycle of the pulse charge current matters for the battery life cycle. Improper selection of the duty cycle can result in batteries with shorter life cycles. The next biggest contribution was determined to be the frequency at which the pulse charge current operated. This is understandable as pulsing at the frequencies at which the battery impedance is minimal results in less heating losses, improving the life cycle of the battery.

Table 20: ANOVA table for battery impedance parameters

$R_s(\Omega)$				
Factor	DoF	Sum of squares	Mean square	Contribution to SS
D	2	0.004654	0.002327	18.43%
f	5	0.007104	0.001421	28.13%
T	2	0.013494	0.006747	53.44%
Total		0.025252		
$R_{ct}(\Omega)$				
Factor	DoF	Sum of squares	Mean square	Contribution to SS
D	2	0.003193	0.001596	8.92%
f	5	0.007084	0.001417	19.79%
T	2	0.025525	0.012762	71.30%
Total		0.035802		
$Q_{dl}(Fs^{a-1})$				
Factor	DoF	Sum of squares	Mean square	Contribution to SS
D	2	0.70633	0.35317	31.83%
f	5	1.12199	0.2244	50.56%
T	2	0.39094	0.19547	17.62%
Total		2.21926		

From Table 20, many inferences can be made as to which factors affect which battery impedance parameter the most. The ambient temperature at which the battery was charged contributed significantly to the battery impedance parameters, R_{ct} , and R_s , while the frequency at which the battery was pulsed at contributed the second largest portion to the sum of squares. Temperature does affect the aging rate of the battery with higher temperature leading to early battery aging. Q_{dl} , however, had frequency contributing the largest amount to the sum of squares, with duty cycle contributing the next largest amount.

With this information, different decisions can be made to increase battery life cycle while improving battery charge and energy efficiencies and reducing charge time.

7.3.4 Summary of experimental results

The influence of pulse charging parameters and ambient temperature at which the battery is charged on LiPo battery impedance parameters and life cycle has been determined. Battery impedance parameter values increased as the number of charge and discharge cycles increased. This is due to the various side chemical reactions that occur in the battery as it ages. The byproducts of these reactions impact the battery impedance. Batteries subjected to pulse charging at 50% duty cycle at room temperature had lower impedance values compared to batteries subjected to CC-CV at the same temperature. Results from the accelerated aging of the battery indicated that pulse charging at the optimal values, $f = 12.6kHz$ (f_{Zmin}) and $D = 0.5$, resulted in an increase of an additional 100 cycles when compared to the benchmark method CC-CV. In terms of determining which factor and factor levels of the pulse charge current affected the life cycle of the batteries, Taguchi OA approach was used. It was deduced that the duty cycle of the pulse charge current played a major role in battery life cycle extension, followed by ambient temperature at which the

battery is charged. Factor levels corresponding to $f = 12.6kHz$ (f_{zmin}), $D = 0.5$, and $T = 23\text{ }^{\circ}\text{C}$ had the greatest impact on the battery life cycle.

This work has demonstrated the impact of pulse charge current factors and factor levels on the life cycle of the battery. Accelerated life cycle tests have also proven that batteries subjected to pulse charging at the optimal parameters can result in longer life cycles when compared to batteries subjected to the CC-CV charging algorithm.

8. CONCLUSION

With consumers of electronic devices seeking faster charging and longer battery runtime, battery charging methods are becoming very important. The pulse charging algorithm has been shown to be a promising method to obtain better battery charge and energy efficiencies while drastically reducing charge time. This work has proposed pulse charger designs based on battery characteristics for both portable and IoT applications.

A pulse charger for IoT applications has been presented. This pulse charger design is based on altering duty cycles according to battery polarization characteristics. The performance of this charging system was verified through experimental results. The proposed pulse charging algorithm was used to charge two different li-ion batteries with different cathode chemistries. Experiments indicate that charging these batteries at the frequency at which their impedance is minimum produced the best battery charge efficiency. The proposed battery charging system produced better battery charge efficiencies and charge times when compared with the benchmark CC-CV charging technique. A battery charge efficiency improvement of 3.15% and a charge time reduction of 37.35% was achieved for a 100 mAh li-ion battery.

With pulse chargers having different parameters whose combinations could result in different output performance metrics, it was necessary to determine which pulse charge current parameters resulted in optimal performance. This work has proposed a new technique to experimentally search for the optimal parameters for the pulse charging of a LiPo battery by using Taguchi orthogonal arrays. This approach can be extended to both large battery capacities, such as those used in

electric vehicles, and smaller battery capacities, such as those used in portable electronic applications. This technique provides the optimal parameters that maximize battery charge and energy efficiencies while decreasing charge time. The approach can also be extended to select factors and factor levels that maximize or minimize any preferred output response. The design of the Taguchi OA, the experimental procedure, the design of the pulse charger, and the analysis of the output responses data have been presented. The optimal parameters for the pulse charging of a 3.7V 600 mAh LiPo battery was determined to be 50% duty cycle, which gives an equal time for the battery to absorb and redistribute charge efficiently, a frequency equal to the frequency at which the minimum ac impedance of the battery occurs, which minimizes the energy losses in the battery, and room temperature, which is ideal for most applications. When compared with the benchmark CC-CV charge method, operating the pulse charger at these parameters increased battery energy and charge efficiencies by 11.3% and 1.5% respectively, and decreased charge time by 47.6%. This work has demonstrated that by using the methods presented herein, optimal parameter values of a pulse charger can be determined.

This work also investigated the impact of pulse charging and its parameters on battery impedance parameters and life cycle. By subjecting the batteries under test to accelerated aging processes, batteries that were pulse charged at optimal parameters could obtain about 100 more cycles when compared to batteries that were subjected to CC-CV charging technique. Battery impedance parameter values increased as the number of charge and discharge cycles increased for both pulse and CC-CV charged batteries. The duty cycles and ambient temperature at which the battery was charged also impacted the battery impedance parameters.

8.1 Contributions

Battery charging is a very important process that must take into account safety, battery characteristics, and the expectations of the consumer. In this work, a pulse charger for coin cells used in IoT applications has been designed. This pulse charger took into account the battery internal chemical processes, i.e. polarization characteristics, to ensure fast charging without compromising battery charge efficiencies. A design procedure was established and can be implemented by researchers who are interested in the art of pulse charging.

Since the pulse charge current has different parameters or factors which results in different output performance metrics, an optimization method where by circuit designers can choose which output performance metric to optimize was proposed. This optimization procedure produced results that can aid designers choose which pulse charger current factors and factor levels to maximize in order to obtain a certain output performance metric. The design procedure that has been presented can be replicated for various battery capacities, thereby extending the number of applications the proposed optimization technique can be used for.

The life cycle of the battery under pulse charging conditions has also been determined. The factor and factor levels that contribute to increased battery life cycle were determined and this information can be used by numerous researchers when designing pulse charging systems.

8.2 Future research direction

Battery charging is always going to play an important role in the life of the electronic device consumer. It will be important to continue developing improved charging methods that focus on safety, reduce charging time more drastically, improve battery runtime, and increase the battery

life cycle. Different battery chemistries, which have much higher energy density levels than li-ion batteries, are still under development and it will be important to start developing universal charging algorithms that can be used for any battery chemistry. Focus should be placed on safe charging while still reducing charge time and increasing efficiencies.

Other potential areas for research include a low power consumption, highly efficient, and small form factor in-situ battery characteristics measurement approach that continually monitors the battery characteristics and alters battery charging parameters based on the measured results. As battery characteristics change as they age, a charging method whereby continuous optimal operation is achieved is needed. There is also the potential of integrating a machine learning approach where the battery charging system can learn from its usage behavior and alter charging parameters in anticipation of the predicted behavior.

The battery charging market is ever evolving and it is important to keep up with this ever-changing market.

REFERENCES

- [1] ReportsnReports, "Global Rechargeable Battery Market," Technavio, Infiniti Research Limited10970, January 2016.
- [2] C. Pillot, "Battery Market Development for Consumer Electronics, Automotive, and Industrial: Materials: Requirements & Trends," presented at Batteries 2014 event, Nice, France, 2014.
- [3] Taiyou Research, "Global Market for Lithium-Ion Batteries – Forecast, Trends & Opportunities 2014 – 2020," Research and Markets, Global, ID: 2599948, July 2013.
- [4] marketsandmarkets.com, "Supercapacitor Market by Type (Double Layer, Pseudocapacitor, and Hybrid) - 2022|," MarketsandMarkets, Report code: SE 2310, November. 2016.
- [5] Bob Dunstan and Richard Petrie, "Universal Serial Bus Power Delivery Specification Revision 2.0, Version 1.3," USB Implementers Forum, Inc.," January 12, 2017.
- [6] C. Hota and P.K. Srimani, "Distributed Computing and Internet Technology" in *Proceedings of 9th International Conference, ICDCIT 2013, Bhubaneswar, India, February 5-8, 2013*, Springer, 2013.
- [7] G.V. Piqué and H.J. Bergveld, "State-of-the-Art of Integrated Switching Power Converters," in *Analog Circuit Design: Low Voltage Low Power; Short Range Wireless Front-Ends; Power Management and DC-DC*, M. Steyaert, A. van Roermund, and A. Baschiroto, Dordrecht: Springer Netherlands, 2012, pp. 259-281.

- [8] A. Iyengar, A. Tripathi, A. Basarur, and I. Roy, "Unified Power Management Framework for Portable Media Devices," *2007 IEEE International Conference on Portable Information Devices*, Orlando, FL., pp. 1-5, 2007.
- [9] Seongsoo Lee and T. Sakurai, "Run-time power control scheme using software feedback loop for low-power real-time applications," in *Proceedings of 2000. Design Automation Conference. (IEEE Cat. No.00CH37106)*, pp. 381-386, 2000.
- [10] V. Delaluz, M. Kandemir, N. Vijaykrishnan, A. Sivasubramaniam, and M. J. Irwin, "DRAM energy management using software and hardware directed power mode control," in *Proceedings HPCA Seventh International Symposium on High-Performance Computer Architecture*, pp. 159-169, 2001.
- [11] Y. H. Lu, T. Simunic and G. De Micheli, "Software controlled power management," in *Proceedings of the Seventh International Workshop on Hardware/Software Codesign (CODES '99)*, pp. 157-161, 1999.
- [12] D. Brunelli, L. Benini, C. Moser, and L. Thiele, "An Efficient Solar Energy Harvester for Wireless Sensor Nodes," *2008 Design, Automation and Test in Europe*, Munich, 2008, pp. 104-109. "
- [13] G. Chen, M. Fojtik, D. Kim, D. Fick, J. Park, M. Seok *et al.* "Millimeter-scale nearly perpetual sensor system with stacked battery and solar cells," *2010 IEEE International Solid-State Circuits Conference - (ISSCC)*, San Francisco, CA, 2010, pp. 288-289.

- [14] Z. Abdin, M.A. Alim, R. Saidur, M.R. Islam, W. Rashmi and S. Mekhilef, "Solar energy harvesting with the application of nanotechnology," *Renewable and Sustainable Energy Reviews*, vol. 26, pp. 837-852, 2013.
- [15] S. Carreon-Bautista, L. Huang and E. Sanchez-Sinencio, "An Autonomous Energy Harvesting Power Management Unit with Digital Regulation for IoT Applications," *IEEE Journal of Solid-State Circuits*, vol. 51, pp. 1457-1474, 2016.
- [16] M. AbdElFattah, A. Mohieldin, A. Emira and E. Sanchez-Sinencio, "A low-voltage charge pump for micro scale thermal energy harvesting," *2011 IEEE International Symposium on Industrial Electronics*, Gdansk, pp. 76-80, 2011.
- [17] J. Zarate-Roldan, S. Carreon-Bautista, A. Costilla-Reyes and E. Sanchez-Sinencio, "A Power Management Unit with 40 dB Switching-Noise-Suppression for a Thermal Harvesting Array," *IEEE Transactions on Circuits and Systems I: Regular Papers*, vol. 62, pp. 1918-1928, 2015.
- [18] S. Yoon, S. Carreon-Bautista and E. Sanchez-Sinencio, "An Area Efficient Thermal Energy Harvester with Reconfigurable Capacitor Charge Pump for IoT Applications," *IEEE Transactions on Circuits and Systems II: Express Briefs*, vol. PP, pp. 1, 2018.
- [19] M. AbdElFattah, A.N. Mohieldin, A. Emira, A.K. Hussien and E. Sanchez-Sinencio, "Ultra-low-voltage power management unit for thermal energy harvesting applications," *10th IEEE International NEWCAS Conference*, Montreal, QC, pp. 381-384, 2012.

- [20] L. Xin and Y. Shuang-Hua, "Thermal energy harvesting for WSNs", *2010 IEEE international conference on systems man and cybernetics (SMC)*, pp 3045–3052, 2010 .
- [21] G. Papotto, F. Carrara, and G. Palmisano, "A 90-nm CMOS threshold-compensated RF energy harvester," *IEEE J Solid-State Circuits*, vol. 46, no. 9, pp. 1985-1997, September 2011.
- [22] J.H. Lee, W.J. Jung, J.W. Jung, J.E. Jang, and J.S. Park, "A matched RF charger for wireless RF power harvesting system," *Microwave and Optical Technology Letters*, vol. 57, no. 7, pp. 1622-1625, 2015.
- [23] M. Nalini, J. V. N. Kumar, R. M. Kumar, and M. Vignesh, "Energy harvesting and management from ambient RF radiation," in *2017 International Conference on Innovations in Green Energy and Healthcare Technologies (IGEHT)*, pp. 1-3, 2017.
- [24] M. A. Abouzied, K. Ravichandran, and E. Sanchez-Sinencio, "A Fully Integrated Reconfigurable Self-Startup RF Energy-Harvesting System with Storage Capability," *IEEE Journal of Solid-State Circuits*, vol. 52, pp. 704-719, 2017.
- [25] A.N. Rodriguez, F.R.G. Cruz, and R.Z. Ramos, "Design of 900 Mhz AC to DC converter using native CMOS device of TSMC 0.18 micron technology for RF energy harvest application," *Universal Journal Electrical and Electronic Engineering*, vol. 3, no. 3, pp. 99-105, 2015.
- [26] S.S. Chouhan, M. Nurmi and K. Halonen, "Efficiency enhanced voltage multiplier circuit for RF energy harvesting," *Microelectronics Journal*, vol. 48, pp. 95-102, 2016.

- [27] H. Jabbar, Y.S. Song and T.T. Jeong, "RF energy harvesting system and circuits for charging of mobile devices," *IEEE Transactions Consumer Electronics*, vol. 56, no. 1, pp. 247-253, 2010.
- [28] Suntan Technology Company, "ELECTRIC DOUBLE LAYER CAPACITOR-GOLD CAPACITOR," TS12S-R datasheet, 2008.
- [29] Illinois Capacitor, "RJD- Rechargeable Li-ion Batteries," RJD Series datasheet, 2016.
- [30] Geoff Gordon, Qualcomm Technologies (2016, April 13). Qualcomm Quick Charge: accelerating hundreds of devices and accessories [Online]. Available: <https://www.qualcomm.com/news/onq/2016/04/13/qualcomm-quick->.
- [31] Qnovo Inc., "Fundamentals of Qnovo adaptive charging in lithium ion batteries," December. 2015.
- [32] J. M. Amanor Boadu, M. Abouzied and E. Sanchez-Sinencio, "An Efficient and Fast Li-ion Battery Charging System Using Energy Harvesting or Conventional Sources," *IEEE Transactions on Industrial Electronics*, vol. PP, pp. 1, 2018.
- [33] J.M. Amanor BOADU, A. Guiseppi-Elie and E. Sanchez-Sinencio, "Search for Optimal Pulse Charging Parameters for Li-ion Polymer Batteries Using Taguchi Orthogonal Arrays," *IEEE Transactions on Industrial Electronics*, vol. PP, pp. 1, 2018.
- [34] Global Market Insights Inc., "Stationary Battery Storage Market Size - Growth Forecast Report 2030;" Global Market Insights Inc., Report ID GMI1892, July 2017.

- [35] H. Ibrahim, A. Ilinca and J. Perron, "Energy storage systems—Characteristics and comparisons," *Renewable and Sustainable Energy Reviews*, vol. 12, pp. 1221-1250, 2008.
- [36] I. Dincer and M.A. Rosen, "Thermal Energy Storage: Systems and Applications", 2nd ed, pp. 51-82, John Wiley & Sons, Ltd., 2010.
- [37] B.E. Conway, "Electrochemical supercapacitors", pp. 11-31, Kluwer Acad., New York, 1999.
- [38] L.L. Zhang and X.S. Zhao, "Carbon-based materials as supercapacitor electrodes," *Chemical Society Reviews*, vol. 38, pp. 252-2531, Aug 19, 2009.
- [39] J.R. Miller and A. Burke, "Electrochemical Capacitors: Challenges and Opportunities for Real-World Applications", *Electrochemical Society Interface*, vol. 17, pp. 53-57, 2008.
- [40] J. Wang, F. Kang and B. Wei, "Engineering of MnO₂-based nanocomposites for high-performance supercapacitors," *Progress in Materials Science*, vol. 74, pp. 51-124, 2015.
- [41] M.M. Botte G.G., "Handbook of industrial chemistry and biotechnology-Electrochemical Energy Storage:Applications, Processes, and Trends," J.A. Kent, New York,: Springer, 2012.
- [42] C. Wang, E. Zhou, W. He, X. Deng, J. Huang, M. Ding, X. Wei, X. Liu and X. Xu, "NiCo₂O₄-Based Supercapacitor Nanomaterials," *Nanomaterials*, vol. 7, no. 2, Feb. 2017.
- [43] David Linden and Thomas B. Reddy, "Linden's handbook of batteries", 4th ed., McGraw Hill Professional New York, 2011.

- [44] A.K. Shukla, S. Venugopalan, and B. Hariprakash, "Nickel-based rechargeable batteries," *Journal of Power Sources*, vol. 100, no. 1-2, pp. 125-148, 2001.
- [45] L. Energizer Brands, "Nickel Metal Hydride (NiMH) Handbook and Application Manual," 2018.
- [46] R.A. Huggins, "Lead-Acid Batteries," in *Energy Storage*, R.A. Huggins, pp. 237-250, Boston, MA: Springer US, 2010.
- [47] A. I. Harrison, "Lead Acid Standby Power Batteries in Telecommunications - "Horses for Courses"," in *Telecommunications Energy Conference, 1981. INTELEC 1981*, pp. 72-77, 1981.
- [48] A. I. Harrison, "Valve regulated lead acid batteries for standby power applications," in *Proceedings of Thirteenth International Telecommunications Energy Conference - INTELEC 91*, pp. 14-19, 1991.
- [49] D.A.J. Rand, L.S. Holden, G.J. May, R.H. Newnham, and K. Peters, "Valve-regulated lead/acid batteries," *Journal of Power Sources*, vol. 59, no. 1-2, pp. 191-197, March-April, 1996.
- [50] J. Tarascon and M. Armand, "Issues and challenges facing rechargeable lithium batteries," *Nature*, vol. 414, pp. 359, 2001.
- [51] Global Industry Analysts, "Consumer Batteries- A Global Strategic Business report," Global Industry Analysts Inc., Report ID 338752, May 2016.

- [52] marketsandmarkets.com, "Battery Market by Transport, Type, Geography - 2021," Markets and Markets Research Private Ltd., Report code: AT 2836, April 2016.
- [53] Grand View Research, "Battery Market Size, Share | Industry Research Report, 2024," Grand View Research, Report ID: 978-1-68038-846-6, May. 2016.
- [54] Statista (2018, April 24) , "Lithium ion batteries - main manufacturers in 2018,"[Online] Available: <https://www.statista.com/statistics/235323/lithium-batteries-top-manufacturers/>
- [55] Variant Market Research, "Lithium-Ion Battery Market | Material Type | Industry Vertical | Analysis | Size | Trend and Forecast 2015 - 2024," Variant Market Research, Report ID: LB18082, May 2017.
- [56] A.K. Geim, "Graphene: Status and Prospects," *Science*, vol. 324, pp. 1530-1534, Jun 19, 2009.
- [57] X. Huang, X. Qi, F. Boey, and H. Zhang, "Graphene-based composites," *Chemical Society Reviews*, vol. 41, pp. 666-686, 2012.
- [58] M. Liang and L. Zhi, "Graphene-based electrode materials for rechargeable lithium batteries," *Journal of Materials Chemistry*, vol. 19, pp. 5871-5878, Aug 11, 2009.
- [59] M. Yu, R. Li, M. Wu, and G. Shi, "Graphene materials for lithium–sulfur batteries," *Energy Storage Materials*, vol. 1, pp. 51-73, 2015.
- [60] Z. Wu, G. Zhou, L. Yin, W. Ren, F. Li, and H. Cheng, "Graphene/metal oxide composite electrode materials for energy storage," *Nano Energy*, vol. 1, pp. 107-131, Jan. 2012.

- [61] Y. Li and J. Lu, "Metal–Air Batteries: Will They Be the Future Electrochemical Energy Storage Device of Choice?" *ACS Energy Lett.*, vol. 2, pp. 1370-1377, 2017.
- [62] F. Li, T. Zhang, and H. Zhou, "Challenges of non-aqueous Li-O₂ batteries: electrolytes, catalysts, and anodes," *Energy & Environmental Science*, vol. 6, pp. 1125-1141, Mar 20, 2013.
- [63] S.R. Narayanan, G.K.S. Prakash, A. Manohar, B. Yang, S. Malkhandi, and A. Kindler, "Materials challenges and technical approaches for realizing inexpensive and robust iron–air batteries for large-scale energy storage," *Solid State Ionics*, vol. 216, pp. 105-109, May, 2012.
- [64] J. Lee, S. Tai Kim, R. Cao, N. Choi, M. Liu, K.T. Lee, and J. Cho, "Metal-Air Batteries with High Energy Density: Li-Air versus Zn-Air," *Advanced Energy Materials*, vol. 1, pp. 34-50, Jan 1, 2011.
- [65] M.M. Ottakam Thotiyl, S.A. Freunberger, Z. Peng, and P.G. Bruce, "The Carbon Electrode in Nonaqueous Li–O₂ Cells," *J.Am.Chem.Soc.*, vol. 135, pp. 494-500, 2013.
- [66] Y. Li and H. Dai, "Recent advances in zinc-air batteries," *Chemical Society Reviews*, vol. 43, pp. 5257-5275, Jul 7, 2014.
- [67] Y. Cho, I. Park, H. Lee, and J. Kim, "Aluminum anode for aluminum–air battery – Part I: Influence of aluminum purity," *Journal of Power Sources*, vol. 277, pp. 370-378, Mar 1, 2015.

- [68] S. Choi, D. Lee, G. Kim, Y.Y. Lee, B. Kim, J. Moon, and W. Shim, "Shape-Reconfigurable Aluminum–Air Batteries," *Advanced Functional Materials*, vol. 27, Sep 20, 2017.
- [69] Renata Batteries, "ZA675 maratone+," Technical Datasheet, December. 2011.
- [70] Y.J. Nam, D.Y. Oh, S.H. Jung and Y.S. Jung, "Toward practical all-solid-state lithium-ion batteries with high energy density and safety: Comparative study for electrodes fabricated by dry- and slurry-mixing processes," *Journal of Power Sources*, vol. 375, pp. 93-101, 2018.
- [71] K., K, Luntz, A, Viswanathan, V, Chiang, YM, Chen, Z, "Review-Practical Challenges Hindering the Development of Solid State Li Ion Batteries," *J. Electrochem. Soc.*, vol. 164, pp. A1744, 2017.
- [72] C. Yu, Eck, E R H van, H. Wang, S. Basak and Z. Li, "Accessing the bottleneck in all-solid state batteries, lithium-ion transport over the solid-electrolyte-electrode interface," *Nature Communications*, vol. 8, pp. 1-9, 2017.
- [73] Y. Zhou, X. Rui, W. Sun, Z. Xu, Y. Zhou, W. Jern Ng, Q. Yan, and E. Fong, "Biochemistry-Enabled 3D Foams for Ultrafast Battery Cathodes," *ACS Nano*, vol. 9, pp. 4628-4635, Apr 28,. 2015.
- [74] Prieto Battery Inc (2018, April 27), "A closer look at Prieto Battery innovation: Foam technology" 2015 [Online] Available: <https://www.prietobattery.com/how-it-works-2/foam/>.

- [75] C.K. Chan, R.A. Huggins, Y. Cui, G. Liu, K. McIlwrath, X.F. Zhang, and H. Peng, "High-performance lithium battery anodes using silicon nanowires," *Nature Nanotechnology*, vol. 3, pp. 31-35, Jan. 2008.
- [76] S. Grugeon, J. Tarascon, L. Dupont, S. Laruelle, and P. Poizot, "Nano-sized transition-metal oxides as negative-electrode materials for lithium-ion batteries," *Nature*, vol. 407, pp. 496-499, Sep 28, 2000.
- [77] H. Kim, D. A. Boysen, J. M Newhouse, B. L Spatocco, B. Chung, P. J Burke, and *et al*, "Liquid Metal Batteries: Past, Present, and Future," *Chemical Reviews*, vol. 113, pp. 2075, Mar 1, 2013.
- [78] M. Winter and R.J. Brodd, "What Are Batteries, Fuel Cells, and Supercapacitors?" *Chem.Rev.*, vol. 104, pp. 4245-4270, 2004.
- [79] Gurbinder Kaur, "Solid Oxide Fuel Cell Components", pp. 50-55, DE: Springer Verlag, 2016.
- [80] S. Wang, W. Quan, Z. Zhu, Y. Yang, Q. Liu, Y. Ren, and *et al*, "Lithium titanate hydrates with superfast and stable cycling in lithium ion batteries," *Nature Communications*, vol. 8, pp. 627, 2017.
- [81] N. Nitta, F. Wu, J.T. Lee, and G. Yushin, "Li-ion battery materials: present and future," *Materials Today*, vol. 18, pp. 252-264, 2015.
- [82] A. Shukla and P. Kumar, "Materials for Next-Generation Lithium Batteries", *Current Science*, vol. 94, 2008.

- [83] B.L. Ellis, K.T. Lee, and L.F. Nazar, "Positive Electrode Materials for Li-Ion and Li-Batteries," *Chem. Mater.*, vol. 22, pp. 691-714, 2010.
- [84] F.F.C. Bazito and R.M. Torresi, "Cathodes for lithium ion batteries: the benefits of using nanostructured materials," *Journal of the Brazilian Chemical Society*, vol. 17, pp. 627-642, Aug. 2006.
- [85] Y. Mekonnen, A. Sundararajan, and A. I. Sarwat, "A review of cathode and anode materials for lithium-ion batteries," *SoutheastCon 2016*, pp. 1-6, 2016.
- [86] W.H. Meyer, "Polymer electrolytes for lithium-ion batteries," *Advanced Materials* (Deerfield Beach, Fla.), vol. 10, pp. 439-448, Apr. 1998.
- [87] J.R. Owen, "Rechargeable lithium batteries," *Chem.Soc.Rev.*, vol. 26, pp. 259-267, 1997.
- [88] G. Li, Z. Li, P. Zhang, H. Zhang, and Y. Wu, "Research on a gel polymer electrolyte for Li-ion batteries," *Pure and Applied Chemistry*, vol. 80, pp. 2553-2563, Jan 1., 2008.
- [89] V. Etacheri, R. Marom, R. Elazari, G. Salitra and D. Aurbach, "Challenges in the development of advanced Li-ion batteries: a review," *Energy & Environmental Science*, vol. 4, pp. 3243, 2011.
- [90] A. Manuel Stephan, "Review on gel polymer electrolytes for lithium batteries," *European Polymer Journal*, vol. 42, pp. 21-42, 2006.
- [91] B. Scrosati and J. Garche, "Lithium batteries: Status, prospects and future," *Journal of Power Sources*, vol. 195, pp. 2419-2430, 2010.

- [92] S.J. An, J. Li, C. Daniel, D. Mohanty, S. Nagpure and D.L. Wood, "The state of understanding of the lithium-ion-battery graphite solid electrolyte interphase (SEI) and its relationship to formation cycling," *Carbon*, vol. 105, pp. 52-76, 2016.
- [93] H.J. Bergveld, W.S. Kruijt and F. Toolenaar, "Battery Management Systems : Design by Modelling", Dordrecht: Springer Netherlands, 2010 .
- [94] C. A. Lundgren, K. Xu, T. Richard Jow, J. Allen, S. S. Zhang, "Handbook of Electrochemical Energy", pp. 449-494, Springer Berlin Heidelberg, 2017,.
- [95] A. Jossen, "Fundamentals of battery dynamics," *Journal of Power Sources*, vol. 154, pp. 530-538, 2006.
- [96] V.S. Muralidharan, "Warburg impedance - basics revisited," *Anti-Corros. Methods Mater.*, vol. 44, pp. 26-29, 1997.
- [97] S. Rodrigues, N. Munichandraiah and A.K. Shukla, "A review of state-of-charge indication of batteries by means of a.c. impedance measurements," *Journal of Power Sources*, vol. 87, pp. 12-20, 2000.
- [98] J. -P. Diard, B. Le Gorrec, and C. Montella, "Handbook of Electrochemical Impedance Spectroscopy-Electrical Circuits containing CPEs;" Bio-logic, March 29, 2013.
- [99] H. He, R. Xiong and J. Fan, "Evaluation of Lithium-Ion Battery Equivalent Circuit Models for State of Charge Estimation by an Experimental Approach," *Energies*, vol. 4, pp. 582-598, Mar 29, 2011.

- [100] F. Saidani, F. X. Hutter, R.-G. Scurtu, W. Braunwarth, and J. N. Burghartz, "Lithium-ion battery models: a comparative study and a model-based powerline communication," *Advances in Radio Science*, vol. 15, pp. 83-91, Sep 1., 2017.
- [101] L. Zhang, H. Peng, Z. Ning, M. Zhongqiang and C. Sun, "Comparative Research on RC Equivalent Circuit Models for Lithium-Ion Batteries of Electric Vehicles", *Applied Sciences*, vol. 7. 2017.
- [102] U. Westerhoff, K. Kurbach, F. Lienesch and M. Kurrat, "Analysis of Lithium-Ion Battery Models Based on Electrochemical Impedance Spectroscopy," *Energy Technology*, vol. 4, pp. 1620-1630, 2016.
- [103] J.E.B. Randles, "Kinetics of rapid electrode reactions," *Discuss. Faraday Soc.*, vol. 1, pp. 11-19, 1947.
- [104] D. Andre, M. Meiler, K. Steiner, C. Wimmer, T. Soczka-Guth and D.U. Sauer, "Characterization of high-power lithium-ion batteries by electrochemical impedance spectroscopy. I. Experimental investigation," *Journal of Power Sources*, vol. 196, pp. 5334-5341, 2011.
- [105] I. Dincer, "Comprehensive Energy Systems", pp. 842, San Diego: Elsevier, 2018.
- [106] Scribner Associates (2016 September 28), "ZView® For Windows," [Online] Available: <http://www.scribner.com/software/68-general-electrochemistr376-zview-for-windows/> .

- [107] BioLogic Science Instruments (2016 September 1), "EC-Lab® software," [Online] Available: <http://www.bio-logic.net/software/ec-lab-software/>
- [108] Global Industry Analysts, "Battery Chargers – Global Strategic Business Report," Electronics.ca Publications., Report ID: 344098, March 2017.
- [109] D.R. Ely and R.E. García, "Heterogeneous Nucleation and Growth of Lithium Electrodeposits on Negative Electrodes," *Journal of the Electrochemical Society*, vol. 160, pp. A668, January 01. 2013.
- [110] J.Y. Song, Y.Y. Wang, and C.C. Wan, "Review of gel-type polymer electrolytes for lithium-ion batteries," *Journal of Power Sources*, vol. 77, pp. 183-197, 1999.
- [111] Q. Wang, P. Ping, X. Zhao, G. Chu, J. Sun, and C. Chen, "Thermal runaway caused fire and explosion of lithium ion battery," *Journal of Power Sources*, vol. 208, pp. 210-224, 2012.
- [112] D. Belov and M. Yang, "Investigation of the kinetic mechanism in overcharge process for Li-ion battery," *Solid State Ionics*, vol. 179, pp. 1816-1821, 2008.
- [113] S.S. Choi and H.S. Lim, "Factors that affect cycle-life and possible degradation mechanisms of a Li-ion cell based on LiCoO₂," *Journal of Power Sources*, vol. 111, pp. 130-136, 2002.
- [114] Weixiang Shen, Thanh Tu Vo and A. Kapoor, "Charging algorithms of lithium-ion batteries: An overview," *2012 7th IEEE Conference on Industrial Electronics and Applications (ICIEA)*, Singapore, pp. 1567-1572, 2012.

- [115] P. H. Cheng and C. L. Chen, "High efficiency and nondissipative fast charging strategy," *IEE Proceedings - Electric Power Applications*, vol. 150, pp. 539-545, 2003.
- [116] A.A. Hussein and I. Batarseh, "A Review of Charging Algorithms for Nickel and Lithium Battery Chargers," *IEEE Transactions on Vehicular Technology*, vol. 60, no. 3, pp. 830-838, 2011.
- [117] V.L. Teofilo, L.V. Merritt, and R.P. Hollandsworth, "Advanced lithium ion battery charger," *The Twelfth Annual Battery Conference on Applications and Advances*, Long Beach, CA., pp. 227-231, 1997.
- [118] M.J. Isaacson, R.P. Hollandsworth, P.J. Giampaoli, F.A. Linkowsky, A. Salim, and V.L. Teofilo, "Advanced lithium ion battery charger," *IEEE Aerospace and Electronic Systems Magazine*, vol. 12, no. 11, pp. 193-198, 2000.
- [119] F. Rezzi, L. Collamati, M. Costagliola and M. Cutrupi, "Battery Management in Mobile Devices," in *Frequency References, Power Management for SoC, and Smart Wireless Interfaces: Advances in Analog Circuit Design 2013*, pp. 147-168, A. Baschirotto, K.A.A. Makinwa and P. Harpe, Cham: Springer International Publishing, 2014.
- [120] Chih-Chiang Hua and Meng-Yu Lin, "A study of charging control of lead-acid battery for electric vehicles," in *Proceedings of the 2000 IEEE International Symposium on Industrial Electronics, 2000. ISIE 2000*, pp. 140 vol.1, 2000.

- [121] H. Asadi, S. Kaboli, M. Oladazimi, and M. Safari, "A review on Li-ion battery charger techniques and optimize battery charger performance by fuzzy logic," *International Conference on Information and Intelligent Computing*, vol. 18, pp. 89-96, 2011.
- [122] Shun-Chung Wang and Yi-Hua Liu, "A PSO-Based Fuzzy-Controlled Searching for the Optimal Charge Pattern of Li-Ion Batteries," *Transactions on Industrial Electronics*, vol. 62, pp. 2983-2993, 2015.
- [123] Z. Ullah, B. Burford, and S. Dillip, "Fast intelligent battery charging: neural-fuzzy approach," *Aes-M*, vol. 11, pp. 26-34, 1996.
- [124] P. J. Cheng, C. H. Cheng, and S. B. Hong, "Optimal battery chargers for photovoltaic system based on fuzzy theory and Taguchi method," in *2013 International Conference on Advanced Robotics and Intelligent Systems*, pp. 70-75, 2013.
- [125] A.B. Khan and W. Choi, "Optimal Charge Pattern for the High Performance Multi-Stage Constant Current Charge Method for the Li-ion Batteries," *Transactions on Energy Conversion*, vol. PP, pp. 1, 2018.
- [126] Y. H. Liu and Y. F. Luo, "Search for an Optimal Rapid-Charging Pattern for Li-Ion Batteries Using the Taguchi Approach," *IEEE Transactions on Industrial Electronics*, vol. 57, pp. 3963-3971, 2010.
- [127] A. Abdollahi, N. Raghunathan, X. Han, G.V. Avvari, B. Balasingam, K.R. Pattipati, and Y. Bar-Shalom, "Battery charging optimization for OCV-resistance equivalent circuit model," *2015 American Control Conference (ACC)*, Chicago, IL, pp. 3467-3472, 2015.

- [128] Yi-Hwa Liu, Jen-Hao Teng, and Yu-Chung Lin, "Search for an optimal rapid charging pattern for lithium-ion batteries using ant colony system algorithm," *IEEE Transactions on Industrial Electronics*, vol. 52, pp. 1328-1336, 2005.
- [129] C. Liu, S. Wang, Y. Liu, and M. Tsai, "An optimum fast charging pattern search for Li-ion batteries using particle swarm optimization," *The 6th International Conference on Soft Computing and Intelligent Systems, and The 13th International Symposium on Advanced Intelligence Systems*, Kobe, pp. 727-732, 2012.
- [130] W. Shen, T. Tu Vo, and A. Kapoor, "Charging algorithms of lithium-ion batteries: An overview," *2012 7th IEEE Conference on Industrial Electronics and Applications (ICIEA)* pp. 1567-1572, 2012.
- [131] J.-J. Chen, F.-C. Yang, C.-C. Lai, Y.-S. Hwang, and R.-G. Lee, "A High-Efficiency Multimode Li-Ion Battery Charger With Variable Current Source and Controlling Previous-Stage Supply Voltage," *IEEE Transactions on Industrial Electronics*, vol. 56, pp. 2469-2478, 2009.
- [132] B.G. Kim, F.P. Tredeau, and Z.M. Salameh, "Fast chargeability lithium polymer batteries," *2008 IEEE Power and Energy Society General Meeting - Conversion and Delivery of Electrical Energy in the 21st Century*, Pittsburgh, PA, pp. 1-5, 2008.
- [133] Maxim Integrated (2018 March 26), "Switch-Mode, Linear, and Pulse Charging Techniques for Li+ Battery in Mobile Phones and PDAs," August. 2002. [Online] Available: <https://www.maximintegrated.com/en/app-notes/index.mvp/id/913>

- [134] Roland van Roy, "Switching Battery Chargers," Richtek Application Note, January. 2017.
- [135] Linear Technology Corporation, "Battery Charging and Management Solutions High Performance Analog ICs," Application Note: Vol.7, 2016.
- [136] Matt Schindler, "Lithium-ion-battery charging techniques for mobile phones and PDAs," *Wireless Design & Development*, vol. 9, pp. 12, Nov 1, 2001.
- [137] C. H. Lin, C. Y. Hsieh, and K. H. Chen, "A Li-Ion Battery Charger With Smooth Control Circuit and Built-In Resistance Compensator for Achieving Stable and Fast Charging," *IEEE Transactions on Circuits and Systems I: Regular Papers*, vol. 57, pp. 506-517, 2010.
- [138] L. Chih-Min, "Linear battery charger," US patent 7759905B2, Jul 20,. 2010.
- [139] C.-H. Lin, H.-W. Huang, and K.-H. Chen, "Built-in resistance compensation (BRC) technique for fast charging Li-Ion battery charger," *2008 IEEE Custom Integrated Circuits Conference*, San Jose, CA, pp. 33-36, 2008.
- [140] K. Chung, S. Hong, and O. Kwon, "A Fast and Compact Charger for an Li-Ion Battery Using Successive Built-In Resistance Detection," *IEEE Transactions on Circuits and Systems II: Express Briefs*, vol. 64, no. 2, pp. 161-165, 2017.
- [141] C.-H. Lin, C.-Y. Hsieh, and K.-H. Chen, "A Li-Ion Battery Charger with Smooth Control Circuit and Built-In Resistance Compensator for Achieving Stable and Fast Charging," *IEEE Transactions on Circuits and Systems II: Express Briefs*, vol. 57, pp. 506-517, 2010.

- [142] S.-. Tseng, T.-. Shih, S.-. Fan, and G.-. Chang, "Design and implementation of lithium-ion/lithium-polymer battery charger with impedance compensation," *2009 International Conference on Power Electronics and Drive Systems (PEDS)*, pp. 866-870, 2009.
- [143] Min Chen and G.A. Rincon-Mora, "Accurate, Compact, and Power-Efficient Li-Ion Battery Charger Circuit," *IEEE Transactions on Circuits and Systems II: Express Briefs*, vol. 53, pp. 1180-1184, 2006.
- [144] H. Nguyen-Van, T. Nguyen, V. Quan, M. Nguyen, and L. Pham-Nguyen, "A topology of charging mode control circuit suitable for long-life Li-Ion battery charger," *2016 IEEE Sixth International Conference on Communications and Electronics (ICCE)*, pp. 167-171, 2016.
- [145] C.C. Su, Y.W. Liu, and C.C. Hung, "A dual-input high-efficiency li-ion battery charger with current-mode smooth transition and ripple reduction circuits," *2017 IEEE 60th International Midwest Symposium on Circuits and Systems (MWSCAS)*, pp. 468-471, 2017.
- [146] J.-J. Chen, F.-C. Yang, C.-C. Lai, Y.-S. Hwang, and R.-G. Lee, "A High-Efficiency Multimode Li-Ion Battery Charger with Variable Current Source and Controlling Previous-Stage Supply Voltage," *IEEE Transactions of Industrial Electronics*, vol. 56, pp. 2469-2478, 2009.
- [147] Y.-S. Hwang, S.-C. Wang, F.-C. Yang and J.-J. Chen, "New Compact CMOS Li-Ion Battery Charger Using Charge-Pump Technique for Portable Applications," *IEEE Transactions on Circuits and Systems I: Regular Papers*, vol. 54, no. 4, pp. 705-712, 2007.

- [148] B. Do Valle, C.T. Wentz and R. Sarpeshkar, "An Area and Power-Efficient Analog Li-Ion Battery Charger Circuit," *IEEE Transactions on Biomedical Circuits and Systems*, vol. 5, no. 2, pp. 131-137, 2011.
- [149] H. Han, Y. Choi, S. Choi and R. Kim, "A High Efficiency LLC Resonant Converter with Wide Ranged Output Voltage Using Adaptive Turn Ratio Scheme for a Li-Ion Battery Charger," pp. 1-6, 2016.
- [150] Y. Choi, S. Choi and R. Kim, "An integrated voltage-current compensator of LLC resonant converter for Li-ion battery charger applications," *2016 IEEE Vehicle Power and Propulsion Conference (VPPC)*, Hangzhou , pp. 3783-3790, 2016.
- [151] K. Park, Y. Choi, S. Choi and R. Kim, "Design consideration of CC-CV controller of LLC resonant converter for Li-ion battery charger," *2015 IEEE 2nd International Future Energy Electronics Conference (IFEEEC)*, Taipei, pp. 1-6, 2015.
- [152] Y-C Hsieh and C-S Huang, "Li-ion battery charger based on digitally controlled phase-shifted full-bridge converter," *IET Power Electronics*, vol. 4, pp. 242, Feb 1,. 2011.
- [153] J. Graw and H. Zimmermann, "Charging multiple batteries using the boost-flyback converter," *2012 IEEE International Energy Conference and Exhibition (ENERGYCON)*, Florence, pp. 963-967, 2012.
- [154] U. Yilmaz, A. Kircay and S. Borekci, "PV system flyback converter controlled PI control to charge battery under variable temperature and irradiance," *2017 Electronics*, Palanga, pp. 1-6, 2017.

- [155] R.-H. Peng, T.-W. Tsai, K.-H. Chen, Z. H. Tai, Y. H. Cheng, C. C. Tsai, and *et al*, "Switching-based charger with continuously built-in resistor detector (CBIRD) and analog multiplication-division unit (AMDU) for fast charging in Li-Ion battery," *2013 Proceedings of the ESSCIRC (ESSCIRC)*, Bucharest, pp. 157-160, 2013.
- [156] T.-C. Huang, R.-H. Peng, T.-W. Tsai, K.-H. Chen, and C.-L. Wey, "Fast Charging and High Efficiency Switching-Based Charger with Continuous Built-In Resistance Detection and Automatic Energy Deliver Control for Portable Electronics", *IEEE Journal of Solid-State Circuits*, vol. 49, no. 7, pp. 1580-1594, 2014.
- [157] M. Jeong, S. Kim, and C. Yoo, "Switching Battery Charger Integrated Circuit for Mobile Devices in a 130-nm BCDMOS Process," *IEEE Transactions on Power Electronics*, vol. 31, no. 11, pp. 7943-7952, 2016.
- [158] J.-N. Lou, X.-B. Wu, and M.-L. Zhao, "Switch-mode multi-power-supply Li-ion battery charger with power-path management," *2010 10th IEEE International Conference on Solid-State and Integrated Circuit Technology*, Shanghai, pp. 527-529, 2010.
- [159] R. Pagano, M. Baker, and R. E. Radke, "A 0.18 μ m Monolithic Li-Ion Battery Charger for Wireless Devices Based on Partial Current Sensing and Adaptive Reference Voltage," *IEEE Journal of Solid - State Circuits*, vol. 47, pp. 1355, Jun 1, 2012.
- [160] T. Kang, C. Kim, Y. Suh, H.I Park, B. Kang, and D. Kim, "A design and control of bi-directional non-isolated DC-DC converter for rapid electric vehicle charging system," *2012*

Twenty-Seventh Annual IEEE Applied Power Electronics Conference and Exposition (APEC), Orlando, FL pp. 14-21, 2012.

- [161] T. T. Ha, D.-Y. Chung, D. Park, H.-S. Lee, and J.W. Lee, "A buck DC-DC converter using automatic PFM/PWM mode change for high-efficiency Li-ion battery charger," *2014 International SoC Design Conference (ISOCC)*, Jeju, pp. 238-239, 2014.
- [162] David H Wilson, "Method of charging storage batteries," US Patent US1126667A, June 27, 1914.
- [163] F.B. Diniz, L.E.P. Borges and B.d.B. Neto, "A comparative study of pulsed current formation for positive plates of automotive lead acid batteries," *Journal of Power Sources*, vol. 109, pp. 184-188, 2002.
- [164] L.T. Lam, H. Ozgun, O.V. Lim, J.A. Hamilton, L.H. Vu, D.G. Vella and D.A.J. Rand, "Pulsed-current charging of lead/acid batteries — a possible means for overcoming premature capacity loss?" *Journal of Power Sources*, vol. 53, pp. 215-228, 1995.
- [165] H. Ikeda, S. Minami, S.J. Hou, Y. Onishi and A. Kozawa, "Nobel High Current Pulse Charging Method for Prolongation of Lead-acid Batteries," *Journal of Asian Electric Vehicles*, vol. 3, pp. 681-687, 2005.
- [166] L.-R. Chen, "A Design of an Optimal Battery Pulse Charge System by Frequency-Varied Technique," *IEEE Transactions on Industrial Electronics*, vol. 54, pp. 398-405, 2007.

- [167] L.-R. Chen, "Design of Duty-Varied Voltage Pulse Charger for Improving Li-Ion Battery-Charging Response," *IEEE Transactions on Industrial Electronics*, vol. 56, pp. 480-487, 2009.
- [168] M. D. Yin, J. Youn, D. Park, and J. Cho, "Efficient Frequency and Duty Cycle Control Method for Fast Pulse-Charging of Distributed Battery Packs by Sharing Cell Status," in *2015 IEEE 12th Intl Conf on Ubiquitous Intelligence and Computing and 2015 IEEE 12th Intl Conf on Autonomic and Trusted Computing and 2015 IEEE 15th Intl Conf on Scalable Computing and Communications and Its Associated Workshops (UIC-ATC-ScalCom)*, pp. 1813-1818, 2015.
- [169] F. Savoye, P. Venet, M. Millet, and J. Groot, "Impact of Periodic Current Pulses on Li-Ion Battery Performance," *IEEE Transactions on Industrial Electronics*, vol. 59, pp. 3481-3488, 2012.
- [170] L.-R. Chen, J.-J. Chen, C.-M. Ho, S.-L. Wu, and D.-T. Shieh, "Improvement of Li-ion Battery Discharging Performance by Pulse and Sinusoidal Current Strategies," *IEEE Transactions on Industrial Electronics*, vol. 60, pp. 5620-5628, 2013.
- [171] J. Li, E. Murphy, J. Winnick, and P.A. Kohl, "The effects of pulse charging on cycling characteristics of commercial lithium-ion batteries," *Journal of Power Sources*, vol. 102, pp. 302-309, 2001.

- [172] F. Savoye, P. Venet, M. Millet, and J. Groot, "Impact of Periodic Current Pulses on Li-Ion Battery Performance," *IEEE Transactions on Industrial Electronics*, vol. 59, pp. 3481-3488, 2012.
- [173] P.E. de Jongh and P.H.L. Notten, "Effect of current pulses on lithium intercalation batteries," *Solid State Ionics*, vol. 148, pp. 259-268, 2002.
- [174] S. Tobishima and J. Yamaki, "A consideration of lithium cell safety," *Journal of Power Sources*, vol. 81-82, pp. 882-886, 1999.
- [175] T. Ohsaki, T. Kishi, T. Kuboki, N. Takami, N. Shimura, Y. Sato, M. Sekino, and A. Satoh, "Overcharge reaction of lithium-ion batteries," *Journal of Power Sources*, vol. 146, pp. 97-100, 2005.
- [176] M.Z. Mayers, J.W. Kaminski, and T.F. Miller, "Suppression of Dendrite Formation via Pulse Charging in Rechargeable Lithium Metal Batteries," *J.Phys.Chem.C*, vol. 116, pp. 26214-26221, 2012.
- [177] B.K. Purushothaman, P.W. Morrison and U. Landau, "Reducing Mass-Transport Limitations by Application of Special Pulsed Current Modes," *Journal of the Electrochemical Society*, vol. 152, pp. J33, 2005.
- [178] C. Oladimeji and P. Moss, "Performance of Commercial LiCoO₂ Battery Under Pulse Current Charging Using Varying Duty Cycles," presented at the 225th *Electrochemical Society Meeting Abstracts*, Orlando, Florida May 11-15, 2014.

- [179] B. N. Popov, B. S. Haran, A. Durairajan, R. White, Y. Podrazhansky, and R. C. Cope, "Studies on capacity fade of Li-ion cells cycled using pulse and DC charging protocols," presented at the *197th Electrochemical Society meeting*, Toronto, Canada, May 2000.
- [180] M. Di Yin, J. Cho, and D. Park, "Pulse-Based Fast Battery IoT Charger Using Dynamic Frequency and Duty Control Techniques Based on Multi-Sensing of Polarization Curve," *Journal of Energies*, vol. 9, pp. 209, Mar 1, 2016.
- [181] B.K. Purushothaman and U. Landau, "Rapid Charging of Lithium-Ion Batteries using Pulsed Currents," *Journal of the Electrochemical Society*, vol. 153, pp. A533, 2006.
- [182] Markets and Markets, "Internet of Things (IoT) Market by Software Solution - Global Forecast to 2022" Research and Markets, Report ID: 4308780, Jun 15, 2017.
- [183] Digi-Key's European Editors (2018 March 25), "Selecting Batteries for IoT Devices," [Online] Available: <https://www.digikey.com/en/articles/techzone/2014/aug/selecting-batteries-for-iot-devices>
- [184] Ji. Jiang, Q. Liu, C. Zhang, and W. Zhang, "Evaluation of Acceptable Charging Current of Power Li-Ion Batteries Based on Polarization Characteristics," *IEEE Transactions on Industrial Electronics*, vol. 61, pp. 6844-6851, 2014.
- [185] Cadence Design Systems Inc. (2018 March 28), "Virtuoso ADE Product Suite," [Online] Available: https://www.cadence.com/content/cadence-www/global/en_US/home/tools/custom-ic-analog-rf-design/circuit-design/virtuoso-ade-product-suite.html.

- [186] Ani Fayezi and Kerry Lacanette (2018 March 17), "Keep Designs Cool with a Tiny, Low-Power Temperature Sensor," Maxim Integrated Blog, November 14, 2017. [Online] Available: <https://www.maximintegrated.com/en/design/blog/low-power-temperature-sensor.html>
- [187] The MOSIS Service (2018 March 14), "Account Types Available to Academic Institutions," The MOSIS Service, USC Information Sciences Institute 2018. [Online] Available: <https://www.mosis.com/you-are/academic-institutions>
- [188] Ametek Scientific Instruments, "VersaSTAT 4 | Potentiostat Galvanostat" Princeton Applied Research, VersaSTAT Series datasheet, 2017.
- [189] Zivelab, "EIS Software Package: Electrochemical Impedance Spectroscopy," Designing the solution for electrochemistry application note, May, 2015.
- [190] *Panasonic Lithium Batteries Technical Handbook*, Matsushita Battery Industrial Co. Ltd, 2002, pp. 64-86.
- [191] C. Harm and K. Timm, "Battery charger with thermal runaway protection," U.S Patent 5214370 A, Sept. 13, 1991.
- [192] Y. Saito, "Thermal behaviors of lithium-ion batteries during high-rate pulse cycling," *Journal of Power Sources*, vol. 146, pp. 770-774, 2005.

- [193] K. Onda, T. Ohshima, M. Nakayama, K. Fukuda, and T. Araki, "Thermal behavior of small lithium-ion battery during rapid charge and discharge cycles," *Journal of Power Sources*, vol. 158, pp. 535-542, 2006.
- [194] R.K. Roy, "Design of experiments using the Taguchi approach", New York: Wiley, 2001, pp. 8-23.
- [195] K. K. Hockman and D. Berengut, "Design of experiments," *Chemical Engineering*, vol. 102, no. 11, pp. 142-147, 1995.
- [196] G. Taguchi, "Experimental designs", Tokyo, Japan: Maruzen Publishing Company, 1976.
- [197] S. C. Wang, J. W. Huang, Y. H. Liu, and C. H. Hsieh, "The implementation of consecutive orthogonal array method on searching optimal five step charging pattern for Lithium-ion batteries," in *2011 9th World Congress on Intelligent Control and Automation*, pp. 358-363, 2011.
- [198] W.-C. Weng, F. Y., V. Demir, and A. Elsherbeni, "Optimization using Taguchi method for electromagnetic applications," in *2006 First European Conference on Antennas and Propagation*, pp. 1-6, 2006.
- [199] R. Dudhe, S. Ayyalusamy, and T. Desai, "Optimization of BAW Resonator for Wireless Applications using Taguchi's Orthogonal Array Method" *COMSOL Conference*, 2015..

- [200] C. C. Hsu, C. S. Chien, T. Y. Wei, Y. T. Li, and H. F. Li, "Taguchi DoE for ceramic substrate SMT defects improvement," *11th International Microsystems, Packaging, Assembly and Circuits Technology Conference (IMPACT)*, pp. 381-384, 2016.
- [201] K. S. Kim, K. T. Jung, J. M. Kim, J. P. Hong and S. I. Kim, "Taguchi robust optimum design for reducing the cogging torque of EPS motors considering magnetic unbalance caused by manufacturing tolerances of PM," *IET Electric Power Applications*, vol. 10, pp. 909-915, 2016.
- [202] K. Dehnad, "Quality control, robust design, and the Taguchi method", Pacific Grove, Calif: Wadsworth & Brooks/Cole, 1989, pp. 12-13.
- [203] *NIST/SEMATECH e-Handbook of Statistical Methods* (2017 March) [Online]. Available: <http://www.itl.nist.gov/div898/handbook/pri/section5/pri56.htm>.
- [204] M.S. Phadke, "Quality engineering using robust design", Prentice Hall, 1989.
- [205] S. C. Wang, Y. L. Chen, Y. H. Liu and Y. S. Huang, "A fast-charging pattern search for li-ion batteries with fuzzy-logic-based Taguchi method," in *2015 IEEE 10th Conference on Industrial Electronics and Applications (ICIEA)*, pp. 855-859, 2015.
- [206] Y. H. Liu and Y. F. Luo, "Search for an Optimal Rapid-Charging Pattern for Li-Ion Batteries Using the Taguchi Approach," *IEEE Transactions on Industrial Electronics*, vol. 57, pp. 3963-3971, 2010.

- [207] Renata Batteries, "Article Safety Data Sheet- Lithium Ion/Polymer Batteries," Lithium Ion Polymer Battery pack, ICP/AHB series, Dec. 3, 2013.
- [208] L. Pauling, "General Chemistry", Dover Publications, 1988, pp.551 - 576
- [209] L. Ahmadi, M. Fowler, S.B. Young, R.A. Fraser, B. Gaffney, and S.B. Walker, "Energy efficiency of Li-ion battery packs re-used in stationary power applications," *Sustainable Energy Technologies and Assessments*, vol. 8, pp. 9-17, 2014.
- [210] R. Lu, A. Yang, Y. Xue, L. Xu, and C. Zhu, "Analysis of the key factors affecting the energy efficiency of batteries in electric vehicle," *World Electric Vehicle Journal*, vol. 4, 2010.
- [211] S.S. Choi and H.S. Lim, "Factors that affect cycle-life and possible degradation mechanisms of a Li-ion cell based on LiCoO₂," *Journal of Power Sources*, vol. 111, pp. 130-136, 2002.
- [212] K. Onda, T. Ohshima, M. Nakayama, K. Fukuda and T. Araki, "Thermal behavior of small lithium-ion battery during rapid charge and discharge cycles," *Journal of Power Sources*, vol. 158, pp. 535-542, 2006.
- [213] Japan Electronics and Information Technology Industries Association and Battery Association of Japan, "A guide to the safe use of secondary lithium ion batteries in notebook-type personal computers," April. 2007.
- [214] N. Williard, B. Sood, M. Osterman, and M. Pecht, "Disassembly methodology for conducting failure analysis on lithium-ion batteries," *J. Mater. Sci.: Mater. Electron.*, vol. 22, pp. 1616, 2011.

- [215] S. Jeong, M. Inaba, R. Mogi, Y. Iriyama, T. Abe and Z. Ogumi, "Surface Film Formation on a Graphite Negative Electrode in Lithium-Ion Batteries: Atomic Force Microscopy Study on the Effects of Film-Forming Additives in Propylene Carbonate Solutions," *Langmuir*, vol. 17, pp. 8281-8286, 2001.
- [216] R. Scipioni, P.S. Jørgensen, D. Ngo, S.B. Simonsen, Z. Liu, *et al*, "Electron microscopy investigations of changes in morphology and conductivity of LiFePO₄/C electrodes," *Journal of Power Sources*, vol. 307, pp. 259-269, 2016.
- [217] Stefanie Freitag, Christina Berger, Jeff Gelb and T.B. Christian Weisenberger, "Li-Ion Battery Components – Cathode, Anode, and, Separator – Imaged at Low Accelerating Voltages With ZEISS FE-SEMs," Zeiss White Paper, Carl Zeiss Microscopy GmbH, November. 2016.
- [218] L. Kong, Y. Xing, and M.G. Pecht, "In-Situ Observations of Lithium Dendrite Growth," *IEEE Access*, vol. 6, pp. 8387-8393, 2018.
- [219] F. Orsini, A. Du Pasquier, B. Beaudoin, J.M. Tarascon, M. Trentin, N. Langenhuizen, E. De Beer and P. Notten, "In situ Scanning Electron Microscopy (SEM) observation of interfaces within plastic lithium batteries," *Journal of Power Sources*, vol. 76, pp. 19-29, 1998.
- [220] J.Y. Chan, J.H. Kim, N. Seunghoon, C.R. Park and S.J. Yang, "Rational Design of Nanostructured Functional Interlayer/Separator for Advanced Li–S Batteries," *Adv. Funct. Mater.*, vol. 0, pp. 1707411, 2018.

- [221] S. Jeong, M. Inaba, Y. Iriyama, T. Abe, and Z. Ogumi, "Surface film formation on a graphite negative electrode in lithium-ion batteries: AFM study on the effects of co-solvents in ethylene carbonate-based solutions," *Electrochimica Acta*, vol. 47, pp. 1975-1982, 2002.
- [222] W. Waag, S. Käbitz, and D.U. Sauer, "Experimental investigation of the lithium-ion battery impedance characteristic at various conditions and aging states and its influence on the application," *Applied Energy*, vol. 102, pp. 885-897, 2013.
- [223] D. Aurbach, E. Zinigrad, Y. Cohen, and H. Teller, "A short review of failure mechanisms of lithium metal and lithiated graphite anodes in liquid electrolyte solutions," *Solid State Ionics*, vol. 148, pp. 405-416, 2002.
- [224] J. Shim, R. KostECKI, T. Richardson, X. Song, and K.A. Striebel, "Electrochemical analysis for cycle performance and capacity fading of a lithium-ion battery cycled at elevated temperature," *Journal of Power Sources*, vol. 112, pp. 222-230, 2002.
- [225] P. Ramadass, A. Durairajan, B.S. Haran, R.E. White, and B.N. Popov, "Capacity fade studies on spinel based Li-ion cells," *Seventeenth Annual Battery Conference on Applications and Advances. Proceedings of Conference (Cat. No.02TH8576)*, Long Beach, CA, pp. 25-30, 2002.
- [226] Y. Ito and Y. Ukyo, "Performance of LiNiCoO₂ materials for advanced lithium-ion batteries," *Journal of Power Sources*, vol. 146, pp. 39-44, 2005.

- [227] D. Zhang, B.S. Haran, A. Durairajan, R.E. White, Y. Podrazhansky, and B.N. Popov, "Studies on capacity fade of lithium-ion batteries," *Journal of Power Sources*, vol. 91, pp. 122-129, 2000.
- [228] U. Tröltzsch, O. Kanoun, and H. Tränkler, "Characterizing aging effects of lithium ion batteries by impedance spectroscopy," *Electrochimica Acta*, vol. 51, pp. 1664-1672, 2006.
- [229] J. Vetter, P. Novák, M.R. Wagner, C. Veit, K.-. Möller, J.O. Besenhard, M. Winter, M. Wohlfahrt-Mehrens, C. Vogler and A. Hammouche, "Ageing mechanisms in lithium-ion batteries," *Journal of Power Sources*, vol. 147, pp. 269-281, 2005.
- [230] TestEquity, "TestEquity 107 Benchtop Temperature Chamber (Environmental Chamber)," Operation and service manual, 2008-2009.
- [231] G. Ning, B. Haran and B.N. Popov, "Capacity fade study of lithium-ion batteries cycled at high discharge rates," *Journal of Power Sources*, vol. 117, pp. 160-169, 2003.
- [232] F. Leng, C.M. Tan, and M. Pecht, "Effect of Temperature on the Aging rate of Li Ion Battery Operating above Room Temperature," *Scientific Reports*, vol. 5, pp. 12967, 2015.
- [233] P. Ramadass, B. Haran, R. White, and B.N. Popov, "Capacity fade of Sony 18650 cells cycled at elevated temperatures: Part I. Cycling performance," *Journal of Power Sources*, vol. 112, pp. 606-613, 2002.

- [234] K. Amine, J. Liu and I. Belharouak, "High-temperature storage and cycling of C-LiFePO₄/graphite Li-ion cells," *Electrochemistry Communications*, vol. 7, pp. 669-673, 2005.

APPENDIX

The benchmark CC-CV charging algorithms were implemented by various commercial linear and switch-mode chargers. The CC-CV algorithm-based chargers used are

- Microchip MCP73831/2
- Texas Instruments BQ24271
- Texas Instruments BQ25100

Another designed CC-CV based charger used is shown in Fig. A-1.

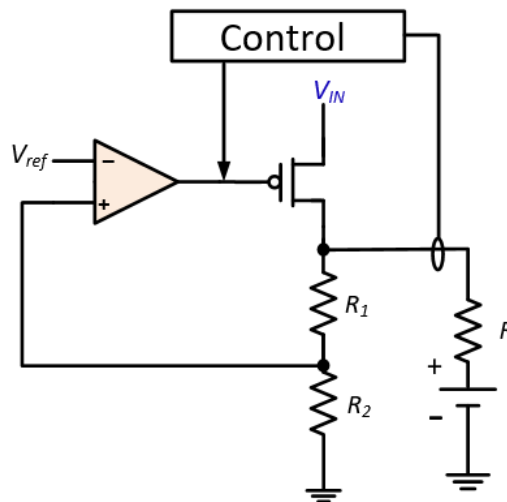


Figure A-1: Charger for coin cells

The fuel gauge and coulomb counter for SoC measurements used were Maxim Integrated MAX 17043 and Analog Devices LTC4150, respectively. The temperature sensor used was Microchip Technology MCP9808 digital temperature sensor.

The experimental test setups are shown in the figures below. A typical charging and discharging setup is shown in Fig. A-2, while a battery undergoing an EIS is shown in Fig. A-3. The setups

might change depending on what experiment is being performed. The batteries under test are always placed in the temperature chamber.

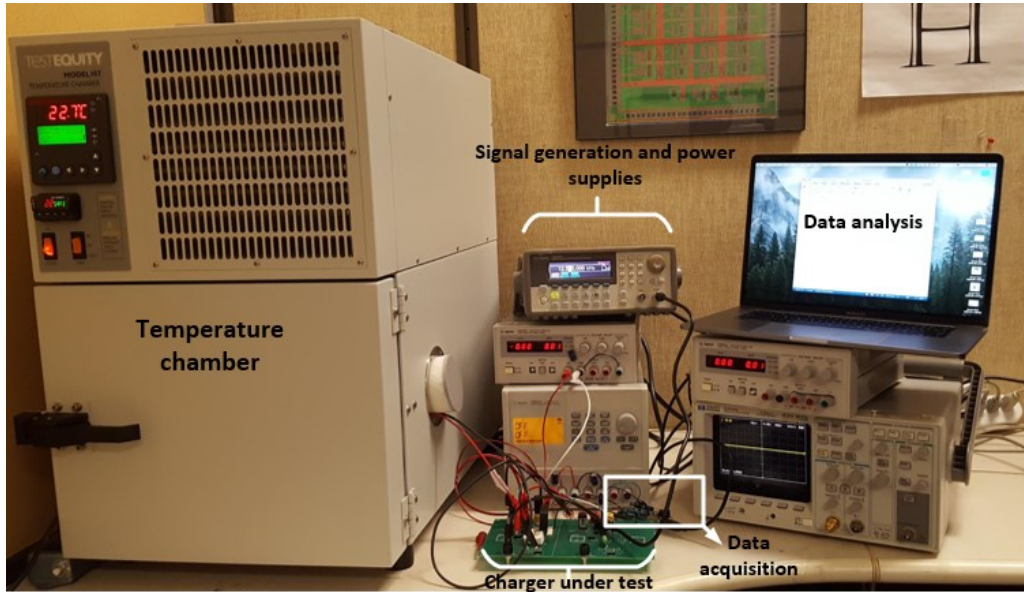


Figure A-2: A typical setup for charging and discharging



Figure A-3: Battery undergoing EIS